TKK Dissertations 94
Espoo 2007

PROGRESSIVE FLOODING OF A DAMAGED PASSENGER SHIP

Doctoral Dissertation

Pekka Ruponen

Helsinki University of Technology
Department of Mechanical Engineering
Ship Laboratory

TKK Dissertations 94
Espoo 2007

PROGRESSIVE FLOODING OF A DAMAGED PASSENGER SHIP

Doctoral Dissertation

Pekka Ruponen

Dissertation for the degree of Doctor of Science in Technology to be presented with due permission of the Department of Mechanical Engineering for public examination and debate in Auditorium K216 at Helsinki University of Technology (Espoo, Finland) on the 16th of November, 2007, at 12 noon.

Helsinki University of Technology
Department of Mechanical Engineering
Ship Laboratory

Teknillinen korkeakoulu
Konetekniikan osasto
Laivalaboratorio

Distribution:
Helsinki University of Technology
Department of Mechanical Engineering
Ship Laboratory
P.O. Box 5300 (Tietotie 1)
FI - 02015 TKK
FINLAND
URL: http://www.tkk.fi/Units/Ship/
Tel. +358-(0)9-451 3501
Fax +358-(0)9-451 4173
E-mail: leila.silonsaari@tkk.fi

ISBN 978-951-22-9012-3
ISBN 978-951-22-9013-0 (PDF)
ISSN 1795-2239
ISSN 1795-4584 (PDF)
URL: http://lib.tkk.fi/Diss/2007/isbn9789512290130/

TKK-DISS-2362

Yliopistopaino
Helsinki 2007

ABSTRACT OF DOCTORAL DISSERTATION	HELSINKI UNIVERSITY OF TECHNOLOGY P.O. BOX 1000, FI-02015 TKK http://www.tkk.fi

Author Pekka Ruponen

Name of the dissertation
Progressive Flooding of a Damaged Passenger Ship

Manuscript submitted 11.05.2007	Manuscript revised 13.09.2007
Date of the defence 16.11.2007	
☒ Monograph	☐ Article dissertation (summary + original articles)

Department	Department of Mechanical Engineering
Laboratory	Ship Laboratory
Field of research	Naval Architecture
Opponent(s)	Prof. Apostolos Papanikolaou and Dr. Patrik Rautaheimo
Supervisor	Prof. Jerzy Matusiak
Instructor	Prof. Jerzy Matusiak

Abstract

Progressive flooding inside a damaged passenger ship was studied with time-domain simulations. A novel computational method was developed for this purpose. Typically, the layout of the watertight compartments in this ship type contains numerous openings and rooms with complex geometry. In the voids the flooding can also result in air compression since the ventilation of these rooms is restricted due to the relatively small air pipes. These factors are significant for time-accurate simulation of progressive flooding.

The developed method is based on pressure correction technique. This iterative and implicit approach is suitable for time-accurate simulations. The progress of the floodwater is considered on the basis of the hydrostatic pressure (i.e. the water height) in the flooded rooms. The widely used hydraulic model, based on Bernoulli's equation, is used for the calculation of the flow velocities. The pressure-correction equation is formed from the conservation of mass and the linearization of Bernoulli's equation. The ship is considered as a staggered and unstructured grid, where the hydrostatic and air pressures are solved in the centers of the rooms and the flow velocities in the openings. Also the counter pressure due to air compression and the resulting airflows can be solved. All water levels are considered to be flat and parallel to the sea level. The main emphasis of the study is on the calculation of the flooding inside the damaged ship, and therefore, a simple quasi-stationary approach is used for the evaluation of the ship motions. The standard procedures of the NAPA software are utilised for this. In addition, it is assumed that the sea is calm.

The developed simulation method has been extensively validated by comparing simulation results with the measurement data from model tests for progressive flooding and air compression in a damaged box-shaped barge. The results of the validation show very good correspondence between the simulations and the measurements.

The applicability of the developed simulation method has been tested by performing simulations of cross-flooding and extensive progressive flooding for a 40 000 GT passenger ship design. The latter test case involves flooding through leaking and collapsed structures and slow down-flooding in a large and complex system of rooms and openings.

Keywords progressive flooding, damage stability, pressure correction, passenger ship

ISBN (printed)	978-951-22-9012-3	ISSN (printed)	1795-2239
ISBN (pdf)	978-951-22-9013-0	ISSN (pdf)	1795-4584
Language	English	Number of pages	128
Publisher	Helsinki University of Technology, Ship Laboratory		
Print distribution	Helsinki University of Technology, Ship Laboratory		

☒ The dissertation can be read at http://lib.tkk.fi/Diss/2007/isbn9789512290130/

VÄITÖSKIRJAN TIIVISTELMÄ	TEKNILLINEN KORKEAKOULU PL 1000, 02015 TKK http://www.tkk.fi

Tekijä Pekka Ruponen

Väitöskirjan nimi
Progressiivinen vuoto vaurioituneessa matkustajalaivassa

Käsikirjoituksen päivämäärä 11.05.2007	Korjatun käsikirjoituksen päivämäärä 13.09.2007
Väitöstilaisuuden ajankohta 16.11.2007	
☒ Monografia	☐ Yhdistelmäväitöskirja (yhteenveto + erillisartikkelit)

Osasto	Konetekniikan osasto
Laboratorio	Laivalaboratorio
Tutkimusala	Laivatekniikka
Vastaväittäjä(t)	Prof. Apostolos Papanikolaou ja TkT Patrik Rautaheimo
Työn valvoja	Prof. Jerzy Matusiak
Työn ohjaaja	Prof. Jerzy Matusiak

Tiivistelmä

Työssä tutkittiin aikatason simuloinneilla progressiivisen vuodon etenemistä vaurioituneessa matkustajalaivassa. Tätä tarkoitusta varten kehitettiin uudentyyppinen laskentamenetelmä. Matkustajalaivan vesitiiviissä osastoissa on usein lukuisia monimutkaisia tiloja ja niitä yhdistäviä aukkoja. Lisäksi ilmanvaihto void-tiloissa on usein rajoitettu pienten ilmaputkien takia, joten vuoto voi aiheuttaa myös ilman kokoonpuristumista. Nämä tekijät ovat merkittäviä simuloitaessa progressiivista vuotoa ajan suhteen tarkasti.

Kehitetty uudentyyppinen laskentamenetelmä perustuu painekorjaustekniikkaan. Tämä iteratiivinen ja implisiittinen menetelmä soveltuu hyvin ajan suhteen tarkkaan laskentaan. Vuotoveden etenemisen laskenta pohjautuu siinä hydrostaattisiin paineisiin, eli veden korkeuksiin, vuodon saaneissa tiloissa. Laajalti käytettyä hydraulista mallia (Bernoullin yhtälö) sovelletaan virtausnopeuksien laskentaan. Laivaa käsitellään limitettynä ja rakenteettomana laskentahilana, jossa hydrostaattinen paine ja ilmanpaine ratkaistaan tilojen keskellä ja virtausnopeudet tiloja yhdistävissä aukoissa. Myös ilman vastapaine ja siitä seuraavat ilmavirtaukset voidaan ratkaista. Kaikki nestepinnat oletetaan horisontaaleiksi tasoiksi. Tutkimuksen pääpaino on vuodon etenemisen laskennassa, joten laivan liikkeiden määrittämiseen käytetään yksinkertaista kvasistaattista lähestymistapaa. Tässä hyödynnettiin NAPA-ohjelmiston standardimenetelmiä. Lisäksi oletetaan, että meri on tyyni.

Kehitetty simulointimenetelmä on perusteellisesti validoitu vertaamalla laskennallisia tuloksia laatikkolaivan mallilla tehtyihin mittauksiin vuodon etenemisestä ja ilman puristumisesta. Tulokset osoittavat hyvän vastaavuuden laskennan ja mittausten välillä.

Menetelmän soveltuvuutta käytäntöön on testattu simuloimalla poikittaisvuotoa ja laajaa progressiivista vuotoa 40 000 GT:n kokoisessa matkustajalaivassa. Progressiivisen vuodon tapauksessa on otettu huomioon myös vuoto vaurioituneiden ja sortuneiden rakenteiden läpi sekä hidas alasvirtaus monimutkaisessa ja laajassa tilojen ja aukkojen muodostamassa systeemissä.

Asiasanat progressiivinen vuoto, vuotovakavuus, painekorjaus, matkustajalaiva

ISBN (painettu)	978-951-22-9012-3	ISSN (painettu)	1795-2239
ISBN (pdf)	978-951-22-9013-0	ISSN (pdf)	1795-4584
Kieli	englanti	Sivumäärä	128
Julkaisija	Teknillinen korkeakoulu, Laivalaboratorio		

Painetun väitöskirjan jakelu Teknillinen korkeakoulu, Laivalaboratorio

☒ Luettavissa verkossa osoitteessa http://lib.tkk.fi/Diss/2007/isbn9789512290130/

Preface

The research for this thesis was carried out in the Ship Laboratory of Helsinki University of Technology (TKK) during the years 2003–2007. The research was funded by Napa Ltd and Tekes (Finnish funding agency for technology and innovation). The last phase of the work was funded by the graduate school of the Department of Mechanical Engineering. The financial support is gratefully acknowledged.

I want to express my gratitude to Professor Jerzy Matusiak, the supervisor of this thesis, for his guidance throughout the period of my work. I would also like to thank Prof. Timo Siikonen for his inspiring lectures and for introducing me to computational fluid dynamics.

I want to thank Markku Larmela from Napa Ltd for his help with the implementation of the simulation method to the NAPA software and Tom Sundell for his comments and support.

I am grateful to Tommi Mikkola from TKK Ship Laboratory for the interesting discussions on numerical hydrodynamics. Pentti Tukia and the personnel at the workshop of the laboratory are thanked for their valuable help with the model tests.

I would also like to thank Anna-Lea Routi and Erik Routi from Aker Yards for providing the ship design for the case study and Mikko Vartiainen for his comments and for testing the simulation method.

Particular thanks are due to Christopher Ridgewell for checking the language of this dissertation.

I am also grateful to all my friends and colleagues at TKK Ship Laboratory and Napa Group during these years.

Finally, I would like to thank my parents and my brother for their support during my studies.

Helsinki 11.5.2007

Pekka Ruponen

Contents

Nomenclature

A	area (of an opening)
A_{coll}	effective area of a collapsed door
A_{eff}	effective area of a potential opening
A_{leak}	effective area of a leaking door
A_{ratio}	ratio between leak and collapse areas
A_{tot}	total area of an opening
b	width of an opening
C_d	discharge coefficient, additional indices tell whether the opening is submerged on 1 or 2 sides
D	effective diameter of a pipe
$\mathbf{F}$	body force vector
g	acceleration due to gravity
h	height from the reference level
H_{coll}	critical pressure head for collapsing
H_{leak}	critical pressure head for leaking
H_o	height of an opening from the reference level
H_w	water height from the reference level
ΔH_{eff}	effective pressure head
ΔH_o	vertical distance between the lowest and highest point of an opening
K'	dimensional pressure loss coefficient
k_L	pressure loss coefficient (non-dimensional)
l	length
L	length of a pipe
L_o	length of an opening line
L_{pp}	length of the ship (between perpendiculars)
M	moment

$\dot{m}$	mass flow
$\Delta\dot{m}$	mass balance
m_{ship}	mass of the intact ship
$\mathbf{n}$	normal vector
P	total pressure (sum of hydrostatic pressure and air pressure)
p	air pressure
p_0	atmospheric air pressure
Δp	air pressure difference
Q	volumetric flow through an opening or pipe
S	surface, bounding a control volume
S_{fs}	area of the free surface (permeability taken into account)
S_{geom}	geometrical area of the free surface (permeability excluded)
T	draught of the ship
t	time
$\mathbf{U}$	velocity vector
u	flow velocity
Δt	time step
V_a	volume of air
V_{net}	net volume (permeability taken into account)
V_w	volume of floodwater
α	under-relaxation factor
β	inclination angle of an opening line
δH	convergence criterion for water heights
δp	convergence criterion for air pressures
ε	surface roughness (particular size of grains)
ϕ	heeling angle of the ship
λ	surface roughness coefficient
μ	permeability

ρ_0	density of air at the atmospheric pressure
ρ_a	density of air
ρ_w	density of water
θ	trim angle of the ship
Ω	control volume
∇	volume of the buoyancy
	nabla operator $\{\partial/\partial x, \partial/\partial y, \partial/\partial z\}$

Abbreviations

BL	baseline
CGSTAB	conjugate gradient stabilized
DOF	degree of freedom
GA	general arrangement
GT	gross tonnage
HARDER	Harmonization of rules and design rationale
IMO	International Maritime Organization
ITTC	International Towing Tank Conference
MARIN	Maritime Research Institute Netherlands
RANSE	Reynolds averaged Navier-Stokes equations
SLF	Sub-Committee on Stability and Load Lines and on Fishing Vessels Safety (IMO)
SOLAS	Safety of Life at Sea
SPH	smoothed particle hydrodynamics
SVD	singular value decomposition
TKK	Helsinki University of Technology (Teknillinen korkeakoulu)

TTF	time-to-flood
VOF	volume of fluid
WT	watertight

1 Introduction

1.1 Objectives

The main objective of this thesis was to develop a fast and accurate simulation method for progressive flooding of a damaged passenger ship. The size of passenger ships has been growing for decades, and nowadays many ships can accommodate several thousand people. Therefore, the safety of these ships is of the uttermost importance, both in the design phase and onboard in the event of accident.

When a ship is damaged, for example due to a collision or grounding, water starts to flood in. The internal openings and non-watertight subdivision in the watertight (WT) compartments can have a significant effect on the motions of the ship during the flooding process. Between the intact position and the final damaged condition, if equilibrium can be found, the flooding ship can pass through intermediate stages that can be more hazardous than the final condition. Therefore, it is important to be able to evaluate these intermediate stages. Practically, the only feasible and accurate way to do this is time-domain simulation of the flooding process and the motions of the damaged ship. Moreover, the simulation will give an estimation of the available time for orderly evacuation and abandonment, where there is a risk that the ship will capsize or sink. Within this thesis, the time period between the start of the flooding and the equilibrium condition is referred to as time-to-flood (TTF). However, if the ship capsizes or sinks, a corresponding term time-to-capsize or time-to-sink is considered to be more appropriate.

Flooding simulations could also be performed for the actual damage case onboard the damaged ship or ashore, on the basis of the measurements by water level sensors. However, in this case the results must be available in a short time in order to provide help for the decision support system. Therefore, the simulation method has to be fast and capable of calculating progressive flooding time-accurately in complex systems of compartments and openings.

This study concentrates on simulation of progressive flooding, i.e. a process, where the floodwater can proceed to undamaged compartments of the ship through the internal openings and connections, such as, doors, staircases, pipes and ducts. The internal layout of a passenger ship is typically very complex and there can be dense non-watertight subdivisions within the watertight compartments. Consequently, the

progressive flooding in such compartments can involve dozens of rooms that are connected to each other through various openings and pipes.

In addition to studying progressive flooding cases, time domain simulation is a very efficient tool for analyzing and improving various cross-flooding arrangements, *Peters et al (2003)*. In these cases, the effects of air pipes can also be significant due to the compression of air that delays the equalizing flooding to the undamaged side, *Vredeveldt and Journée (1991)* and *Vartiainen (2006)*. Therefore, it is necessary that the simulation tool can also deal with airflows.

Normally the calculation of the damaged stability of ships is based on the assumption that all damaged compartments are flooded immediately. However, according to the draft Explanatory Notes for the revised SOLAS (Safety of Life at Sea) chapter II-1, (*IMO MSC.1/Circ.1226, 2007*), calculations for intermediate stages of flooding are not needed whenever the equalization is considered to be instantaneous, i.e. when the equalization is of a duration less than 60 s. This raises a question on how to calculate the required time for the equalization. The *IMO Resolution A.266 (VIII)* provides a simple formula for estimation of the equalization time in typical cross-flooding arrangements, but it cannot be applied to more complex systems. Time-accurate flooding simulation provides the most realistic approach for the calculation of the intermediate stages throughout the whole flooding process and for assessing the time-to-flood.

Since the early 1990s, several time-domain simulation methods for the motions of a damaged ship have been developed in various institutes. These are briefly reviewed in the next section. However, in most of these studies the main emphasis has been on the modelling of the motions of a ro-ro vessel with a flooded vehicle deck in a severe sea state. Furthermore, most of these methods originate from time-domain simulation models for intact ships in waves and the handling of floodwater is simply added to an existing computer code. Effective simulation of progressive flooding for dozens of compartments has rarely been considered to be of interest, and the flooding of large passenger ships without a vehicle deck is considered only in a few studies as the main emphasis has been on the calculation of the motions and their coupling with the flooded water.

1.2 Review of Flooding Simulation Methods

The time-domain simulation methods for damage stability and progressive flooding have been developed for about two decades. The capsizing of the car passenger ferry

"Herald of Free Enterprise" in 1987 and the sinking of the ferry "Estonia" in 1994 have had a major influence on this work. Therefore, it is easy to understand why so much effort has been put to the problem of water on the vehicle deck. However, recently also the performance based damage stability of large passenger ships has been studied with simulations. This has become feasible since the calculation capacity of the computers has improved a lot. The most significant approaches on the flooding simulation are briefly reviewed in the following paragraphs.

The first flooding simulation methods were developed for the estimation of the intermediate phases during the flooding by using a simple hydraulic model for the calculation of the flooding rates. *Spouge (1986)* has presented simulations of the capsizing of the ro-ro passenger vessel "European Gateway". The asymmetric distribution of the floodwater was taken into account by using a semi-empirical offset for the center of gravity of the floodwater. *Sen and Konstantinidis (1987)* have described a similar method, where all water levels are considered to be horizontal. The motions of the ship were considered to be quasi-stationary in both studies.

Later the hydraulic flow model was combined with the solution of the simplified dynamic roll motion of the damaged ship, while the other degrees-of-freedom were considered to be quasi-stationary, *Vredeveldt and Journée (1991)*. This method was also validated with model tests for the cross-flooding in a box-shaped ship. A similar approach was later used in *Xia et al. (1999)*. In both cases, also the compression of air was taken into account and the sea was assumed to be calm. *Xia et al. (1999)* also applied artificial damping in the hydraulic model in order to improve the numerical stability of the method.

Turan and Vassalos (1994) have presented a similar simulation method with a coupled system of sway, heave and roll motions together with instantaneous trim. Also the excitation forces due to irregular seas were taken into account. However, approximated constant flooding rates were used instead of time dependent solutions. This method has been used for a ro-ro vessel with a flooded vehicle deck. An improved version with application of Bernoulli's equation for the volumetric flows was soon presented in *Vassalos and Turan (1994)*. Further simulations for ro-ro vessels with comparisons to experimental data have been presented in *Vassalos et al. (1998b)*.

Santos and Guedes Soares (2000) and *Santos et al. (2002)* have applied a 6 degree-of-freedom (DOF) time-domain simulation tool for the transient flooding of a ro-ro ship in calm water. The large flow obstacles in the flooded compartments were modelled so

that the transient asymmetric flooding could be taken into account, yet all water levels were considered to be horizontal.

Vermeer et al. (1994) have enhanced the method from *Vredeveldt and Journée (1991)* by including the coupling of dynamic roll, sway and yaw motions with the memory effect taken into account, and *Journée et al. (1997)* have further improved it to full 6 DOF approach. They have also presented some validation results, showing that the predicted results are satisfactory when the sloshing effect is minimal. In the cases where sloshing was significant, the calculation method predicted much larger roll angles. In both papers, flooding was considered to take place in calm sea. *Vassalos et al. (1998a)* and *Vassalos (2000)* presented a non-linear coupled 6 DOF method with the memory effect taken into account for the flooding of a damaged ro-ro ship in irregular waves.

Zaraphonitis et al. (1997) presented a 6 DOF method for the motions of a damaged ship in waves with the memory effect in the radiation forces. The mass of the floodwater was assumed to be concentrated at its center of gravity and sloshing was neglected. Further developments and applications have been presented in *Papanikolaou et al. (2000a)*, *Papanikolaou et al. (2000b)*, *Spanos and Papanikolaou (2001)*, *Spanos et al. (2002)* and *Papanikolaou and Spanos (2002)*. This simulation method has also been used for the analysis of the capsizing and sinking of the ro-ro ferry "Express Samina", *Papanikolaou et al. (2003)*.

In the simple approach the surface of the floodwater is considered to remain horizontal, independent of the motions of the ship. *Papanikolaou et al. (2000a)* applied the so called "lump mass" concept to model the free surface. The mass of the flooded water is considered to be concentrated on its center of gravity, moving over a predefined surface domain. The floodwater keeps its surface as a plane, that is movable. Validation of this approach is presented in *Papanikolaou and Spanos (2002)* along with comparisons to calculations with a Reynolds averaged Navier-Stokes equations (RANSE) solver. This simple approach to sloshing has been further developed and validated in *Jasionowski and Vassalos (2001)*.

Chang and Blume (1998) and *Chang (1999)* have presented a simulation method for damaged ro-ro ships, where the heave, pitch, sway and yaw motions are calculated using response amplitude operators, determined with a strip theory, whereas the roll and surge motions of the ship are simulated using non-linear equations of motion. Furthermore, two different methods are used for the motion of the water in the flooded compartments, depending on the height of the water level. Shallow water equations are

used if the water depth is small when compared to the width of the compartment; otherwise the fluid motion is approximated by that of a point mass, concentrated in the center of gravity of the fluid mass. A more detailed description of the method is given in *Valanto (2002)* and *Valanto (2006)*, along with the results of various simulations. This method is obviously mainly intended for ro-ro vessels with a flooded vehicle deck and the modelling of progressive flooding is not discussed.

Recently, also *Lee et al. (2007)* have performed 6 DOF time domain simulations for a damaged passenger ferry in waves. However, the validation with model tests shows that the roll motion is highly over-estimated.

The previously described studies concentrated on the flooding of ferries. Only very recently, flooding simulations have been performed for progressive flooding of large passenger ships. In the study by MARIN, reported in *van't Veer et al. (2002)*, *van't Veer and Serra (2003)* and *IMO SLF46/INF.3 (2003)*, the motions of a damaged large passenger ship were calculated with a 6 DOF nonlinear method using memory functions. The water flows were calculated with the quasi-stationary hydraulic flow model. Some results from the validation of the applied code with a more simple case of a damaged frigate have been presented in *de Kat and Peters (2002)*. The internal layout of the damaged compartments of a passenger ship was modelled in detail and also the collapsing of non-watertight doors due to the pressure of the floodwater was taken into account. Simulations were performed both in calm seas and in various sea states. Water levels inside the ship were considered to be horizontal and all rooms were assumed to be fully vented. The final results of this extensive study are presented in *van't Veer et al. (2004)* and *van't Veer (2004)*. Recently, also *Ikeda et al. (2004)* and *Vassalos et al. (2005)* have simulated the flooding of a large passenger ship and compared the numerical results with experimental data.

In the 1990s the effect of air compression on the flooding process was taken into account in many studies, e.g. *Vredeveldt and Journée (1991)*, *Vermeer et al. (1994)*, *Journée et al. (1997)* and *Xia et al. (1999)*. However, recently only *Palazzi and de Kat (2002)* have studied the flooding of a damaged frigate with airflow taken into account, both experimentally and numerically. They have concluded that the effect of air should be taken into account since it can have significant effects, especially in the transient flooding phase. Also the interviews with ship designers, reported by *Vartiainen (2006)*, indicate that the effect of air during the flooding is considered to be an important issue, especially in the design of cross-flooding arrangements. However, *van't Veer et al. (2004)* point out that the modelling of all air ducts in a passenger ship is very difficult.

Some of the above mentioned simulation methods have been tested in the ITTC (International Towing Tank Conference) benchmark studies on numerical prediction of damage stability, *ITTC (2002)* and *ITTC (2005)*. The studies have mainly concentrated on the modelling of floodwater dynamics and the roll motion of damaged ro-ro vessels. In the second benchmark study, *ITTC (2005)*, a case involving progressive flooding was also tested. In this case, the deviation of the results with different numerical methods was significant. Unfortunately, the measurement data was inadequate for a proper validation analysis.

It is a widely used assumption that the flooding rates can be calculated as quasi-stationary from Bernoulli's equation on the basis of the pressures on both sides of the opening. *van't Veer and de Kat (2000)* have presented validation results for this flooding model for engine room and accommodation compartments. It was further assumed that all water levels were horizontal. In general, the measured and calculated values for heeling moments and water heights seem to have a good correspondence.

In addition to the simplified approaches, also RANSE computations have been used for simulation of flooding. *van't Veer and de Kat (2000)* have studied the applicability of volume of fluid method (VOF) for the simulation of progressive flooding in an engine room. The results were validated with model tests. The correlation between the calculated and measured water heights was good. So the results were very promising but it was concluded that, for the time being, both the modelling (grid generation) and the calculation were much too slow for efficient flooding simulation, even though the applied cell size (0.33 m in all directions) was rather large. Also *Cho et al. (2005)* have used VOF for flooding of an engine room, excluding the motions of the ship. The results are compared to experimental data. The grid contained about a million cells and the computation time was up to 200 hours. *Woodburn et al. (2002)* have used VOF method, coupled with a 6 DOF method, for the motions of the ship for the flooding of a damaged ro-ro vessel.

As an alternative to the grid based methods, like VOF, particle based methods have also been tested. *González et al. (2003)* have used the smoothed particle hydrodynamics (SPH) method for calculation of the dynamic behavior of a damaged ro-ro ship with a flooded vehicle deck and forced sinusoidal roll motion. *Souto-Iglesias et al. (2004)* have applied SPH method for sloshing in rectangular tanks with baffles. In principle, this case corresponds to a progressive flooding through large open rooms. The correspondence between the numerical and experimental results is good. The SPH method seems to be suitable for capturing the free surface when sloshing is significant.

Skaar et al. (2006) have applied the SPH method for progressive flooding of a ro-ro vessel under forced roll and heave motions. The required number of particles is large and the modelling of the solid walls and boundaries of the computational domain in the case of waves is still considered to be problematic, *Skaar et al. (2006)*. Furthermore, both *González et al (2003)* and *Souto-Iglesias et al. (2004)* state that the calculation process is very slow. Therefore, it can be concluded that for the time being, the SPH is not feasible for practical needs, even through it has some benefits. Consequently, at the moment a simplified modelling of the floodwater surfaces is needed if fast computation times are required.

In all the reviewed simplified methods, the flow through the openings was calculated with a simple hydraulic model, i.e. by applying Bernoulli's equation. Basically, the alternative method is RANSE, with a computational grid that is much denser than the structural subdivision of the ship, or the SPH method. At the moment, RANSE solvers are not fast enough for the practical analysis of the flooding process, *Papanikolaou and Spanos (2002)*, but they can be used for estimation of the pressure losses in various structures. *Pittaluga and Giannini (2006)* have used a commercial RANSE solver for the evaluation of the pressure losses in a cross-flooding tunnel. This kind of RANSE solutions for limited studies can provide valuable data for simulations with the more simplified approach of the hydraulic model.

It can be concluded, that several sophisticated methods have been developed over the last decade, but mainly for the simulation of transient flooding of damaged ro-ro vessels with a flooded vehicle deck.

1.3 Scope of the Work

The main emphasis in the time-domain simulation of damaged ships has mainly concentrated on the modelling of the dynamic motions of the ship in a seaway and the ship-floodwater interaction. This work is intended to provide a better and more accurate approach on the modelling of progressive flooding with a large and complex system of potentially flooded compartments in a modern passenger ship.

The pressure-correction technique, which is well-established in the area of computational fluid dynamics (CFD), is applied for the time-accurate simulation of progressive flooding inside a damaged passenger ship. The widely used hydraulic model is used for the calculation of the flow velocities by applying Bernoulli's equation as the momentum equation. This kind of method has previously been applied to pipe systems,

where the tanks are filled up with fluid (*Patankar, 1980* and *Siikonen, 2001*). However, in the case of progressive flooding, there can be free surfaces. Therefore, the existing methods have been appropriately modified. Furthermore, air compression due to flooding is modelled with the assumption of perfect gas, and Bernoulli's equation for compressible fluid is used for the calculation of airflows in the openings and pipes. This computational approach and its application are believed to be original.

The first ideas of this new approach on flooding simulation were published by the author in *Ruponen (2006a)*. In this thesis, the theory is further developed and applied to real ship geometries. Among the new features, the pressure-correction method is further developed for easier handling of openings with high vertical extent. If there is a weir flow instead of flow through an orifice a slightly modified version of the pressure-correction equation is needed.

The research concentrated on the calculation of progressive flooding and internal airflows inside a damaged passenger ship, especially after the short phase of transient flooding. Therefore, some simplifications were done in the calculation of the motions of the damaged ship. All motions of the ship are assumed to be slow, and hence a quasi-stationary approach is considered to be reasonable. However, it is believed that this method for progressive flooding can be enhanced to include the calculation of the dynamic motions of the ship in waves.

The simulation method is extensively validated by comparing simulation results with experimental data from dedicated model tests (*Ruponen, 2006b*). Furthermore, the applicability for realistic ship geometries is tested with a case study, involving a detailed model of a 40 000 GT (gross tonnage) passenger ship. Two flooding cases are calculated. Firstly, a cross-flooding in a U-shaped void with the counter air pressure taken into account, and secondly an extensive progressive flooding in a large and complex system of rooms and openings. The latter case also involves structures that start to leak and eventually collapse under the pressure of the floodwater.

2 Physical Background

2.1 Flooding Mechanisms

2.1.1 General

The flooding of a damaged ship is a complex process that can involve various phenomena, such as collapsing of non-watertight structures and compression of air. In this section some important topics on the physics of the flooding are presented and their importance and modelling possibilities are discussed.

In general, the flooding process that follows the creation of the damage opening can be divided into three main phases (*IMO SLF46/INF.3, 2003*). Right after the creation of the damage, there is a phase of transient flooding as the water rushes in through the damage opening. This is followed by a phase of progressive flooding as the water floods to undamaged compartments through the internal openings. If the ship does not capsize or sink during these phases, a steady final state is eventually achieved. A schematic representation of these phases is shown in Figure 2.1. This thesis is mainly concentrated on the phase of progressive flooding.

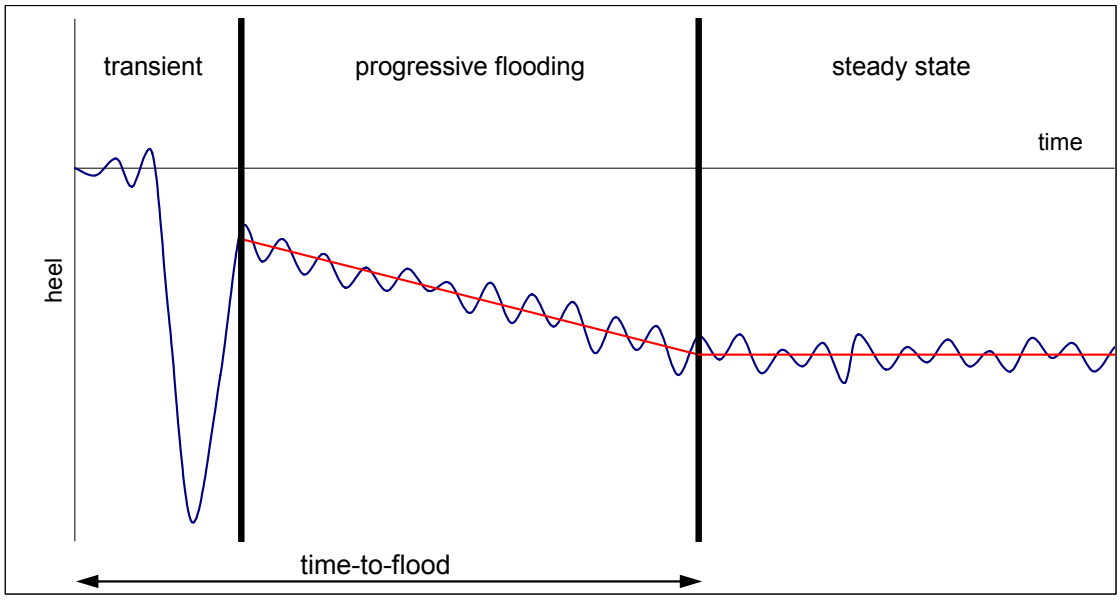

Figure 2.1 Main phases of the flooding process

During the flooding process the ventilation ducts and the strength of the non-watertight subdivision can have significant effects on the intermediate stages and on the extent of the flooding. Therefore, also these mechanisms are discussed in this chapter.

2.1.2 Transient Flooding

During the first phase after the damage, water rushes into the ship through the damage opening. If the opening is large and it is located on the side of the ship, the flooded water causes a large transient heeling moment. As a result, the ship heels rapidly to the damaged side. It is possible that the ship will capsize due to this sudden loading, and therefore, the time-to-capsize can be very short: from only a few seconds to a few minutes.

Several factors, such as the force from the striking vessel, the penetration of the damage and the time, in which the damage is created, can also have a remarkable role. However, these factors are often not known, and thus they are usually ignored in the numerical studies.

In some cases, also the flooding of symmetrical compartments can be a transient phenomenon since the structures inside the flooded compartments can significantly delay the equalization of the floodwater. The term "transient asymmetric flooding of symmetrical compartments" was first introduced by *Spouge (1986)* in his analysis of the capsizing of the ro-ro ferry "European Gateway". The same case was later used in a numerical simulation by *Santos et al. (2002)* for testing a simple modelling technique for compartments with large flow obstacles.

The transient heeling can usually be reduced by allowing cross-flooding to a compartment in the undamaged side of the ship. In the case of a small damage opening or a bottom damage, the transient phase is likely insignificant as the heeling angle will increase slowly.

2.1.3 Progressive Flooding

After the possible phase of transient flooding, the flooding process usually becomes more quasi-stationary. This phase can take from a couple of minutes to several hours, depending on the damage case, internal subdivision and possible counteractions. The main emphasis of this study is on the modelling of this phase.

The water levels in the flooded compartments rise steadily and progressive flooding to other compartments may take place if there are open connections to the flooded compartments. Moreover, the pressure of the floodwater may cause leaking through closed doors or even lead to the collapsing of non-watertight structures. In addition, it is favourable that asymmetric flooding is compensated by allowing flooding through cross-ducts and other passive counter flooding routes in order to decrease the heeling angle. Similarly, down-flooding is sometimes allowed in order to lower the center of gravity, and thus increase the stability of the damaged ship. However, additional free surfaces always have a negative effect on the stability.

The simulations, presented in *van't Veer et al. (2004)*, show that the applied critical pressure head for collapsing of a closed door to a staircase can have a significant effect on the roll motion and time-to-flood. Therefore, it is essential that the simulation method can handle also leaking and collapsing structures. However, there is not much experimental data on the critical pressure heads for typical non-watertight structures. Some values have been presented in *IMO SLF47/INF.6 (2004)* but in general, these are mainly assumptions. The applicability of the proposed values is discussed in detail in *Vartiainen (2006)*. Obviously, dedicated full scale tests on various typical structures would provide valuable information that could be utilized in flooding simulations.

If the ship does not sink or capsize, a steady state is eventually reached. The total elapsed time for the phases of transient and progressive flooding is often referred to as the time-to-flood (TTF), see Figure 2.1. However, it is practical to define further criteria since very large heeling angles can be encountered during the intermediate stages of flooding. *van't Veer et al. (2002)* used a criterion of 15° maximum heel angle, which is reasonable since lowering of the life boats may be difficult with larger heel angles. According to SOLAS, the criterion for this is 20°. If such criteria are applied, TTF is often appropriately referred to as the available time for orderly evacuation and abandonment.

2.1.4 Air compression

The increased air pressure due to compression can have significant effects on the flooding process, especially in the early phases of transient flooding. When a compartment is flooded, the air must escape the inflowing water. If the flooding is fast and the ventilation level of the compartment is reduced, it is possible that the air compression becomes significant, and the compressed air starts to delay the flooding.

When the water level has risen above all openings and pipe inlets, air cannot escape at all and an air pocket is formed. The pressure in the air pocket can still rise as the external hydrostatic pressure increases due to the increasing draft that causes the decrease of the air pocket volume.

In order to take the effects of air into account, it is necessary that air is modelled as a compressible fluid. The biggest problem is that all airflow routes should be modelled. In practice, it is not practical to separately model every ventilation duct. Therefore, some simplifications and assumptions are always needed. In principle, air should always be taken into account when flooding of tanks is simulated since the air pipes are typically rather small when compared to the cross-flooding openings.

2.2 Assumptions

2.2.1 Environment

Accidents that result in flooding can take place in various different sea states, and therefore, environmental factors, such as the sea state and wind must be considered. According to the results of the HARDER (Harmonization of rules and design rationale) project, *Tagg and Tuzcu (2002)*, 90 % of the collision accidents take place in a sea state, where the significant wave height is less than 2.0 m. This statistical fact forms a good basis for a simplified approach on the motions of a damaged ship.

de Kat and van't Veer (2001) have compared model test results for a damaged ferry in calm sea and in irregular waves. In that case, the roll response was very similar in both cases. Furthermore, the roll motions in waves were small when compared to the maximum roll angle due to the transient flooding.

Papanikolaou et al. (2003) have calculated the flooding of the ferry "Express Samina" both in calm water and in a seaway with significant wave height of 2.0 m. The overall time history of the heeling angle is very similar in both cases.

In MARIN's final study on time-to-flood for a large passenger ship, *van't Veer (2004)*, results of simulations in calm sea and in irregular waves with a significant wave height of 2.0 m were compared (Figure 2.2). The case was a large passenger ship with extensive three-compartment damage. Both the heel angle and the volume of flooded water were compared. The results in waves are very comparable to the calm sea results. The wave forces lead to roll variations around the trend, found in calm sea. However, in

higher waves the calm sea approximation can lead to different results. Simulation results in a seaway with a significant wave height of 4.5 m have been presented in *van't Veer and Serra (2003)*. The results indicate that the large motions of the damaged ship lead to very slow progressive flooding through openings above the bulkhead deck. On the other hand, the results start to differ from the calm sea simulations only after a relatively long time.

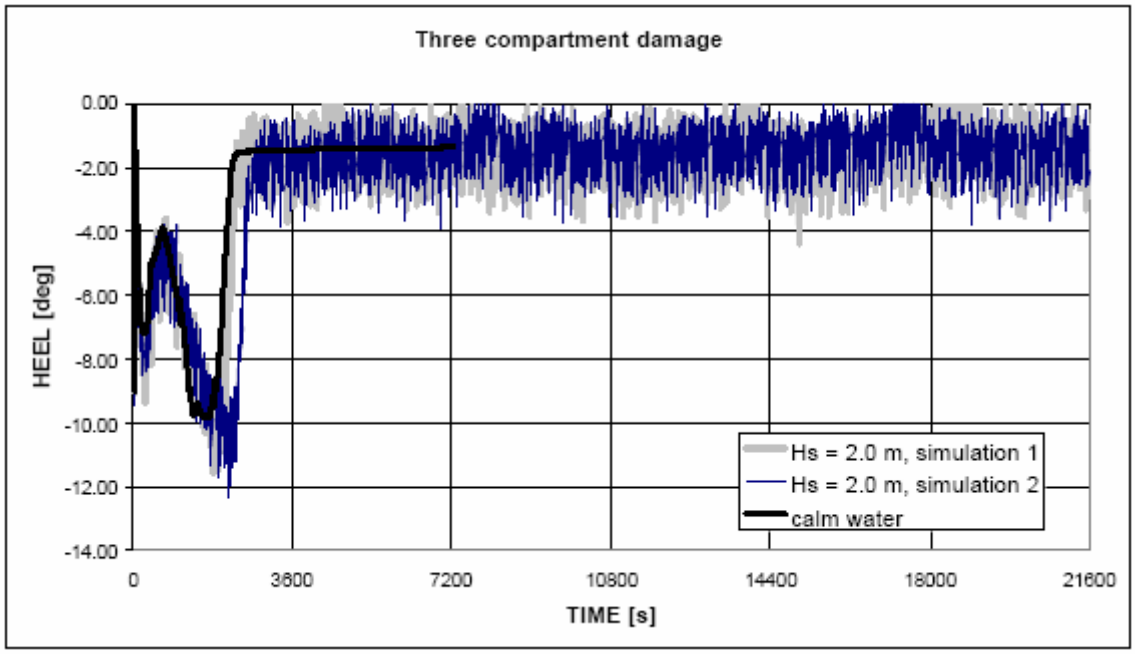

Figure 2.2 Comparison between simulations in calm water and in irregular waves, adopted from MARIN Report No. 19289-1-CPS, *van't Veer (2004)*

On the basis of these results, it is reasonable to assume that the waves do not have a significant effect on the flooding process and motions of a damaged large passenger ship if the significant wave height is less than 2 m. However, it is recognized that in the case of large asymmetric damage, it is possible that the waves and wind may have a more significant effect on the transient heeling in the phase of transient flooding.

This study is mainly concentrated on the development of a new method for the calculation of the progressive flooding in a damaged passenger ship. Thus the non-watertight subdivision of the WT-compartments is rather dense. Therefore, on the basis of the previously described results in literature, it is assumed that the sea is calm. It is

further assumed that the wind speed is low, and hence it has no effect on the ship. It is believed that the effects of the waves and wind can be implemented at a later stage in order to increase the applicability of the method for harsher sea states.

2.2.2 Motions of the Ship

According to *Svensen and Vassalos (1998)*, the analysis of numerous model tests with flooded ro-ro vessels shows that the ship motions will reduce significantly as the amount of water on the deck increases. One reason for this is that the roll damping will increase due to the flooding. Moreover, the restoring moment is increased as the floodwater is considered as added weight. This conclusion on the increase of the roll damping can, at least partly, be extended to other ship types as well.

As discussed in the previous section, it is assumed that the sea is calm. With a further assumption of slow motions, it is possible to apply a quasi-stationary approach to the calculation of the ship motions. In calm water this assumption is generally justified for the trim and heave motions since the time derivatives of these quantities are small. This approach has been successfully used by *Vredeveldt and Journée (1991)* for the simulation of the transient heeling of a box-shaped ship.

As described in section 2.1, fast heeling usually takes place only during the short period of transient flooding, right after the creation of the damage opening. Therefore, the dynamic roll motion is not very significant in the simulations of the progressive flooding phase in calm water. Especially, if the simulation is performed onboard the damaged ship, in which case the initial condition can be obtained from the water level sensors after the phase of transient heeling.

On the basis of these facts, it was decided to adopt a fully quasi-stationary approach to the motions of the ship for the first stage of the development of the simulation method. However, it is recognized that for example in the case of a large asymmetric side damage due to a collision, the transient heeling can be up to two times as large as predicted by the quasi-stationary method, see e.g. *Mustonen (1998)*. The applied equations of motion can be enhanced later in order to increase the applicability of the flooding simulation method. Yet, this simplification forms a good basis for the development of a calculation method for the progressive flooding inside the damaged ship. Furthermore, it should be noted that the collision forces will also affect the transient motions of the ship in the early stages of flooding. According to the model tests, reported in *Tabri et al. (2007)*, the roll motion due to the collision impact can be

significant, depending mainly on the location of the center of gravity and the contact point. In some cases the exclusion of the collision force can also decrease the error that is caused by the assumption of quasi-stationary motions.

2.2.3 Ship-Floodwater Interaction

The floodwater motion can be approximated with the lump mass concept, where the mass of the floodwater is concentrated in its centroid and moving over a predefined surface domain, *Papanikolaou et al. (2000a)*, *Papanikolaou and Spanos (2002)* and *Jasionowski and Vassalos (2001)*.

In the simpler approach the free surfaces are assumed to remain horizontal, independent of the ship motions. Or in other words, the floodwater is in phase with the ship motions. This simplification has been used in most of the previous studies, e.g. *Journée et al. (1997)*, *Santos et al. (2002)*, *Lee et al. (2007)* and in the MARIN study of time-to-flood simulations, *IMO SLF46/INF.3 (2003)* and *van't Veer (2004)*.

The former approach should provide better results if a compartment with a large area, such as a vehicle deck, is flooded and the ship rolls in a seaway. Especially, if the excitation frequency is close to the natural frequency of the fluid motion in the flooded compartment, in which case sloshing of water is likely to happen. The latter approach is considered to be suitable for the cases, where the subdivision of the flooded compartments is dense, as in the case of a passenger ship, since possible sloshing in small rooms will have only a small effect on the motions of the ship. Furthermore, when the sea is considered to be calm, the sloshing is even more likely to be unimportant.

The aim of this study was to develop a fast and efficient simulation method, especially for passenger ships. Therefore, the sloshing of the floodwater is considered to be insignificant, and hence it can be ignored. This means that all water levels are assumed to be flat surfaces, parallel to the sea level. The free surface effect on the stability of the ship is naturally taken into account.

As a result of the above mentioned assumption, also the inertia of the floodwater is neglected and the whole mass of the floodwater is considered to settle down instantaneously. *van't Veer and de Kat (2000)* have compared calculations with this simplified approach to more accurate RANSE computations with the VOF method. The results are very similar, providing justification for applying this simpler approach in the flooding simulations.

2.3 Governing Equations

2.3.1 Conservation of Mass

The conservation of mass, i.e. the equation of continuity, in the integral form is (see e.g. *Paterson, 1997*):

$$\int_{\Omega} \frac{\partial \rho}{\partial t} d\Omega = -\int_{S} \rho \mathbf{U} \cdot \mathbf{n} dS \,, \tag{2.1}$$

where ρ is the density of the fluid, t is time, $\mathbf{U}$ is the velocity vector and S is the surface that bounds the control volume Ω. The normal vector of the surface $\mathbf{n}$ points outwards from the control volume, hence the minus sign on the right hand side of the equation.

2.3.2 Conservation of Momentum

The flooding process is modelled with certain simplifications that were discussed in section 2.2.3. The viscous effects are likely to be relevant only for local phenomena that are excluded by the applied assumptions. Therefore, it is reasonable to consider both water and air as inviscid fluid. The losses in the openings are later taken into account by applying semi-empirical discharge coefficients.

The conservation of momentum for inviscid fluid is governed by Euler's equation:

$$\rho \frac{D\mathbf{U}}{Dt} = \rho \mathbf{F} - \nabla p \,, \tag{2.2}$$

where $\mathbf{U}$ is the velocity vector, $\mathbf{F}$ is the body force and p is the pressure.

It is then further assumed that the flow is stationary (or at least quasi-stationary) and irrotational. Thus, along a streamline from a point A to a point B, this can be presented in the form of Bernoulli's equation (see Appendix A and *Fox and McDonald, 1985*):

$$\int_{A}^{B} \frac{dp}{\rho} + \frac{1}{2}\left(u_B^2 - u_A^2\right) + g\left(h_B - h_A\right) = 0 \,, \tag{2.3}$$

where u is the flow velocity, g is the acceleration due to gravity and h is the height from the reference level.

The considered streamline connects the point A that is in the middle of the compartment and point B that is in the opening. The flow velocity in the center of the compartment is considered to be negligible, i.e. $u_A \approx 0$. In principle, this assumption is valid only for slow flooding of large compartments. However, the previously developed simulation methods (see section 1.2) have worked considerably well with this assumption, and therefore, the same approximation is made also in this study.

The equation (2.3) applies for inviscid flow. However, the pressure losses can be taken into account semi-empirically, by adding a pressure loss term to the equation (2.3). This term is considered to be proportional to the square of the velocity in the opening. Hence the modified version of Bernoulli's equation along a streamline can be written as:

$$\int_A^B \frac{dp}{\rho} + \frac{1}{2}\left(u_B^2 - u_A^2\right) + g\left(h_B - h_A\right) + \frac{1}{2}k_L u_B^2 = 0, \tag{2.4}$$

where k_L is a semi-empirical non-dimensional pressure loss coefficient.

The square of the velocity in the opening can be solved from (2.4), resulting in:

$$u_B^2 = \frac{1}{1+k_L}\left[2g\left(h_A - h_B\right) - 2\int_A^B \frac{dp}{\rho}\right]. \tag{2.5}$$

Hence the flow velocity in the opening is directly proportional to a constant discharge coefficient:

$$C_d = \frac{1}{\sqrt{1+k_L}}. \tag{2.6}$$

A similar approach is used in the *IMO Resolution A.266 (VIII)*, where a flow reduction coefficient is used to represent the losses in the cross-flooding arrangements.

When air pressure is taken as constant, the equation (2.5) for a flow through a small opening with area dA reduces to the usual representation in flooding simulations (e.g. *Vassalos et al., 2000*):

$$dQ = u_B dA = \operatorname{sign}\left(h_B - h_A\right) \cdot C_d \sqrt{2g\left|h_B - h_A\right|} \cdot dA. \tag{2.7}$$

The total volumetric flow through the opening can be obtained by integrating equation (2.7) over the area of the opening.

According to this hydraulic model, water will flow immediately when there is a difference in the pressure heights. In reality, there are delaying effects due to the inertia of the water particles. Apparently, these can be neglected since the previous studies, e.g. *van't Veer and de Kat (2000)*, show that the calculations with this simplification correspond well with the experimental results.

As mentioned above, the losses in the openings and pipes are taken into account with semi-empirical coefficients. Usually, these coefficients are considered to be constant for each opening. However, more accurate results may be obtained if the pressure losses are slightly increased when the water jet discharges to water instead of air.

A general problem in flooding simulation is how to find out the proper discharge coefficients for all openings. This question is not considered in detail in this study but the following is a brief review of the available literature.

Some typical values for various openings and pipes have been presented e.g. in *Blevins (1984)*. However, it should be noted that these are theoretical values and they may not be directly applied to much larger or more complex-shaped openings.

Vassalos et al. (1997) have compared numerical simulations to experimental data and concluded that $C_d = 0.6$ is a good approximation for damage openings. *Katayama and Ikeda (2005)* have studied the effect of the scale on the discharge coefficient for a rectangular sharp-crested opening. They tested two openings with the same shape but different scale. The smaller scale resulted in larger values for the discharge coefficient. Therefore, the application of model tests with a small scale for determining these values for full scale simulations is somewhat questionable. Obviously more studies on the water flow characteristic through typical openings in ships are needed in order to improve the reliability of the flooding simulations.

Pittaluga and Giannini (2006) have presented CFD (computational fluid dynamics) calculations with a commercial RANSE solver for the pressure-losses in cross-flooding tunnels. As a result, they have presented regression equations that can be used for the estimation of the effective discharge coefficient. This kind of RANSE computations for detailed parts of the ship may provide valuable information on the pressure losses in various kinds of openings and cross-flooding arrangements. However, a thorough validation of the applied tools with detailed experimental data should be performed.

2.3.3 Flooded Air Pockets

A complex airflow case may take place when a large air pocket is formed. If the flooding opening is located at least partly in the air pocket. Air is compressed as a result of infloodng water until the pressure in the air pocket is equal to the effective total pressure on the other side of the opening. The principle idea is presented in Figure 2.3, showing the opening k that connects the rooms i and j. Flow through the opening is considered to be impossible when the pressure in the air pocket is:

$$p_i, \geq p_j + \rho_w g\left(H_{w,j} - H_{o,k}\right). \tag{2.8}$$

As a result, it is assumed that the pressure in the air pocket will prevent further flooding. However, in reality the air pressure is not quasi-stationary. Consequently, air will escape from the air pocket in a bubble flow. This phenomenon was observed in the model tests (see section 5.3.2 and *Ruponen, 2006b*). However, due to the very complex nature of the bubble flow, it is difficult to estimate how it will take place in full scale. On the other hand, due to the scaling of air pressures, the relative size of air pockets is smaller in full scale, and therefore, the error due to the simplified approach is also expected to be smaller than in the model scale.

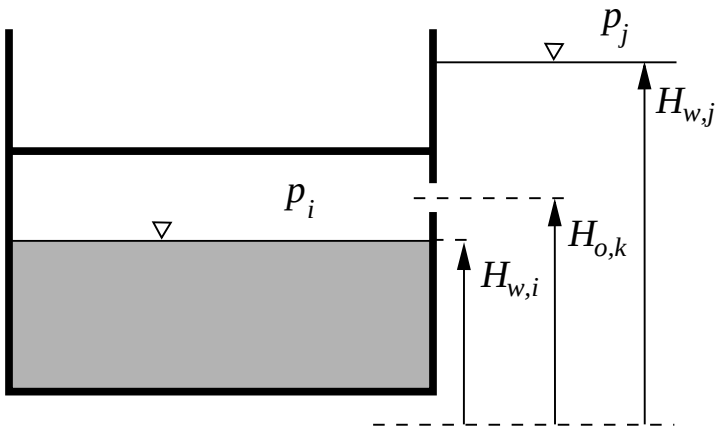

Figure 2.3 Example of a situation, where the pressure in an air pocket (p_i) is considered to prevent further flooding

2.3.4 Equations of Motion

As described in sections 2.2.1 and 2.2.2, it is assumed that the sea is calm and the motions of the damaged ship are slow. Therefore, a quasi-stationary approach is considered to be suitable for calculating the motions of a ship. Consequently, the ship is considered to have only three degrees-of-freedom, namely heel (ϕ), trim (θ) and heave or draft (T). Therefore, the floating position of the damaged ship is governed by the following set of three non-linear equations:

$$\begin{aligned} &M_{heel}(\phi,\theta,T,V_{w,i}) + M_{st,T}(\phi,\theta,T,V_{w,i},m_{ship}) = 0 \\ &M_{trim}(\phi,\theta,T,V_{w,i}) + M_{st,L}(\phi,\theta,T,V_{w,i},m_{ship}) = 0 \\ &\rho_w g \cdot \nabla(\phi,\theta,T,V_{w,i}) - m_{ship} g - \rho_w g \sum_i V_{w,i} = 0, \end{aligned} \tag{2.9}$$

where M_{heel} is the heeling moment and M_{trim} the trimming moment, $V_{w,i}$ is the distribution of floodwater, m_{ship} is the mass of the intact ship, ∇ is the function for the volume of displacement and M_{st} is the static righting moment in transverse (T) or longitudinal (L) direction.

At each time step, the floating position of the ship is evaluated on the basis of the distribution of floodwater inside the flooded compartments, taking into account the initial condition of the ship and the free surfaces of the floodwater and liquid cargo. The standard iterative procedure of the NAPA software is used for this.

3 Numerical Method

3.1 Background

The basic idea of applying the pressure-correction technique for time-domain simulations of progressive flooding was introduced in *Ruponen (2006a)* for ship-like systems of rooms and small openings when the floating position was kept fixed. In this thesis this method is further developed so that it can be applied to a floating ship that has a more complex geometry.

The idea of applying pressure-correction technique for a pipe system was briefly introduced in *Patankar (1980)*. Later, *Siikonen (2001)* has presented this in detail. Both Patankar and Siikonen consider the same case, where a group of tanks, filled with incompressible fluid, are connected by pipes. In the case of flooding in a damaged ship, the situation is more complex since there can be free surfaces in the compartments and also the air pressures and airflows should be taken into account.

Usually flooding simulation methods are based on the volumes of floodwater that are integrated explicitly from the flow velocities that are solved by using Bernoulli's equation. The water height differences for the next time step are then calculated from the volumes of water with the heel and trim angles taken into account. However, in this study, a completely different approach is used and the volumes are calculated on the basis of water heights and the heel and trim angles. This is reasonable since the water height is physically more meaningful than the volume of water since it represents the hydrostatic pressure. Consequently, the progress of the floodwater can be solved implicitly on the basis of the pressures in the rooms and the velocities in the openings.

The principle of a pressure-correction method is that the equation of continuity and the linearized momentum equation are used for the correction of the pressures until the iteration converges and both the continuity and the conservation of momentum are satisfied at the same time.

Throughout the thesis, the estimated values are marked with an asterisk (*) and the corrections with an apostrophe (′). This is a common practice in pressure-correction methods, e.g. *Ferziger and Perić (2002*). Moreover, a dot above a variable is used to represent time derivation. Water is denoted by a lower index w and air with an index a. Compartments are identified by indices i and j and an opening that connects them

by an index k. The flow from i to j is defined to be positive. Time levels are marked with an upper index n.

3.2 Computational Grid

The ship model for flooding simulation can be considered as an unstructured and staggered grid (Figure 3.1). Each modelled room is used as a single computational cell. However, the flux through a cell face is possible only if there is an opening that connects the rooms (cells). As a result, the room arrangement, normally used in the static damage stability calculations, can be used for flooding simulation; only the openings must be defined separately. Furthermore, it may be necessary to include some non-watertight boundaries that are not normally defined in the numerical ship model.

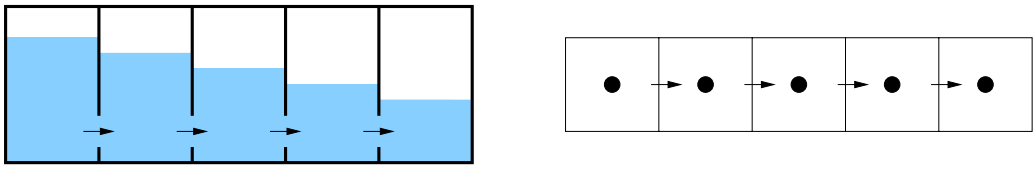

Figure 3.1 The analogy between the ship model for flooding simulation (left) and staggered grid (right)

3.3 Mass Flows

3.3.1 Background

The mass flows through the openings are evaluated by applying the well-established hydraulic model that is based on Bernoulli's equation, as described in section 2.3.2. In the following subsections the equations for mass flow of water ($\dot{m}_{w,k}$) and air ($\dot{m}_{a,k}$) through the opening k are derived from equation (2.4).

At first, let us assume that all openings are so small that they can be considered as single points. Later, in the case of large openings, the mass flow can be calculated simply by integrating the derived equations over the area of the opening. This procedure is described in detail in section 4.4.

Let us consider a streamline from a point A that is inside a flooded compartment to a point B in the opening (Figure 3.2 and Figure 3.3). It is assumed that the flow velocity is negligible far from the opening ($u_A = 0$). Generally, this assumption is valid only for large compartments, subjected to slow flooding. However, the study by *van't Veer and de Kat (2000)* shows good correlation between measurements and calculations with this simple hydraulic model.

The integration of the pressure term in the equation (2.4) depends on whether the fluid is compressible or not. However, also air is often considered to be incompressible when the mass flows are calculated, *Xia et al. (1999)* and *Palazzi and de Kat (2002)*. This approximation is generally justified only if the pressure difference is small. However, it is possible that the air pressure can be relatively large in the flooded compartments, especially if the ventilation ducts are very small when compared to the flooding openings. Therefore, air should be treated as a compressible fluid in order to model the physics as accurately as possible. This will ensure that the error will not increase, even if large pressure differences are encountered.

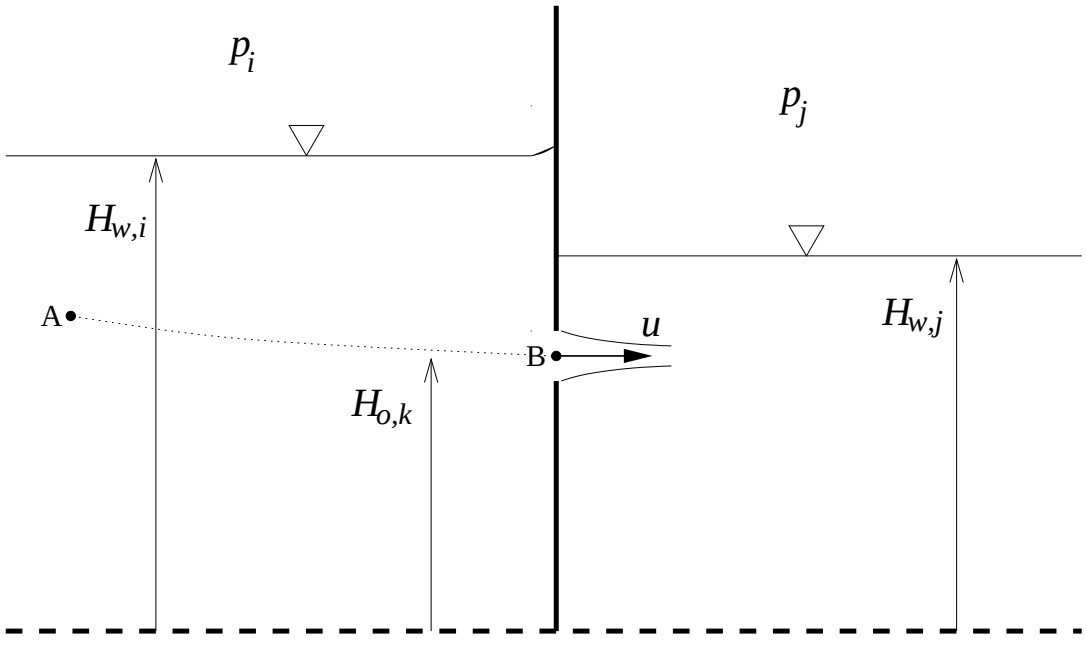

Figure 3.2 Application of Bernoulli's equation for a streamline from the point A to the point B in order to calculate the water flow velocity in the opening

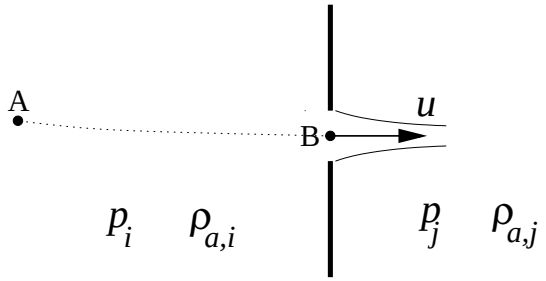

Figure 3.3 Application of Bernoulli's equation for a streamline from the point A to the point B in order to calculate the airflow velocity in the opening

3.3.2 Water Flow

For incompressible fluid, Bernoulli's equation with the pressure losses (2.4) can be written as:

$$p_B - p_A + \rho_w g(h_B - h_A) + \frac{1}{2}\rho_w u_B^2 + \frac{1}{2}\rho_w k_L u_B^2 = 0\,. \tag{3.1}$$

The effective pressure is the sum of air pressure and hydrostatic pressure:

$$P = p + \rho g h\,. \tag{3.2}$$

Consequently, in the case of water flow, the total pressure difference for an opening k that connects the compartments i and j is:

$$\left(P_i - P_j\right)_k = p_i - p_j + \rho_w g \cdot \left[\max\left(H_{w,i} - H_{o,k}, 0\right) - \max\left(H_{w,j} - H_{o,k}, 0\right)\right], \tag{3.3}$$

where H_w is the height of the water level and H_o is the height of the opening, measured from the same horizontal reference level, and p is the air pressure.

Furthermore, the velocity in the opening (point B) can be expressed on the basis of the mass flow:

$$u_B \equiv u_k = \frac{\dot{m}_k}{\rho A_{eff,k}}, \tag{3.4}$$

where A_{eff} is the effective geometrical area of the opening, taking into account the possible structural changes, such as collapsing of a closed door (see section 4.4.3).

As a result, Bernoulli's equation for water flow through the opening k, that connects the compartments i and j (positive flow from i to j), can be written in a form of a pressure loss:

$$\frac{1}{2}\rho_w \dot{m}_{w,k}\left|\dot{m}_{w,k}\right|\frac{1+k_{L,k}}{\rho_w^2 A_{eff,k}^2} = P_i - P_j . \tag{3.5}$$

The absolute value is used to define the direction of the flow. The pressure losses can be taken into account by applying a discharge coefficient. The pressure loss and discharge coefficients are related, as presented in equation (2.6), so that:

$$1 + k_L = \frac{1}{C_d^2} . \tag{3.6}$$

Let us define a dimensional pressure loss coefficient:

$$K' = \frac{1}{\rho \cdot C_d^2 \cdot A_{eff}^2} . \tag{3.7}$$

As a result, equation (3.5) can be written as:

$$\frac{1}{2}K'_{w,k}\dot{m}_{w,k}\left|\dot{m}_{w,k}\right| = P_i - P_j . \tag{3.8}$$

Water flow through the opening is calculated by using this equation.

3.3.3 Airflow

In the case of airflow, the potential energy does not have a significant role, and therefore, the terms involving *h* in the equation (2.4) can be ignored.

Bernoulli's equation for compressible fluid depends on the modelled relation between the density and the pressure. In this study, the flooding process is assumed to be isothermal, so that Boyle's law can be applied and the density of air is linearly dependent on the pressure:

$$\rho_a = \frac{\rho_0}{p_0} p , \tag{3.9}$$

where ρ_0 is the density of air at the atmospheric pressure p_0.

Therefore, equation (2.4) for a streamline from the point A that is located in the middle of the air pocket to the point B in the opening (Figure 3.3) can be written as:

$$\frac{p_0}{\rho_0}\cdot[\ln(p_B)-\ln(p_A)]+\frac{1}{2}u_B^2+\frac{1}{2}k_L u_B^2=0\,. \tag{3.10}$$

The velocity in the opening can be expressed on the basis of the mass flow according to equation (3.4). Therefore, for an opening k that connects rooms i and j (positive flow from i to j), equation (3.10) can be written as:

$$\frac{1}{2}\frac{\dot{m}_{a,k}|\dot{m}_{a,k}|}{\rho_{a,k}^2 A_{eff,k}^2}(1+k_L)=\frac{p_0}{\rho_0}\cdot\ln\left(\frac{p_i}{p_j}\right). \tag{3.11}$$

The pressure losses can be taken into account in a form of a discharge coefficient using equation (3.6). Consequently, equation (3.11) can be expressed as:

$$\frac{1}{2}\dot{m}_{a,k}|\dot{m}_{a,k}|\frac{1}{\rho_{a,k}^2 C_d^2 A_{eff,k}^2}=\frac{p_0}{\rho_0}\cdot\ln\left(\frac{p_i}{p_j}\right). \tag{3.12}$$

Furthermore, by applying the dimensional pressure loss coefficient, as defined in equation (3.7), the following equation is obtained:

$$\frac{1}{2}K'_{a,k}\dot{m}_{a,k}|\dot{m}_{a,k}|=\min(p_i,p_j)\cdot\ln\left(\frac{p_i}{p_j}\right), \tag{3.13}$$

since:

$$\frac{p_0}{\rho_0}\rho_{a,k}=\min(p_i,p_j) \tag{3.14}$$

is the relevant air pressure in the opening (i.e. in the point B on the streamline, see Figure 3.3).

Equation (3.13) is used for the evaluation of airflows since it is possible that there can be large pressure differences between the compartments. Therefore, the airflows can be fast and the compressibility effects can become significant. However, the airflows are approximated by applying Bernoulli's equation for incompressible fluid when the pressure-correction equations are derived. The pressure-correction method is iterative, and therefore, this approximation has proved to be good enough, leading to the

convergence on the solution of compressible airflow. Furthermore, this assumption significantly simplifies the pressure-correction equation.

3.4 Mass Balances

3.4.1 Background

Mass balance equations are used for calculating the residuals of the equations of continuity. The pressures are corrected so that the residuals are eventually zero after the iteration has converged. That is when both the equations of continuity and Bernoulli's equation are satisfied at the same time. There are two equations for the mass balance since water and air are treated separately.

3.4.2 Mass Balance for Water

Water is an incompressible fluid and hence the density is constant. Furthermore, the flow velocity is assumed to be perpendicular to the surface of the openings. Consequently, the dot product of the velocity and the area of the opening is the volumetric flow through the opening. Therefore, the equation of continuity (2.1) for water can be written in a discrete form:

$$\rho_w \frac{dV_{w,i}}{dt} = -\rho_w \sum_k Q_{w,k} \,, \tag{3.15}$$

where ρ_w is the density of water, $V_{w,i}$ is the volume of water in the compartment i and $Q_{w,k}$ is the volumetric water flow through the opening k that is connected to the compartment i. Outflow from the compartment is considered to be positive.

The time derivative of the volume of water can be approximated by:

$$\frac{dV_{w,i}}{dt} \approx S_{fs,i} \frac{dH_{w,i}}{dt} \equiv S_{fs,i} \dot{H}_{w,i} \,, \tag{3.16}$$

where S_{fs} is the area of the free surface in the compartment and H_w is the water height. This equation is based on the assumption that the area S_{fs} remains nearly constant during a single time step. In general, this applies only if all bulkheads are parallel or when the time step is infinitely short. However, this has proved to be a very practical simplification, allowing efficient solution of the governing equations. As a result, the following equation for the mass balance of water can be formed:

$$\Delta \dot{m}_{w,i} = \rho_w S_{fs,i} \dot{H}_{w,i} + \rho_w \sum_k Q_{w,k} \ . \tag{3.17}$$

The permeability μ_i needs to be taken into account when the area of free surface $S_{fs,i}$ is calculated. Consequently:

$$S_{fs,i} = \mu_i S_{geom,i} \, , \tag{3.18}$$

where $S_{geom,i}$ is the geometrical area of the free surface in the room i.

In order to minimize the error due to the assumption of constant area of free surface, a more accurate estimation for the applied area can be used:

$$S_{fs,i} = \frac{1}{2} \cdot \left[S^n_{fs,i} + S^{approx}_{fs,i} \right]. \tag{3.19}$$

Thus the applied area is the average of the free surface in the beginning of the time step (n) and the linear approximation for the new value. The approximation for the new area of surface is based on the volumetric net flow from the previous time step, so that:

$$S^{approx}_{fs,i} = \mu_i \cdot S\left(V^n_{w,i} - \Delta t \cdot \sum_k Q^n_{w,k} \right), \tag{3.20}$$

where Δt is the time step. The effects of this simplification are discussed in section 4.5.

The iteration has converged and the equation of continuity (3.15) is satisfied with a reasonable accuracy when the absolute value of the mass balance is smaller than the applied convergence criterion.

The water height H_w is used to represent the hydrostatic pressure, and therefore, it can change even if the compartment is full of water. However, these changes do not affect the equation of continuity since the volume of water is then constant. Therefore, the time derivative term in the equation (3.17) must be set to zero when the compartment is full of water.

3.4.3 Mass Balance for Air

Air is a compressible fluid, and hence also the density is variable. Therefore, it is practical to use mass flow instead of volumetric flow. Consequently, the equation of continuity (2.1) for air in a discrete form can be written as:

$$\frac{d(\rho_{a,i}V_{a,i})}{dt} = -\sum_k \dot{m}_{a,k} \,, \tag{3.21}$$

where $V_{a,i}$ is the volume of air and $\rho_{a,i}$ is the density of air in the compartment i and $\dot{m}_{a,k}$ is a mass flow of air through an opening k that is connected to the compartment i. Outflow from the compartment is considered to be positive.

The equation (3.21) can be rearranged and expanded into:

$$\frac{d(\rho_a V_a)_i}{dt} + \sum_k \dot{m}_{a,k} = V_{a,i}\frac{d\rho_{a,i}}{dt} + \rho_{a,i}\frac{dV_{a,i}}{dt} + \sum_k \dot{m}_{a,k} = 0 \,. \tag{3.22}$$

The time derivative for the volume of air is:

$$\frac{dV_{a,i}}{dt} = -\frac{dV_{w,i}}{dt} = \sum_k Q_{w,k} \,, \tag{3.23}$$

since the total volume of the compartment is constant ($V_{w,i} + V_{a,i} = V_{net,i}$) and the equation of continuity for water (3.15) defines the time derivative for the volume of water.

It is assumed that the density of air is linearly dependent on the air pressure, equation (3.9). Therefore, the time derivative of the density of air can be linearized as follows:

$$\frac{d\rho_a}{dt} \approx \frac{\partial \rho_a}{\partial p}\dot{p} = \frac{\rho_0}{p_0}\dot{p} \,. \tag{3.24}$$

When the equations (3.9), (3.23) and (3.24) are substituted into the equation (3.22), the following equation for the mass balance of air is obtained:

$$\Delta\dot{m}_{a,i} = V_{a,i}\frac{\rho_0}{p_0}\dot{p}_i + \frac{\rho_0}{p_0}p_i\sum_k Q_{w,k} + \sum_k \dot{m}_{a,k} \,. \tag{3.25}$$

The iteration has converged and the equation of continuity for air (3.21) is satisfied with a reasonable accuracy when the absolute value of the mass balance is smaller than the applied convergence criterion.

3.5 Computation of the Time Derivatives

Generally, the three-level second order implicit time discretization method (see e.g. *Ferziger and Perić, 2002*) is applied in order to ensure time accurate results. Consequently, the time derivative of the water height H_w is:

$$\frac{dH_w^{n+1}}{dt} \equiv \dot{H}_w^{n+1} \approx \frac{3H_w^{n+1} - 4H_w^n + H_w^{n-1}}{2\Delta t}, \tag{3.26}$$

where Δt is the time step and the upper indices mark the time discretization. The time derivative of the air pressure ($\dot{p}^{n+1}$) is evaluated by using the same method.

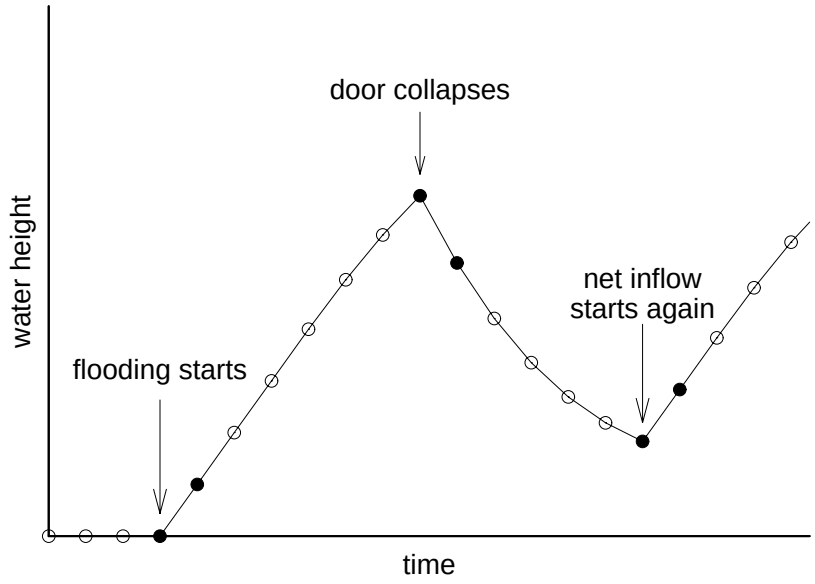

Figure 3.4 Examples of cases, where implicit Euler is used for the calculation of the time derivatives (black dots)

The first order implicit Euler method:

$$\frac{dH_w^{n+1}}{dt} \equiv \dot{H}_w^{n+1} \approx \frac{H_w^{n+1} - H_w^n}{\Delta t} \tag{3.27}$$

has to be used in the time step that follows a discontinuity in the time derivative. Such a situation can occur for example when an empty compartment is flooded or a down-flooding hatch is opened by the pressure of the floodwater. Figure 3.4 shows three examples of the cases, where the implicit Euler method has to be applied.

3.6 Pressure-Correction Equations

3.6.1 Background

The pressures are corrected on the basis of the continuity equations until both the momentum equations (Bernoulli) and the continuity equations are satisfied at the same time. The pressure-correction equations are formed by the mass balances and the linearization of the momentum equations. The solution of the equations gives the pressure corrections H'_w and p'. Consequently, the updated pressures for the next iteration round are:

$$\begin{aligned} H_{w,i} &= H^*_{w,i} + \alpha \cdot H'_{w,i} \\ p_i &= p^*_i + \alpha \cdot p'_i \quad . \end{aligned} \tag{3.28}$$

Some under-relaxation is needed in order to ensure convergence, and hence the solved corrections are multiplied by the under-relaxation factor α. Typically values between 0.5 and 0.8 are sufficient. It has been found out that slightly more under-relaxation is useful if also the air pressures are solved, especially if the volumes of the air pockets or the time derivatives of the pressures are very small.

3.6.2 Water Height Corrections

The density of water is constant, and therefore, the linearization of Bernoulli's equation, see Appendix B, results in:

$$K'_{w,k} \left| \dot{m}^*_{w,k} \right| \dot{m}'_{w,k} = P'_i - P'_j \, , \tag{3.29}$$

where the notations that were described in sections 3.1 and 3.3.2 are used.

The mass flows that satisfy the equations of continuity can be expressed as a sum of mass flow according to the pressures from the previous iteration round and the correction to the mass flow, so that:

$$\dot{m}^{n+1}_{w,k} = \dot{m}^*_{w,k} + \dot{m}'_{w,k} \, . \tag{3.30}$$

Furthermore, volumetric flow can be used for water since the density is constant:

$$\rho_w Q^{n+1}_{w,k} = \rho_w \left(Q^*_{w,k} + Q'_{w,k} \right). \tag{3.31}$$

Similarly, the corresponding water height can be expressed as:

$$H_{w,i}^{n+1} = H_{w,i}^{*} + H'_{w,i} \,. \tag{3.32}$$

Equation (3.32) is substituted into the equation for the time derivative of water height (3.26). The resulting equation and the volumetric flow, equation (3.31), are then substituted into the mass balance equation (3.17), resulting in:

$$\rho_w S_{fs,i} \dot{H}_{w,i}^{*} + \rho_w S_{fs,i} \frac{3}{2} \frac{H'_{w,i}}{\Delta t} + \rho_w \sum_k Q_{w,k}^{*} + \rho_w \sum_k Q'_{w,k} = 0 \,. \tag{3.33}$$

If the implicit Euler method (3.27) is used for computation of the time derivative, the coefficient 3/2 is replaced by a unity.

Moreover, the volumetric flow, equation (3.31), is substituted into the linearized Bernoulli's equation (3.29), resulting in:

$$\rho_w^2 K'_{w,k} \left| Q_{w,k}^{*} \right| Q'_{w,k} = \left(P'_i - P'_j \right)_{eff,k} \,. \tag{3.34}$$

Consequently, the sum of the mass flow corrections is:

$$\rho_w \sum_k Q'_{w,k} = \sum_k \frac{\left(P'_i - P'_j \right)_{eff,k}}{K'_{w,k} \rho_w \left| Q_{w,k}^{*} \right|} \,. \tag{3.35}$$

The total pressure correction P' is the sum of the corrections to the air pressure p' and to the hydrostatic pressure, i.e. the water height correction H'_w. On the basis of equation (3.3), the latter is included only if the water reaches the opening ($H_{w,i} > H_{o,k}$), and therefore:

$$P'_i = p'_i + \rho_w g \cdot \max\left[\operatorname{sign}\left(H_{w,i} - H_{o,k} \right), 0 \right] \cdot H'_{w,i} \,. \tag{3.36}$$

The equations (3.35) and (3.36) are then substituted into the equation (3.33), resulting in the following pressure-correction equation:

$$\sum_k \frac{p'_i - p'_j + \rho_w g \cdot \left[\max\left(\operatorname{sign}\left(H_{w,i} - H_{o,k} \right), 0 \right) \cdot H'_{w,i} - \max\left(\operatorname{sign}\left(H_{w,j} - H_{o,k} \right), 0 \right) \cdot H'_{w,j} \right]}{K'_{w,k} \rho_w \left| Q_{w,k}^{*} \right|}$$

$$+ \underline{\underline{\frac{3}{2} \frac{\rho_w S_{fs,i}}{\Delta t} H'_{w,i}}} = -\rho_w \sum_k Q_{w,k}^{*} - \underline{\underline{\rho_w S_{fs,i} \dot{H}_{w,i}^{*}}} = -\Delta \dot{m}_{w,i}^{*} \,. \tag{3.37}$$

The right hand side is equal to the mass balance, equation (3.17), but the sign is the opposite. Water height is used to represent hydrostatic pressure, and therefore, the underlined terms are set to zero if the compartment is full of water since the time derivative of the real physical water height is then zero.

In practice, it is more appropriate to solve corrections of hydrostatic pressure, instead of water height corrections, so that:

$$\rho_w g \cdot H'_{w,i} = \left(\rho_w g H_w\right)_i', \tag{3.38}$$

especially if compression of air is taken into account and air pressure corrections are solved simultaneously. As a result, both corrections are of the same magnitude, which is favourable for the numerical solution of the pressure-correction equations.

3.6.3 Air Pressure Corrections

The new air pressure is the sum of the initial guess value and the correction:

$$p_i^{n+1} = p_i^* + p_i' . \tag{3.39}$$

Similarly, the volume of air in the compartment can be expressed as:

$$V_{a,i}^{n+1} = V_{a,i}^* + V_{a,i}' . \tag{3.40}$$

The pressure-correction method is more complicated for compressible flows since the density is variable. Therefore, the corrected mass flow of air through the opening k can be expressed as:

$$\begin{aligned} \dot{m}_{a,k}^{n+1} &= \dot{m}_{a,k}^* + \dot{m}_{a,k}' \\ &= \left(\rho_{a,k}^* + \rho_{a,k}'\right) \cdot \left(Q_{a,k}^* + Q_{a,k}'\right) \\ &= \rho_{a,k}^* Q_{a,k}^* + \rho_{a,k}^* Q_{a,k}' + Q_{a,k}^* \rho_{a,k}' + \underline{\underline{\rho_{a,k}' Q_{a,k}'}} . \end{aligned} \tag{3.41}$$

The term $\rho_{a,k}^* Q_{a,k}^*$ is the uncorrected mass flow $\dot{m}_{a,k}^*$ and the underlined term is usually neglected since it is of the second order, and therefore, smaller than the other terms, *Ferziger and Perić (2002)*.

Since the density is assumed to depend linearly on the pressure, equation (3.9), the mass flow correction in (3.41) can be expressed as:

$$\dot{m}'_{a,k} = \rho^*_{a,k} Q'_{a,k} + Q^*_{a,k} \rho'_{a,k} = \frac{\rho_0}{p_0} p^*_k Q'_{a,k} + \frac{\rho_0}{p_0} Q^*_{a,k} p'_k \,. \tag{3.42}$$

Bernoulli's equation for incompressible fluid (3.8) is used as an approximation of the version for incompressible flow, equation (3.13). The linearization (see Appendix B) results in the following equation:

$$K'_{a,k} \left(\frac{\rho_0}{p_0} \right)^2 \left[\left(p^*_k \right)^2 \left| Q^*_{a,k} \right| Q'_{a,k} + \left| Q^*_{a,k} \right| Q^*_{a,k} p^*_k p'_k \right] = p'_i - p'_j \,. \tag{3.43}$$

Therefore, the following equation for the correction of the volumetric airflow is obtained:

$$Q'_{a,k} = \frac{p'_i - p'_j - K'_{a,k} \left(\frac{\rho_0}{p_0} \right)^2 \left| Q^*_{a,k} \right| Q^*_{a,k} p^*_k p'_k}{K'_{a,k} \left(\frac{\rho_0}{p_0} \right)^2 \left| Q^*_{a,k} \right| \left(p^*_k \right)^2} \,. \tag{3.44}$$

Equation (3.39) is substituted into the equation for the time derivative of air pressure. The resulting equation and the corrected mass flow (3.41) are then substituted into the mass balance of air, equation (3.25). Consequently, the following equation for the sum of the mass flow corrections is obtained:

$$\sum_k \dot{m}'_{a,k} = -\frac{\rho_0}{p_0} \left[\left(V^*_{a,i} + V'_{a,i} \right) \cdot \left(\dot{p}^*_i + \frac{3}{2} \frac{p'_i}{\Delta t} \right) + \left(p^*_i + p'_i \right) \cdot \sum_k \left(Q^*_{w,k} + Q'_{w,k} \right) \right] - \sum_k \dot{m}^*_{a,k} \,. \tag{3.45}$$

Again, the second order terms are considered to be small, and therefore, they can be ignored. Consequently, equation (3.45) reduces to:

$$\sum_k \dot{m}'_{a,k} = -\frac{\rho_0}{p_0} \left[\dot{p}^*_i V^*_{a,i} + \dot{p}^*_i V'_{a,i} + V^*_{a,i} \frac{3}{2} \frac{p'_i}{\Delta t} + p^*_i \sum_k Q^*_{w,k} + p'_i \sum_k Q^*_{w,k} + p^*_i \sum_k Q'_{w,k} \right] - \sum_k \dot{m}^*_{a,k} \,. \tag{3.46}$$

If implicit Euler method (3.24) is used for computation of the time derivative, the coefficient 3/2 is replaced by a unity.

The sum of the mass flow corrections can also be acquired by applying the equation (3.42) for all openings k that are connected to the room i:

$$\sum_k \dot{m}'_{a,k} = \frac{\rho_0}{p_0} \sum_k \left[p^*_k Q'_{a,k} + Q^*_{a,k} p'_k \right]. \tag{3.47}$$

The equation (3.44) is then substituted into the equation (3.47), resulting in:

$$\sum_k \dot{m}'_{a,k} = \frac{\rho_0}{p_0} \sum_k \left[\frac{p'_i - p'_j}{K'_{a,k} \left(\frac{\rho_0}{p_0} \right)^2 \left| Q^*_{a,k} \right| p^*_k} - \frac{K'_{a,k} \left(\frac{\rho_0}{p_0} \right)^2 \left| Q^*_{a,k} \right| Q^*_{a,k} p^*_k p'_k}{K'_{a,k} \left(\frac{\rho_0}{p_0} \right)^2 \left| Q^*_{a,k} \right| p^*_k} + Q^*_{a,k} p'_k \right]. \tag{3.48}$$

The last two terms compensate each other. Furthermore, the following relation, based on Boyle's law (3.9), is utilized in order to simplify the equation:

$$\frac{\rho_0}{p_0} p^*_k Q^*_{a,k} = \rho^*_{a,k} Q^*_{a,k} = \dot{m}^*_{a,k}. \tag{3.49}$$

As a result, equation (3.48) can be expressed as:

$$\sum_k \dot{m}'_{a,k} = \frac{\rho_0}{p_0} \sum_k \frac{p'_i - p'_j}{K'_{a,k} \left(\frac{\rho_0}{p_0} \right) \left| \dot{m}^*_{a,k} \right|} = \sum_k \frac{p'_i - p'_j}{K'_{a,k} \left| \dot{m}^*_{a,k} \right|}. \tag{3.50}$$

The correction of the volume of air in (3.46) is related to the water height correction due to the assumption of constant area of free surface, equation (3.16). Consequently:

$$V'_{a,i} = -S_{fs,i} H'_{w,i}. \tag{3.51}$$

The corrections to the volumetric water flows are already defined in equation (3.35). Now the equations (3.46) and (3.50) can be combined, taking into account equations (3.35) and (3.51); and the pressure-correction equation for air pressure is obtained:

$$
\begin{aligned}
&\frac{\rho_0}{p_0}\cdot\left(\frac{3}{2}\frac{V^*_{a,i}}{\Delta t}+\sum_k Q^*_{w,k}\right)\cdot p'_i \\
&+\sum_k \frac{p'_i-p'_j}{K'_{a,k}\left|\dot m^*_{a,k}\right|}-\frac{\rho_0}{p_0}S_{fs,i}\dot p^*_i\cdot H'_{w,i} \\
&+\frac{\rho_0}{p_0}p^*_i\cdot\sum_k\frac{p'_i-p'_j}{K'_{w,k}\rho_w^2\left|Q^*_{w,k}\right|} \\
&+\frac{\rho_0}{p_0}p^*_i\cdot\sum_k\frac{\rho_w g\left[\max\left(\operatorname{sign}\left(H_{w,i}-H_{o,k}\right),0\right)\cdot H'_{w,i}-\max\left(\operatorname{sign}\left(H_{w,j}-H_{o,k}\right),0\right)\cdot H'_{w,j}\right]}{K'_{w,k}\rho_w^2\left|Q^*_{w,k}\right|} \\
&=-\frac{\rho_0}{p_0}\left[V^*_{a,i}\dot p^*_i+p^*\sum_k Q^*_{w,k}\right]-\sum_k \dot m^*_{a,k}=-\Delta\dot m^*_{a,i}\,.
\end{aligned}
\tag{3.52}
$$

The right hand side of the equation is equal to the mass balance for air (3.25), but the sign is the opposite.

If the room is full of water, the effective pressure in the room consists of hydrostatic pressure only. However, for numerical reasons, it is convenient to use a constant "artificial air pressure" also for the rooms that are filled up with water. It has proved to be practical to avoid discontinuities in the pressures, and therefore, the following pressure correction is used for the fully flooded rooms:

$$p'_i=0\,. \tag{3.53}$$

3.7 Simplification of the Pressure-Correction Equation

The air pressure correction equation (3.52) can be simplified by ignoring some minor terms. The background for this simplification is the fact that water flow depends on both the air pressures and the hydrostatic pressures while airflow depends only on the air pressures. In general, the coupling term through the change of air volume:

$$\frac{\rho_0}{p_0\rho_w g}S_{fs,i}\dot p^*_i\cdot\rho_w g H'_{w,i} \tag{3.54}$$

is significant only if the time derivative of the air pressure is large or if the free surface area is very large. Usually, the iteration process provides the correct result even if this term is excluded.

Furthermore, the terms, involving the water flow $Q^*_{w,k}$ are practically always smaller than the terms with the airflow $\dot{m}^*_{a,k}$ since they are proportional to the inverse square of the density of water. However, the exclusion of the terms:

$$\frac{\rho_0}{p_0} p_i^* \sum_k \frac{\rho_w g\left[\max\left(\operatorname{sign}\left(H_{w,i} - H_{o,k}\right),0\right)\cdot H'_{w,i} - \max\left(\operatorname{sign}\left(H_{w,j} - H_{o,k}\right),0\right)\cdot H'_{w,j}\right]}{K'_{w,k}\rho_w^2\left|Q^*_{w,k}\right|} \tag{3.55}$$

can cause convergence problems if the area of the opening for airflow is much smaller than the opening for water flow, especially if the air pressure is large and the volumetric water flow is small.

As a result of this simplification, the air pressure corrections and water height corrections can be solved separately. Similar approach was used in the first version of the method (*Ruponen, 2006a*). Consequently, equation (3.45) can be expressed as:

$$\sum_k \dot{m}'_{a,k} = -\frac{\rho_0}{p_0}\left[V^*_{a,i}\left(\dot{p}^*_i + \frac{3}{2}\frac{p'_i}{\Delta t}\right) + \left(p^*_i + p'_i\right)\cdot\sum_k Q^*_{w,k}\right] - \sum_k \dot{m}^*_{a,k} \,. \tag{3.56}$$

This results in a simplified pressure-correction equation:

$$\begin{aligned}\frac{\rho_0}{p_0}\left[\frac{3}{2}\frac{V^*_{a,i}}{\Delta t} + \sum_k Q^*_{w,k}\right]\cdot p'_i + \sum_k \frac{p'_i - p'_j}{K'_{a,k}\left|\dot{m}^*_{a,k}\right|} &= -\frac{\rho_0}{p_0}\left[V^*_{a,i}\dot{p}^*_i + p^*\sum_k Q^*_{w,k}\right] - \sum_k \dot{m}^*_{a,k} \\ &= -\Delta\dot{m}^*_{a,i} \,,\end{aligned} \tag{3.57}$$

which is independent of the water height corrections. Hence the water height and air pressure corrections are only partially coupled. In many cases, this is favourable since the solution of the pressure corrections is then much faster because a system of size $N \times N$ is solved twice during each iteration round instead of one solution of a $2N \times 2N$ system in the fully coupled version, equations (3.37) and (3.52). If the number of flooded rooms is large, this simplification may significantly reduce the computation time.

In most cases, the simplified version can be used since properly applied under-relaxation will ensure the convergence. In fact, increased diagonal terms act just like additional under-relaxation. It has also proven to be practical to apply a small amount of under-relaxation by dividing the diagonal terms with a constant factor (e.g. 0.95).

3.8 Boundary Conditions

The sea and the atmosphere, surrounding the damaged ship, is considered as one single large ghost cell that is used to set the boundary condition for the calculation of progressive flooding inside the ship. The principle is illustrated in Figure 3.5. The boundary condition depends on the floating position, and consequently, the sea level height from the reference level is:

$$H_{w,sea} = f(\phi, \theta, T). \tag{3.58}$$

Therefore, it has to be re-evaluated separately at the beginning of each time step. The air pressure in the ghost cell is the atmospheric pressure:

$$p_{sea} = p_0. \tag{3.59}$$

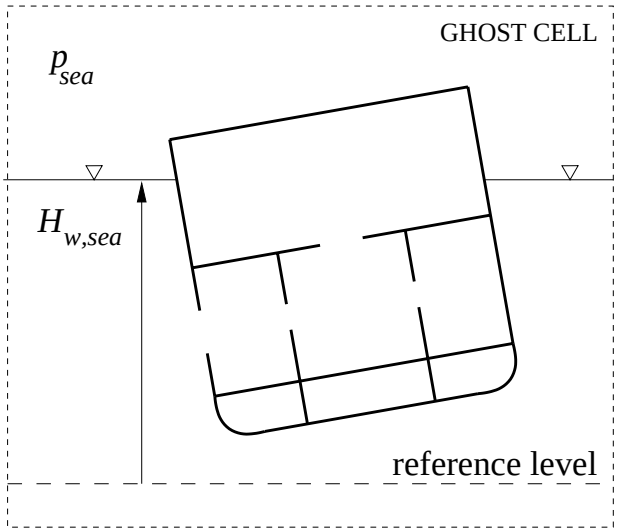

Figure 3.5 Definition of the boundary condition with a ghost cell

It is also practical that some rooms can be modelled as fully ventilated, in which case the air pressure is set to be equal to the atmospheric pressure. These rooms can be considered as additional boundary conditions. In practice, this is handled by setting the correction of air pressure as:

$$p_i' = 0. \tag{3.60}$$

The same approach is used for rooms that are full of water since in that case only the total pressure is used for the calculation of the water flows. It is favourable that the air

pressure is a continuous function of time, and hence, the air pressure is not taken as zero for a filled room.

3.9 Solving the Pressure-Correction Equations

The pressure-correction equations (3.37) and (3.52) form a linear system of equations that can be presented in a matrix form. Thus, for a ship with n potentially flooded rooms:

$$\left[\begin{array}{cccc:cccc} A_{P,1,1} & A_{P,1,2} & \cdots & A_{P,1,n} & A_{PH,1,1} & A_{PH,1,2} & \cdots & A_{PH,1,n} \\ A_{P,2,1} & A_{P,2,2} & \cdots & A_{P,2,n} & A_{PH,2,1} & A_{PH,2,2} & \cdots & A_{PH,2,n} \\ \vdots & \vdots & \ddots & \vdots & \vdots & \vdots & \ddots & \vdots \\ A_{P,n,1} & A_{P,n,2} & \cdots & A_{P,n,n} & A_{PH,n,1} & A_{PH,n,2} & \cdots & A_{PH,n,n} \\ \hdashline A_{HP,1,1} & A_{HP,1,2} & \cdots & A_{HP,1,n} & A_{H,1,1} & A_{H,1,2} & \cdots & A_{H,1,n} \\ A_{HP,2,1} & A_{HP,2,2} & \cdots & A_{HP,2,n} & A_{H,2,1} & A_{H,2,2} & \cdots & A_{H,2,n} \\ \vdots & \vdots & \ddots & \vdots & \vdots & \vdots & \ddots & \vdots \\ A_{HP,n,1} & A_{HP,n,2} & \cdots & A_{HP,n,n} & A_{H,n,1} & A_{H,n,2} & \cdots & A_{H,n,n} \end{array}\right] \cdot \left\{\begin{array}{c} p'_1 \\ p'_2 \\ \vdots \\ p'_n \\ \hdashline \rho_w g H'_{w,1} \\ \rho_w g H'_{w,2} \\ \vdots \\ \rho_w g H'_{w,n} \end{array}\right\} = -\left\{\begin{array}{c} \Delta\dot{m}^*_{a,1} \\ \Delta\dot{m}^*_{a,2} \\ \vdots \\ \Delta\dot{m}^*_{a,n} \\ \hdashline \Delta\dot{m}^*_{w,1} \\ \Delta\dot{m}^*_{w,2} \\ \vdots \\ \Delta\dot{m}^*_{w,n} \end{array}\right\} \quad (3.61)$$

The coefficient matrix consists of four separate sub-matrices $\mathbf{A_P}$, $\mathbf{A_{PH}}$, $\mathbf{A_{HP}}$ and $\mathbf{A_H}$. Consequently, equation (3.61) can be written as:

$$\begin{aligned} \mathbf{A_P} \cdot \mathbf{p'} + \mathbf{A_{PH}} \cdot \rho_w g \mathbf{H'_w} &= -\Delta\dot{\mathbf{m}}^*_{\mathbf{a}} \\ \mathbf{A_{HP}} \cdot \mathbf{p'} + \mathbf{A_H} \cdot \rho_w g \mathbf{H'_w} &= -\Delta\dot{\mathbf{m}}^*_{\mathbf{w}}. \end{aligned} \quad (3.62)$$

Due to the simplification, presented in section 3.7, the sub-matrix $\mathbf{A_{PH}} = \mathbf{0}$, resulting in two linear systems that can be solved consecutively:

$$\begin{aligned} \mathbf{A_P} \cdot \mathbf{p'} &= -\Delta\dot{\mathbf{m}}^*_{\mathbf{a}} \\ \mathbf{A_H} \cdot \rho_w g \mathbf{H'_w} &= -\Delta\dot{\mathbf{m}}^*_{\mathbf{w}} - \mathbf{A_{HP}} \cdot \mathbf{p'}. \end{aligned} \quad (3.63)$$

Most of the off-diagonal elements in each sub-matrix are equal to zero. Hence the matrix is rather sparse. Moreover, due to the equation (3.3), the coefficient matrices can be non-symmetrical also in the case of the simplified version. Therefore, numerical methods for symmetrical matrices cannot be used. In general, iterative methods are considered to be more efficient than direct solution methods since there is no need to find a very accurate solution of the pressure-correction equation. However, the solution should be close enough in order to ensure convergence and to avoid extra pressure-correction iterations. The CGSTAB (conjugate gradient stabilized) method, *van der*

Vorst (1992), has been successfully used in the simulations that are presented in this thesis in chapters 5 and 6.

In the simulations with the fully coupled pressure-corrections, the singular value decomposition (SVD) method has been used due to the more complex form of the coefficient matrix. The major benefit of the simplified pressure-corrections is that the coefficient matrix is concentrated on the diagonal. Consequently, the preconditioning is very easy. However, when the air pressure and water height corrections are fully coupled, the matrix also contains very large off-diagonal terms. In this study, this problem was solved by applying an efficient direct solution method instead of using more complex preconditioning of the matrix with the iterative solution method.

3.10 Convergence Criteria

The pressure-correction iteration is continued until both the mass and momentum conservations are satisfied with a sufficient accuracy. That is when the mass balances, equations (3.17) and (3.25), are practically zero. Therefore, it is reasonable to set suitable criteria for the maximum allowed errors in these equations.

In many CFD applications the L_2-norm is used, and the convergence criterion is of the form:

$$\left\| \Delta \dot{\mathbf{m}}_{\mathbf{w}}^{*} \right\| = \sqrt{\sum_{i} \left| \Delta \dot{m}_{w,i}^{*} \right|^2} \leq criterion \, . \tag{3.64}$$

However, in the flooding simulations it is essential that the iteration has fully converged in all flooded rooms. Therefore, the L_∞-norm is considered to be a more suitable one, and the convergence criterion is of the form:

$$\left\| \Delta \dot{\mathbf{m}}_{\mathbf{w}}^{*} \right\|_{\infty} = \max\left(\left| \Delta \dot{m}_{w,i}^{*} \right| \right) \leq criterion \, . \tag{3.65}$$

Furthermore, the applied criterion should depend on the size of the room since the same flow rate can have different effects on rooms with different sizes.

The following criteria have been used in the simulations that are presented in chapters 5 and 6:

$$\max\left(\frac{\left| \Delta \dot{m}_{w,i}^{*} \right| \cdot \Delta t}{\rho_w S_{fs,i}} \right) \leq \delta H \tag{3.66}$$

and

$$\max\left(\frac{\left|\Delta \dot{m}_{a,i}^{*}\right| \cdot p_0 \cdot \Delta t}{\rho_0 \cdot V_{net,i}}\right) \leq \delta p = \rho_w g \cdot \delta H \,, \tag{3.67}$$

where δH is the maximum negligible water height change and δp is the maximum negligible air pressure change, i.e. the applied convergence criteria. The criteria depend also on the applied time step. In practice this means that smaller residuals are required when a shorter time step is used.

4 Implementation

4.1 Background

The theoretical background for the flooding simulation method was presented in the previous chapter. In the following, a short description of the implementation is given.

Furthermore, various approaches for the opening definition are described in section 4.4, including the required modifications to the pressure-correction equations in the case of openings with high vertical extend.

4.2 Structure of the Simulation Routine

The developed flooding simulation method has been implemented into the NAPA software. The basic structure of the routine is presented in Figure 4.1. The computational grid contains the ship model with all potentially flooded rooms and openings, including the parameters, such as discharge coefficients and permeabilities. The standard NAPA ship model can be used, but usually a more dense subdivision of the compartments is needed.

As an input, the loading condition before the damage is given along with the following parameters of the simulation:

- time step
- convergence criteria
- under-relaxation factor (initial value).

The sea is assumed to be calm, and therefore, the simulation can be stopped if a final equilibrium state is reached. That is when the pressures from the previous time step give a converged solution without any iteration. In practice, this means that a stricter convergence criterion is needed if the progressive flooding is very slow or if a very short time step is used.

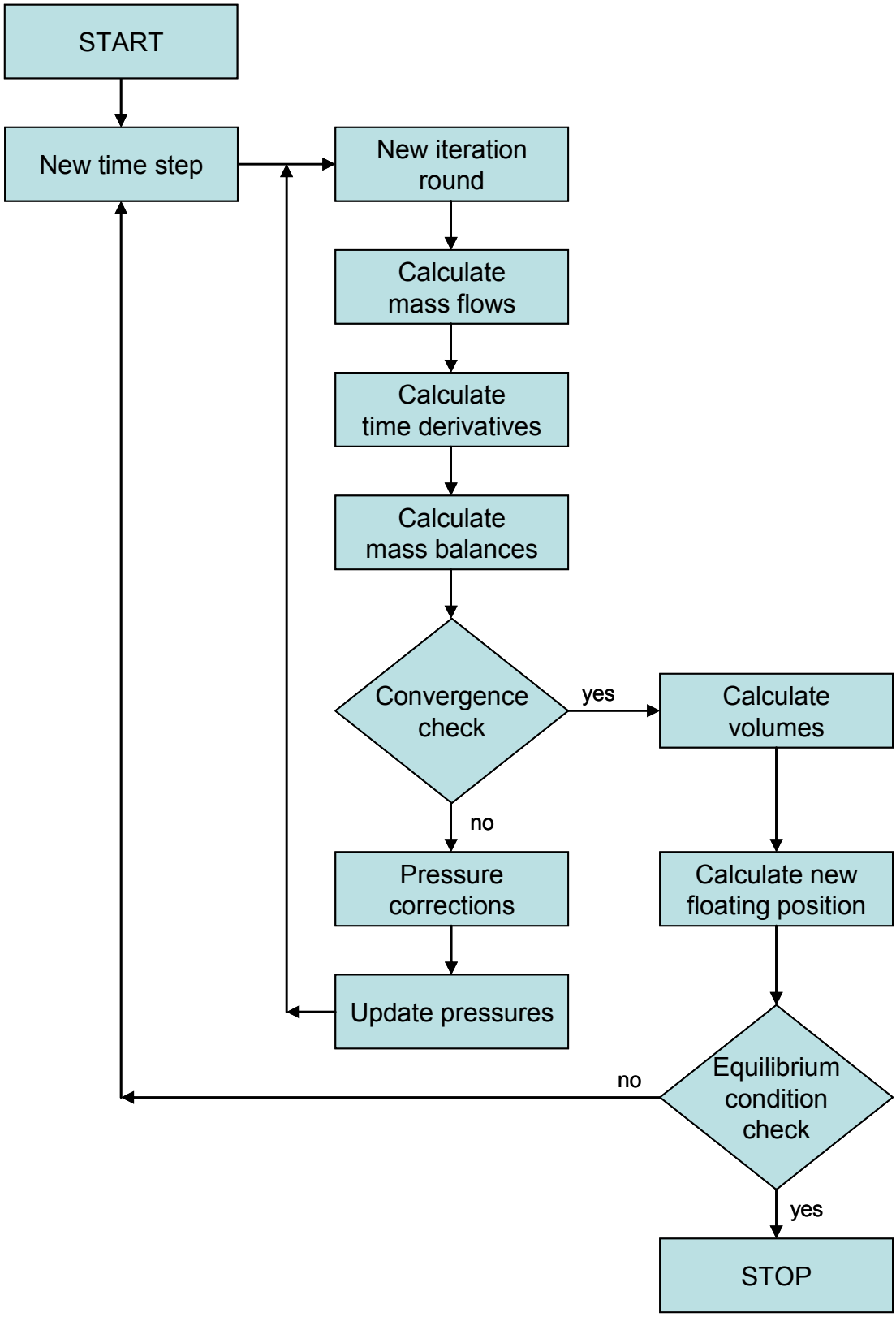

Figure 4.1 Flow chart of the simulation routine

4.3 Calculation of the Floating Position

It is assumed that the motions of the ship are slow, and hence the inertia of the ship and the interaction between the floodwater and the ship are ignored. This means that the motions of the damaged ship are calculated with a quasi-stationary approach. The applied equations of motion were presented in section 2.3.4.

The floating position with three degrees of freedom (heel, trim and draft) is calculated at the end of each time step on the basis of the solved distribution of floodwater inside the ship, and this new floating position is used as an input value for the next time step.

The floating position is calculated with the standard procedures of the NAPA software. In principle, the floating position is iterated so that the forces and moments are in equilibrium. As an input, the volumes of water in each flooded room are given. Also the intact condition with possible liquid in the tanks is taken into account.

4.4 Modelling of the Openings

4.4.1 Tall Openings

Usually the flow rate through an opening is obtained by integrating equation (2.7) over the area of the opening. However, when the pressure-correction technique is applied, as described in chapter 3, special attention is needed since the corrections of the pressures are solved from the linearization of Bernoulli's equation. These aspects are discussed in detail in the following.

The simplest way to model a small opening is a point with a given area in a ship-fixed co-ordinate system. However, for large openings this is not accurate enough. A more realistic, yet simple, representation for an opening with significant vertical height, such as an open door, is a straight line with a given area. A similar approach was used in *Dillingham (1981)* for calculating two-dimensional flow over a bulwark and in *Pawlowski (2003)* for an opening with a constant width. However, in practice this method requires an additional assumption that the flow velocity is always perpendicular to the opening.

The opening line can be considered as three separate openings since the sections $\overline{\mathrm{AB}}$, $\overline{\mathrm{BC}}$ and $\overline{\mathrm{CD}}$ are treated individually, see Figure 4.2.

In chapter 3, the pressure-correction equation was derived by applying the linearization of Bernoulli's equation with the assumption that the opening was just a single point. The result applies to all openings that are submerged on both sides, independent of the size and form of the opening since in that case the flow velocity depends only on the water levels. However, the pressure-correction equation for water heights (3.37) needs to be modified if an opening with large vertical extent is, at least partially, submerged only on one side. The reason for this is that the equation that was derived in section 3.6 was based on the assumption that the water flow velocity is constant over the area of the opening. In the case of large partly submerged openings, this assumption is not valid, as can be seen in Figure 4.2.

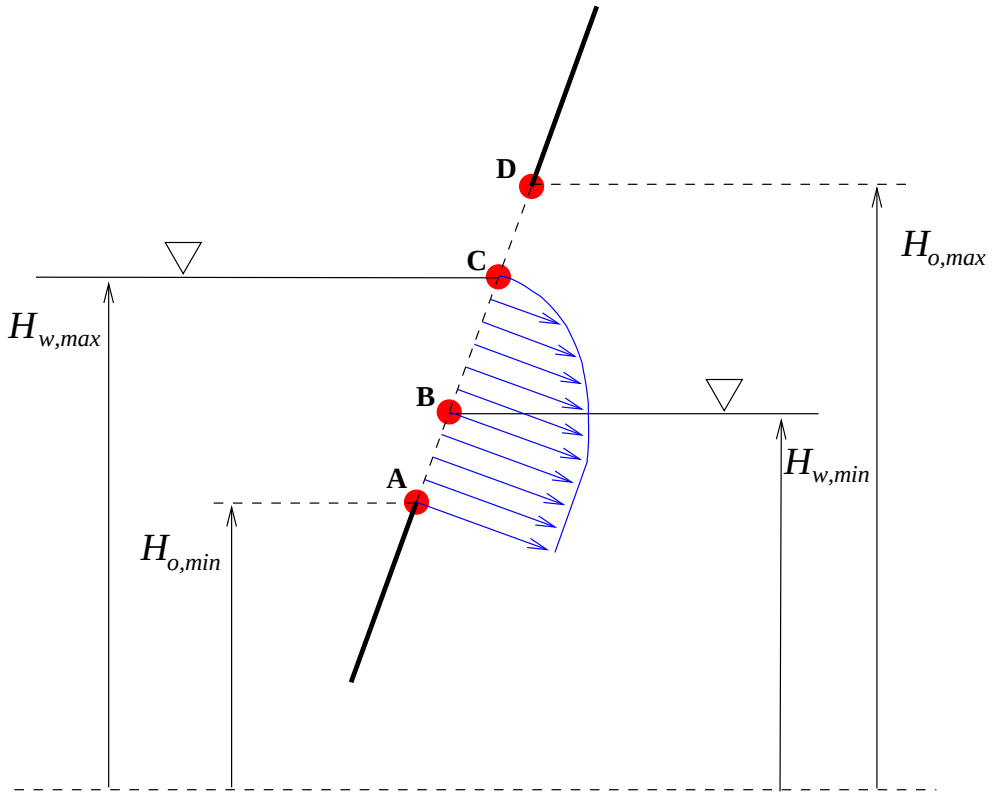

Figure 4.2 Opening line

The section $\overline{AB}$ corresponds to an opening point with the same area, since the flow through this section depends on the both water heights but not on the vertical location of the opening. Consequently, no separate handling is needed.

The section $\overline{CD}$ corresponds to an opening point for airflow, and thus it can be treated with the normal procedures, described in section 3.3.3, since the shape of the opening has no effect on the computation of airflow.

The section $\overline{\mathrm{BC}}$ must be treated in a different way since the volumetric flow through this section must be integrated. This also affects the pressure-correction equation for water heights. The details of the applied methods are described below.

The length of the opening between the points B and C is calculated on the basis of the water heights (Figure 4.2), so that:

$$L_{BC} \equiv \overline{\mathrm{BC}} = \frac{\min\left(H_{o,max}, H_{w,max}\right) - \max\left(H_{o,min}, H_{w,min}\right)}{H_{o,max} - H_{o,min}} \cdot L_o \,, \tag{4.1}$$

where L_o is the total length of the opening (i.e. the distance between the endpoints of the opening, see Figure 4.3). The additional lower indices *min* and *max* refer to the lowest and highest points of the opening line or the lowest and highest water height in the rooms that the opening connects.

The volumetric water flow through the section $\overline{\mathrm{BC}}$ is obtained by integrating the flow velocity u over the corresponding part of the opening line, so that:

$$Q_{w.BC} = b \cdot \int_0^{\overline{\mathrm{BC}}} u \cdot dl \,, \tag{4.2}$$

where b is the width of the opening.

Similarly to the section 2.3.2, let us consider a streamline from the point E that is in the middle of the flooded room, to the point F that is in the opening between the points B and C. The following heights for the points along the streamline are used:

$$\begin{aligned} h_E &= H_C \\ h_F &= H_B + l \cdot \sin\beta, \end{aligned} \tag{4.3}$$

where H_B and H_C are the vertical distances of the points B and C from the horizontal reference level and l is the distance from the point B along the opening line and β is the angle between the opening line and the reference level, see Figure 4.3.

The flow velocity is defined in equation (2.5) and the pressure losses are taken into account in the form of a discharge coefficient, equation (2.6). Consequently, the following equation for the volumetric water flow through the section $\overline{\mathrm{BC}}$ is obtained:

$$Q_{w.BC} = C_{d,1} \cdot b \cdot \int_0^{\overline{\mathrm{BC}}} \sqrt{2g\left[H_{w,max} + \frac{\Delta p}{\rho_w g} - \left(H_B + l \cdot \sin\beta\right)\right]}\, dl \,, \tag{4.4}$$

where $C_{d,1}$ is the discharge coefficient for the opening when the jet discharges into air and Δp is the air pressure difference.

It is practical to assume that the changes of the water heights are rather small, so that $H_{w,max} \approx H_C$ and $H_{w,min} \approx H_B$. Consequently, equation (4.4) can be written as:

$$Q_{w.BC} = C_{d,1} \cdot b \cdot \int_0^{\overline{\mathrm{BC}}} \sqrt{2g\left[H_C + \frac{\Delta p}{\rho_w g} - (H_B + l \cdot \sin\beta) \right]} dl \,. \tag{4.5}$$

This can be evaluated analytically:

$$Q_{w.BC} = C_{d,1} \cdot b \cdot \frac{2 \cdot \sqrt{2g}}{3 \cdot \sin\beta} \left[\left(H_C + \frac{\Delta p}{\rho_w g} - H_B \right)^{\frac{3}{2}} - \left(H_C + \frac{\Delta p}{\rho_w g} - H_B - \overline{\mathrm{BC}} \cdot \sin\beta \right)^{\frac{3}{2}} \right]. \tag{4.6}$$

The inclination angle of the opening line (i.e. the angle between the water levels and the opening, see Figure 4.3), can be evaluated on the basis of the vertical distance between the end points of the opening line (ΔH_o). Consequently:

$$\beta = \arcsin\left(\frac{\Delta H_o}{L_o} \right), \tag{4.7}$$

and therefore:

$$\sin\beta = \frac{\Delta H_o}{L_o} \,. \tag{4.8}$$

Equation (4.6) can be presented in a simpler form since the vertical distance between the points B and C is:

$$H_C - H_B = \overline{\mathrm{BC}} \cdot \sin\beta \,. \tag{4.9}$$

Furthermore, it is assumed that the air pressure difference is small when compared to the difference of the hydrostatic pressures:

$$|\Delta p| << \rho_w g \cdot (H_C - H_B) \,. \tag{4.10}$$

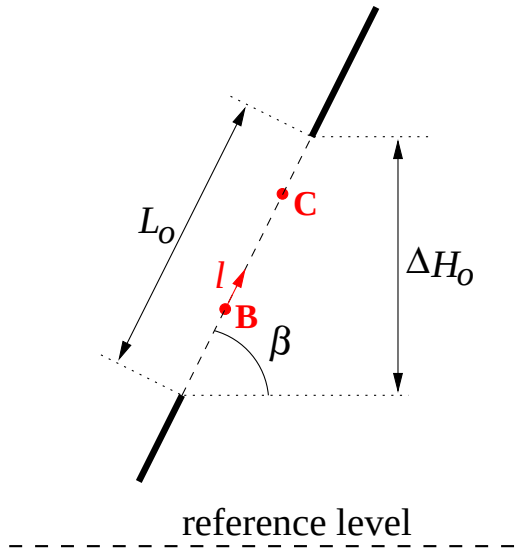

Figure 4.3 The angle between the opening line and the horizontal reference level

Hence, the volumetric flow, equation (4.6), can be approximated with the following equation:

$$Q_{w.BC} = C_{d,1} \cdot b \cdot \frac{2 \cdot \sqrt{2g}}{3 \cdot \sin\beta} (H_C - H_B)^{\frac{3}{2}}. \tag{4.11}$$

The area of the opening between the points B and C is:

$$A_{BC} = b \cdot \overline{\mathrm{BC}} = b \cdot \frac{(H_C - H_B)}{\sin\beta}. \tag{4.12}$$

Therefore, equation (4.11) can be simplified to:

$$\begin{aligned} Q_{w.BC} &= C_{d,1} \cdot b \cdot \frac{2 \cdot \sqrt{2g}}{3 \cdot \sin\beta} (H_C - H_B) \cdot \sqrt{H_C - H_B} \\ &= C_{d,1} \cdot A_{BC} \cdot \frac{2}{3} \sqrt{2g(H_C - H_B)}. \end{aligned} \tag{4.13}$$

The basic form of the rearranged equation for the volumetric flow (4.13) is the same as in the equation for the flow through a one-dimensional opening point, equation (2.7), multiplied by the coefficient 2/3. This relation is used in the following when the pressure-correction equation is derived.

The equation (4.13) can be presented in the form of a pressure loss, similarly to equation (3.8).

The mass flow of water through the section $\overline{\mathrm{BC}}$ is:

$$\dot{m}_{w,BC} = \rho_w \cdot C_{d,1} \cdot A_{BC} \cdot \frac{2}{3}\sqrt{2g\left(H_C - H_B\right)}. \tag{4.14}$$

The square of the mass flow, divided by two is:

$$\frac{1}{2}\dot{m}_{w,BC}\left|\dot{m}_{w,BC}\right| = \rho_w^2 \cdot C_{d,1}^2 \cdot A_{BC}^2 \cdot \frac{4}{9} \cdot g\left(H_C - H_B\right). \tag{4.15}$$

This can be rearranged to:

$$\frac{1}{2} \cdot \left(\frac{1}{\frac{4}{9} \cdot \rho_w \cdot C_{d,1}^2 \cdot A_{BC}^2} \right) \cdot \dot{m}_{w,BC}\left|\dot{m}_{w,BC}\right| = \rho_w g\left(H_C - H_B\right). \tag{4.16}$$

Moreover, this can be simplified by applying the dimensional pressure loss coefficient, defined in (3.7). Therefore, equation (4.16) can be written as:

$$\frac{1}{2} \cdot \frac{9}{4} \cdot K'_w \dot{m}_{w,BC}\left|\dot{m}_{w,BC}\right| = \rho_w g\left(H_C - H_B\right). \tag{4.17}$$

The basic form of this equation is similar to the pressure loss equation for a one-dimensional opening (3.8), but the dimensional pressure loss coefficient is multiplied by a constant factor of 9/4. Therefore, the same form of the pressure-correction equation can be used when this additional coefficient is taken into account. Consequently, the pressure-correction equation (3.37) for water heights in the case of a two-dimensional opening line can be written as:

$$\begin{aligned} &\sum_k \left[\begin{array}{l} \dfrac{p'_i - p'_j}{K'_{w,k}\rho_w\left|Q^*_{w,k}\right|} + \dfrac{H'_{w,i} - H'_{w,j}}{K'_{w,AB,k}\rho_w\left|Q^*_{w,AB,k}\right|} \\ + \dfrac{4}{9} \cdot \dfrac{\max\left[\mathrm{sign}\left(H^*_{w,i} - H^*_{w,j}\right),0\right] \cdot H'_{w,i} - \max\left[\mathrm{sign}\left(H^*_{w,j} - H^*_{w,i}\right),0\right] \cdot H'_{w,j}}{K'_{w,BC,k}\rho_w\left|Q^*_{w,BC,k}\right|} \end{array} \right] \\ &+ \frac{\rho_w S_{fs,i}}{\Delta t} H'_{w,i} = -\Delta\dot{m}^*_{w,i}. \end{aligned} \tag{4.18}$$

The first term on the left hand side takes the effect of air pressures into account. This is independent of the modelling of the opening geometry. The second term applies to the water flow discharging into water since the mass flow depends on the both water heights. The third term on the left hand side is for the water flow discharging into air

since this part of the mass flow only depends on the water height on the maximum pressure side. The fourth (underlined) term is taken into account only if the room is not filled up with water. In principle, the basic form of the pressure-correction equation is exactly the same as in the case of one-dimensional opening points.

Furthermore, the total volumetric water flow through the opening k consists of two parts:

$$Q^*_{w,k} = Q^*_{w,AB,k} + Q^*_{w,BC,k} . \tag{4.19}$$

In order to ensure convergence, discontinuities should be avoided during the iteration process. Therefore, the points B and C are kept constant during the time step. This simplification should not cause significant error if the applied time step is sufficiently short.

The applicability of this implementation was tested by performing comparative simulations, where the high openings were modelled with several individual points, as shown in Figure 4.4. An example of the comparisons is presented in Figure 4.5. In this case, 20 evenly distributed opening points give practically the same result as one opening line. The difference is increased as the number of opening points is decreased. When the whole opening is submerged (volume of floodwater is larger than 10 m^3) the modelling of the opening does not have an effect anymore.

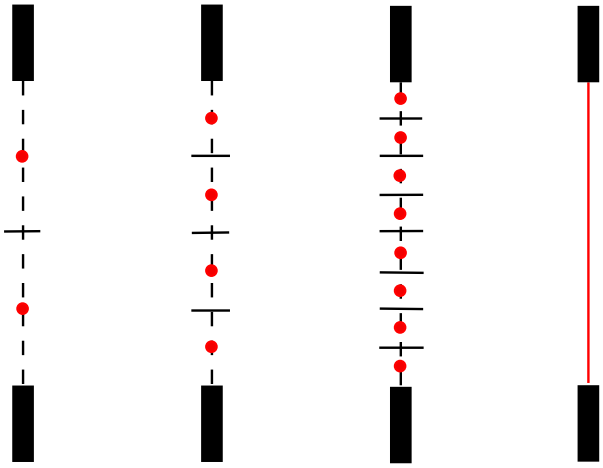

Figure 4.4 Modelling of a tall opening with several opening points (red dots)

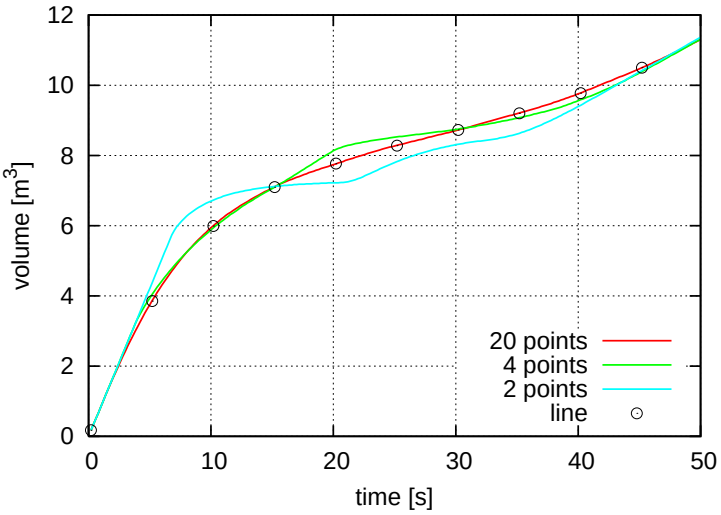

Figure 4.5 Comparison between different modelling techniques for a high open door that is connected to the damaged room (for clarity, only every 25th time step is plotted for the "line")

4.4.2 Very Large Openings

If the opening is very large, both in vertical and transverse or longitudinal directions, the opening can be modelled with several two-dimensional opening lines. The principle is shown in Figure 4.6. In practice, this procedure corresponds to integration in the transverse or longitudinal direction with the trapezoidal method. Consequently, there is no need to further modify the pressure-correction equations since the whole opening can be considered to consist of several high but relatively narrow openings.

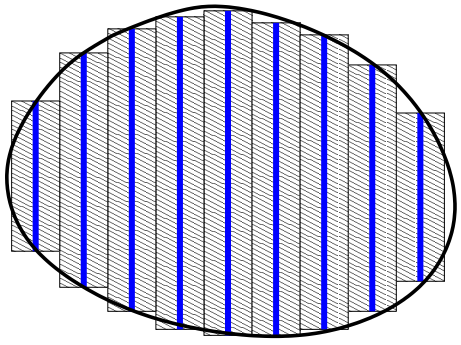

Figure 4.6 Integration over the area of a very large opening that is modelled with several two-dimensional opening lines, marked with the blue lines

4.4.3 Collapsing Structures

The hydrostatic pressure in the flooded compartments may be very significant. The closed doors that are subjected to this pressure may start to bend, causing leaking through the door and progressive flooding to a new compartment. It is also possible that the whole door will eventually collapse under the pressure of the floodwater, in which case a transient large scale flooding between the compartments may take place. Consequently, all potential openings, including the closed doors, must be included in the numerical model of the ship (i.e. in the computational grid).

The effective area of a door that is initially closed depends on the effective pressure head that is acting on the door. The accurate modelling of possible leaking through the door and structural failures, such as bending, is practically impossible. A simplified approach is presented in Figure 4.7, based on the suggestions given in *IMO SLF47/INF.6 (2004)*. The same approach has been used before in similar studies, e.g. in *van't Veer et al. (2004)*.

The effective pressure head that affects the closed door k is defined as:

$$\Delta H_{eff,k} = \frac{\left| P_i - P_j \right|_k}{\rho_w g}, \tag{4.20}$$

on the basis of the total pressure difference, equation (3.3).

It is assumed that the door can withstand the pressure of the floodwater until it starts to leak, when the effective pressure head is larger than H_{leak}. The leaking is modelled by reducing the total area of the opening by multiplying it with the factor:

$$A_{ratio} = \frac{A_{leak}}{A_{tot}}, \tag{4.21}$$

where A_{leak} is the area of the leaking door and A_{tot} is the total area of the door. The possible changes in the discharge coefficient are also included in the effective area ratio.

If the effective pressure head is larger than H_{coll}, the door is assumed to collapse, and the area of the formed opening is equal to the area of the door ($A_{coll} = A_{tot}$). Once the door has started to leak or it has collapsed, it cannot be closed again, even if the pressure head decreases.

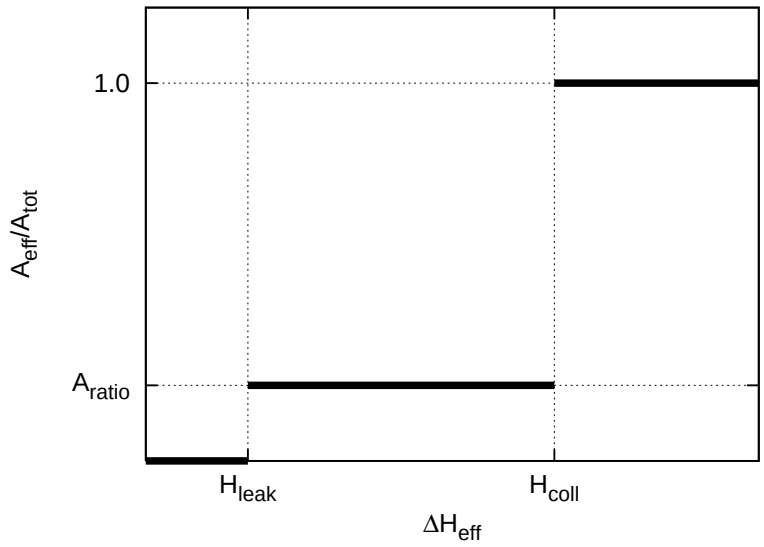

Figure 4.7 Effective area of an initially closed door as a function of the effective pressure head

4.4.4 Pipes

In addition to openings, the floodwater can proceed to other compartments through pipes and ducts. Therefore, the simulation method has to be able to deal with these structures as well.

The simplest way to model a pipe is a straight line with two co-ordinate points that represent the inlet and outlet of the pipe. Thus the possible goose necks, etc. are ignored. Furthermore, all siphon effects are completely excluded. The effective area of the pipe is considered to be constant and the pressure losses are taken into account in a similar way as in the case of openings by applying a discharge coefficient, equation (2.6).

For simplicity, airflow through the pipe is considered to be impossible if at least one end of the pipe is submerged. For the calculation of water flow through a pipe, the highest end of the pipe is used as the reference height for the connection. An illustration of the pipe definition is given in Figure 4.8. Due to the simplification in the modelling, water will start to flow through the pipe already at time t_2 when in reality this takes place when the highest point of the whole pipe is submerged at time t_3.

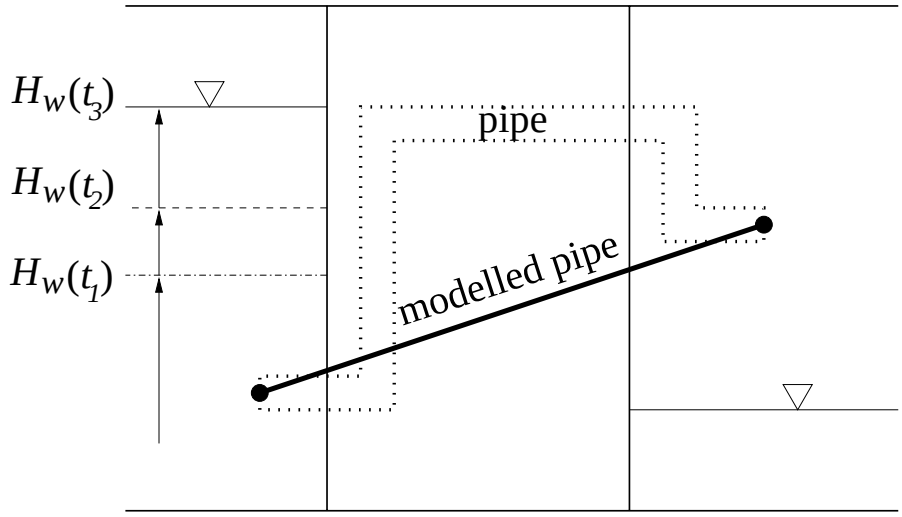

Figure 4.8 Definition for a pipe with a straight line; water will start to flow through the pipe at time t_2 in the simulation, while in reality this takes place only at time t_3

4.5 Modelling of Rooms

The simulation method is based on the assumption that the area of free surface remains constant during the pressure-correction iteration (see section 3.4.2). This can cause significant error, and even numerical problems with the solution of the pressure-correction equation, if there is a large discontinuity in the area as a function of water height. An example of a problematic room is given in Figure 4.9, along with the free surface area as a function of water height with the given angular position.

The rooms can be divided into two categories. A room is concave if it does not contain all the line segments connecting any pair of its points. If the room does contain all the line segments, it is called convex.

Concave rooms can also cause further inaccuracy since two separate air pockets can be formed in one room. Consequently, there can also be two different water heights. The simulation method cannot deal with this properly. This kind of problem can be avoided by modelling the compartment with several smaller convex rooms that are connected through openings. An example of this is shown in Figure 4.10. Therefore, all potentially flooded rooms should be, at least nearly, convex, especially in the vertical direction and particularly if air compression is taken into account.

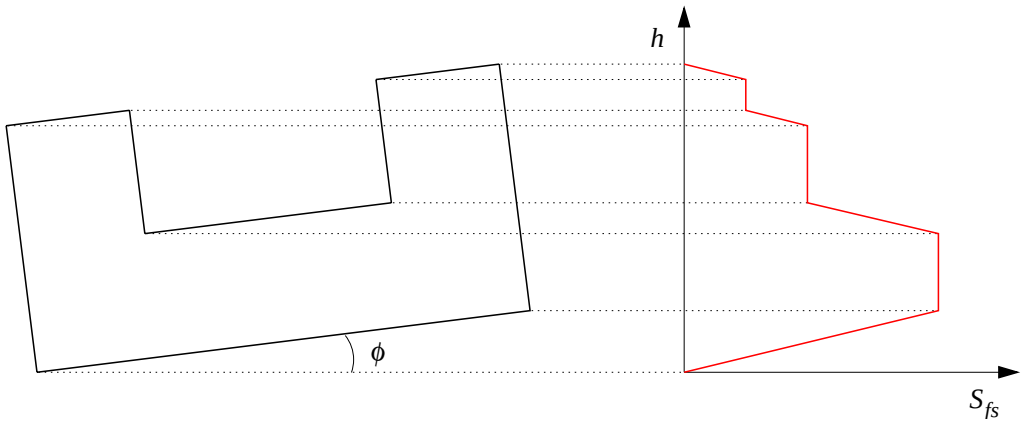

Figure 4.9 Example of a concave room and the area of free surface S_{fs} as a function of the water height h in the room; when at $\phi = 0$ there is a discontinuity

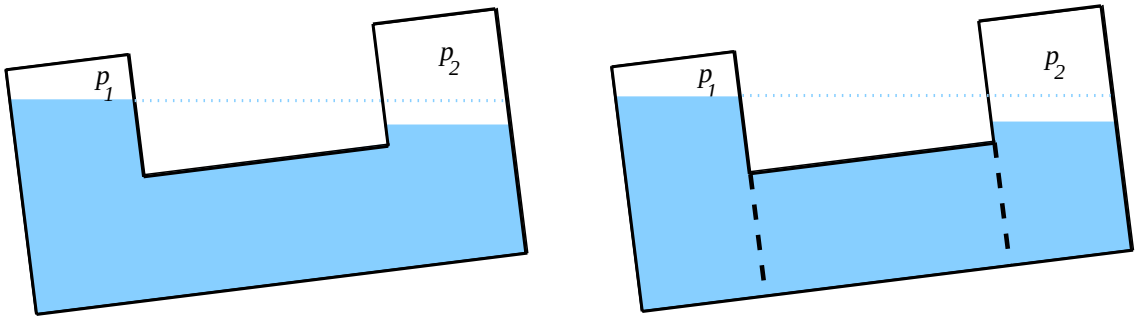

Figure 4.10 Improper modelling of a concave room (left) and proper modelling with three convex rooms and two openings (right)

5 Validation

5.1 Model Tests

Dedicated model tests for progressive flooding of a box-shaped barge (Figure 5.1) were performed in the towing tank of TKK Ship Laboratory in January 2006. A detailed description of the model test setup and the measurements is given in *Ruponen (2006b)*.

The model was constructed of three separate blocks that were connected to each other with the support structures. The plexiglass mid-section contains eight rooms in two compartments. The rooms are connected through internal openings that are open throughout the whole flooding process. The WT-door in the transverse bulkhead on the upper deck can be closed with a tight plate.

The arrangement of the compartments is shown in Figure 5.2 and the identifications are presented in Figure 5.3. The main dimensions and the initial condition for all tests are listed in Table 5.1.

The floating position and the water levels in all flooded compartments were measured throughout the flooding process. Furthermore, the pressure in the air pocket in the double bottom was recorded.

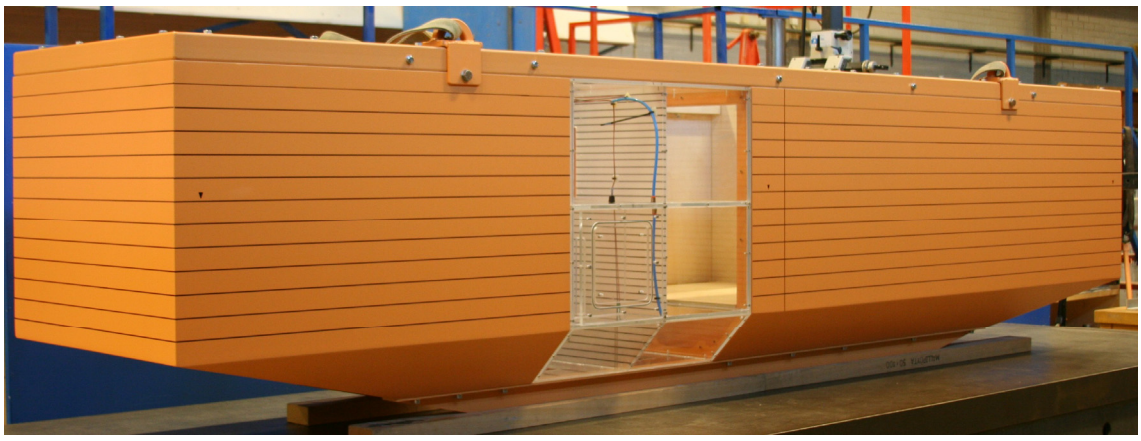

Figure 5.1 The model of the box-shaped barge

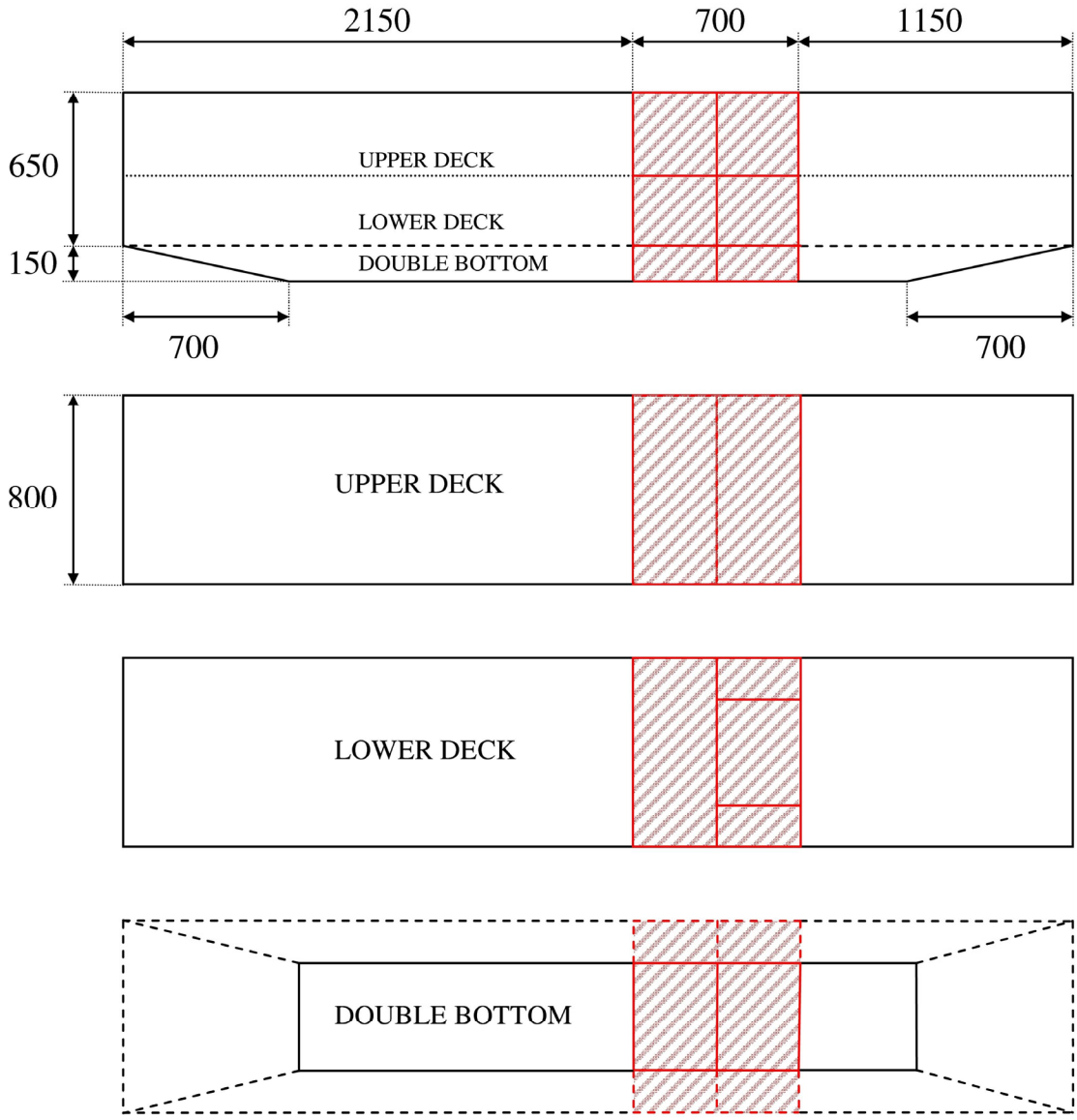

Figure 5.2 General arrangement plan and some dimensions (in mm) of the model; the hatched areas show the flooded compartments.

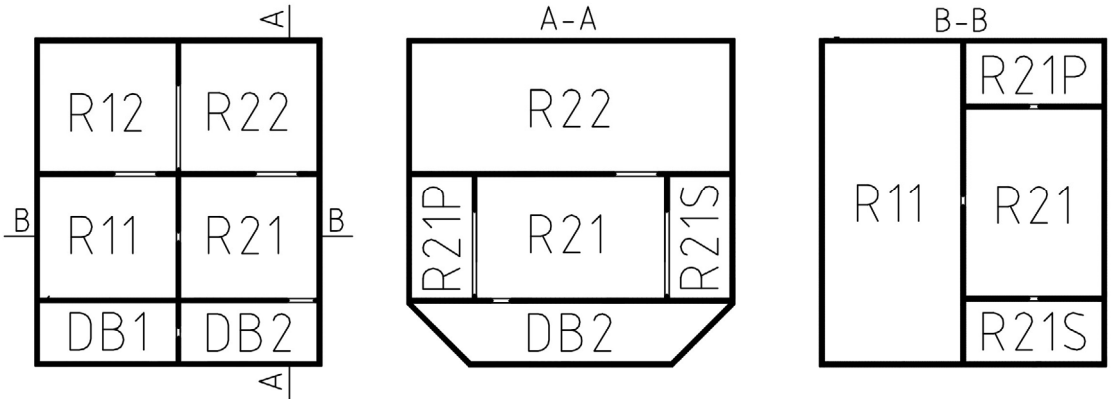

Figure 5.3 Identification of the flooded compartments

Table 5.1 Main dimensions and initial condition

Length over all:	4.000 m
Breadth:	0.800 m
Height (excluding the “backbone” structure):	0.800 m
Draft:	0.500 m
Block coefficient:	0.906
Volume of buoyancy:	1.450 m^3
Initial heel:	0.0°
Initial trim:	0.0°
Vertical center of gravity (intact):	0.278 m
Initial metacentric height:	0.110 m

5.2 Simulations

5.2.1 Motivation

The first results of the validation of the simulation method have been briefly presented in *Ruponen et al. (2006)*. Since then, new simulations have been performed with a more realistic modelling of the openings with large vertical extent. Also the pressure losses in the air pipes have now been taken into account.

5.2.2 Numerical Model of the Barge

A detailed numerical model of the barge was created with the NAPA software in the model scale. The thickness of the plexiglass decks and bulkheads (10 mm) was taken into account but the instrumentation was ignored, so that the permeability in all modelled rooms could be taken as unity.

The double bottom (rooms DB1 and DB2) and the side compartments (R21P and R21S) are modelled to have a restricted level of ventilation, so that ventilation is only possible through the modelled openings and pipes. All other rooms are modelled to be fully ventilated so that the air pressure remains equal to the atmospheric pressure throughout the flooding. In the case of the rooms R11 and R21 this is considered to be realistic since the openings on top of these rooms are large (100 mm × 100 mm). Furthermore, the rooms on the upper deck (R12 and R22) are connected to the atmosphere through large ventilation holes.

The openings with large vertical extent (R21-R21S, R21-R21P and R12-R22) are modelled as lines with a constant width, whilst all other openings are considered as single points with the given area. In the first simulations, *Ruponen et al. (2006)*, all openings were modelled with points. For the openings in vertical direction, several evenly distributed points were used to represent one opening. The new approach is considered to be slightly more realistic.

The applied discharge coefficients were obtained experimentally by draining water through each opening (*Ruponen, 2006b*). These coefficients are listed in , and they are assumed to be independent of the flow condition and the Reynolds number. Consequently, the same coefficient was used also when the jet discharged into water, thus disregarding the increased pressure-losses.

Also the ventilation pipes in the side compartments R21P and R21S were modelled. In the first simulations (*Ruponen et al., 2006*) the pressure losses in the air pipes were disregarded. In the new simulations, these are estimated by using the Darcy formula, e.g. *Walshaw and Jobson (1979)*:

$$\Delta p = \frac{1}{2}\rho k_L u^2 = \frac{1}{2}\rho\lambda\frac{L}{D}u^2, \tag{5.1}$$

resulting in the following pressure loss coefficient:

$$k_L = \lambda \frac{L}{D}, \tag{5.2}$$

where L is the length and D is the diameter of the pipe. The coefficient λ takes the surface roughness into account. The following equation is applied (*Blevins, 1984*):

$$\frac{1}{\sqrt{\lambda}} = 2 \cdot \log_{10}\left(\frac{D}{\varepsilon}\right) + 1.14, \tag{5.3}$$

where ε is the particular size of grains. It is further assumed that the coefficient λ is independent of the Reynolds number. The discharge coefficient for airflow in the pipe is obtained by substituting (5.2) into equation (2.6), resulting in:

$$C_{d,air} = \frac{1}{\sqrt{1 + k_L}} = \frac{1}{\sqrt{1 + \frac{\lambda L}{D}}}. \tag{5.4}$$

Table 5.2 Applied discharge coefficients for the openings (*Ruponen, 2006b*)

Connection	**Size**	C_d
SEA-DB1	60 mm × 40 mm	0.78
SEA-DB2	25 mm × 25 mm	0.83
SEA-R21S	60 mm × 40 mm	0.78
DB1-DB2	Circular hole, D = 20 mm	0.80
DB2-R21	60 mm × 40 mm	0.78
R21-R21S	20 mm × 200 mm	0.75
R21-R21P	20 mm × 200 mm	0.75
R21-R11	D = 20 mm	0.80
R21-R22	100 mm × 100 mm	0.72
R11-R12	100 mm × 100 mm	0.72
R12-R22	80 mm × 200 mm	0.72*
R21S-ATM	Ventilation pipe, D = 7 mm	0.67**
R21P-ATM	Ventilation pipe, D = 7 mm	0.67**
* Assumed to be equal to the C_d for the opening R11-R12 ** Calculated with the Darcy formula		

The length of each pipe is approximately 400 mm and the inner diameter is 7 mm. The surface of a plastic pipe is very smooth, and thus the value for the particular size of grains is approximately $\varepsilon = 0.01$ mm (*Blevins, 1984*). As a result, the discharge coefficient for the airflow in the pipe is 0.67. It can be concluded that the pressure losses in the air pipes are notable but not very significant.

5.2.3 Simulation Parameters

All simulations were performed with a constant time step of 0.05 s. This was selected so that it had no notable effect on the results. An initial under-relaxation coefficient $\alpha = 0.5$ was used. More under-relaxation ($\alpha = 0.1$) was applied near the equilibrium, where the time derivatives of the pressures were very small. This ensured convergence in all cases, even though the computation times were slightly increased due to the larger number of iteration rounds for the last time steps before the final equilibrium condition was reached.

The applied convergence criterion corresponds to a water height difference of 0.01 mm. It was tested that a stricter criterion did not cause any notable difference in the results.

The calculated water heights are converted to a ship-fixed co-ordinate system so that a direct comparison with the measurement data is possible.

The simulations were performed with the simplified approach, where the air pressure corrections were solved first, using the equation (3.57), and the results were used in the solution of the water height corrections, using the equation (3.37). For comparison, some simulations were also performed by applying the fully coupled pressure-corrections, equations (3.37) and (3.52).

5.3 Results

5.3.1 Validation Case A – Side Damage

The damage opening (60 mm × 40 mm) is located in the side of the room R21S and the opening to the double bottom is closed (Test06 in *Ruponen, 2006b*). The progress of the floodwater is presented in Figure 5.4. The damage opening is in line with the internal openings to the side compartments. Hence water flows partly straight from the sea to the room R21, and the flooding phases 1 and 2, as denoted in Figure 5.4, take place partly at the same time. This is clearly visible in the video captures, presented in Figure 5.5.

The results are presented in Figure 5.6 – Figure 5.10. Due to the high initial stability of the model and the almost symmetrical flooding in transverse direction, the heeling angle was very small throughout the whole flooding process and hence it is not included.

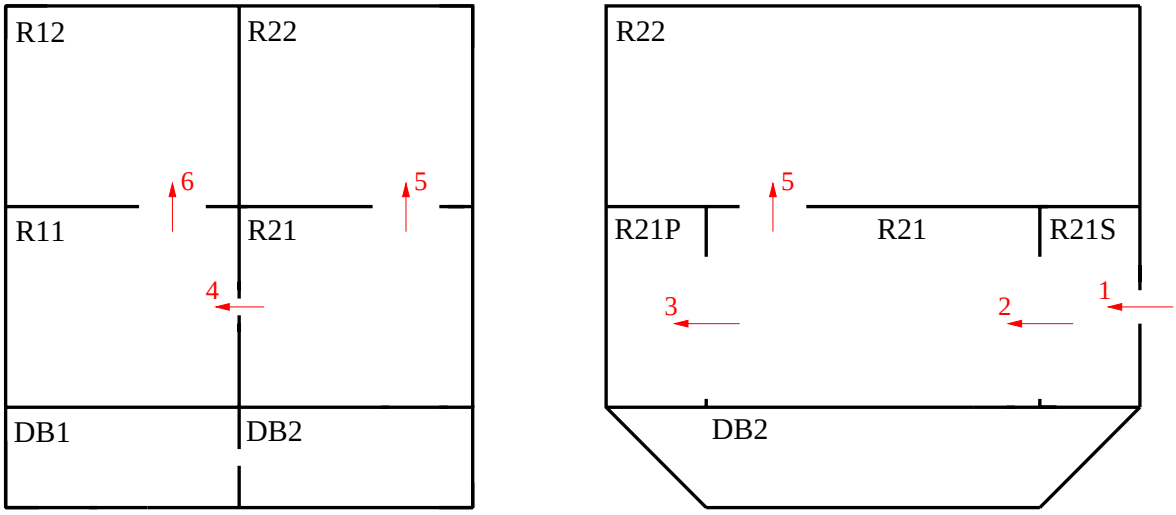

Figure 5.4 Progress phases of the flooding in the validation case A

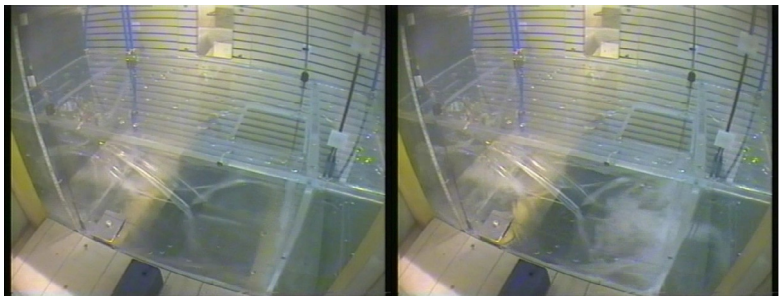

Figure 5.5 Video captures from the start of the flooding in the case A

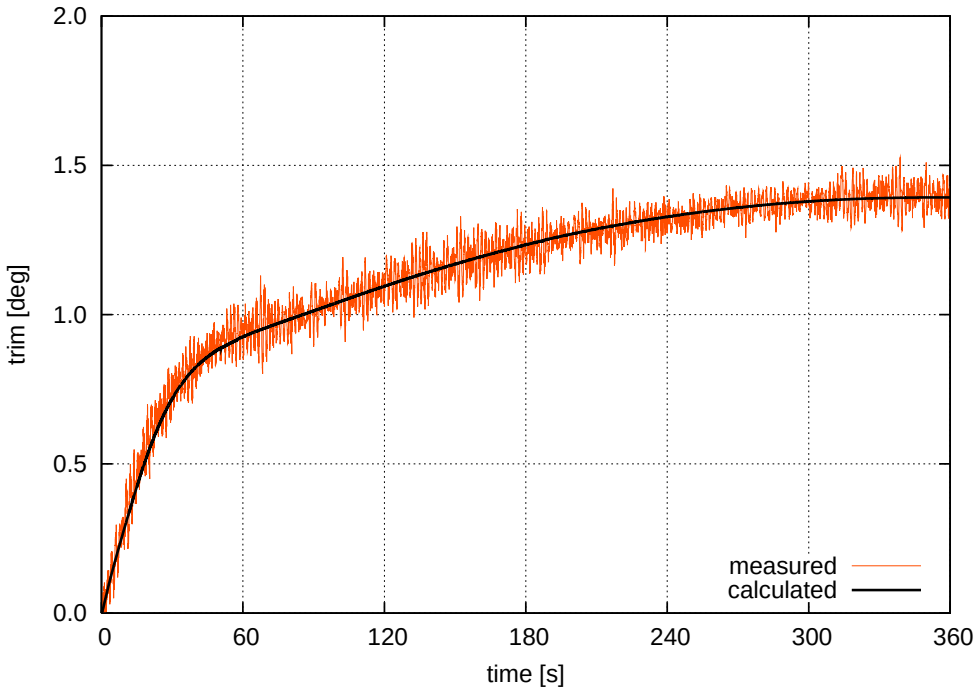

Figure 5.6 Case A – calculated and measured trim angle

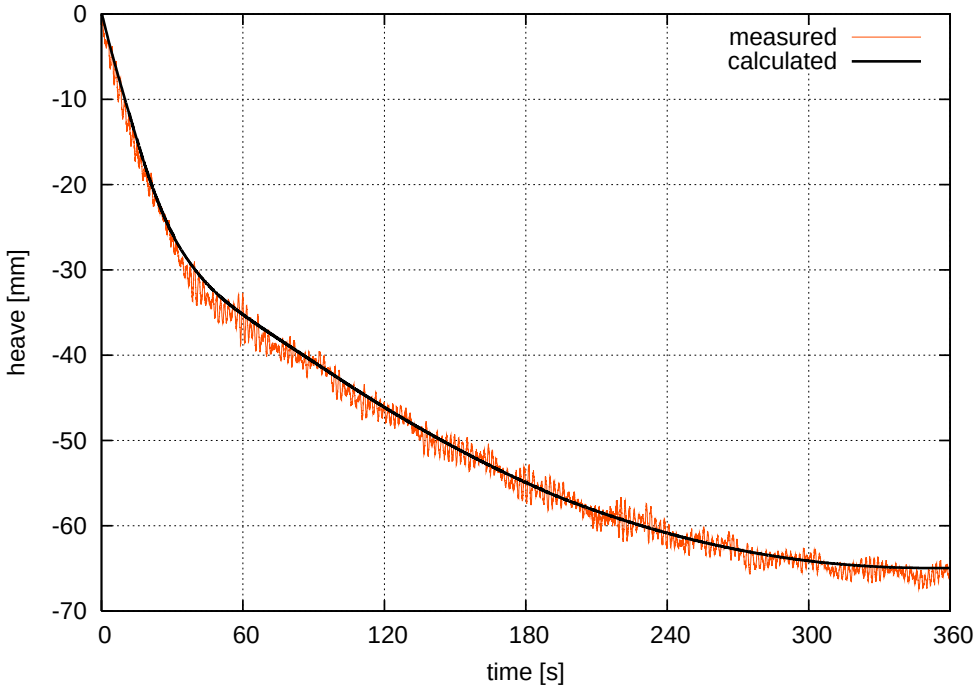

Figure 5.7 Case A – calculated and measured heave motion

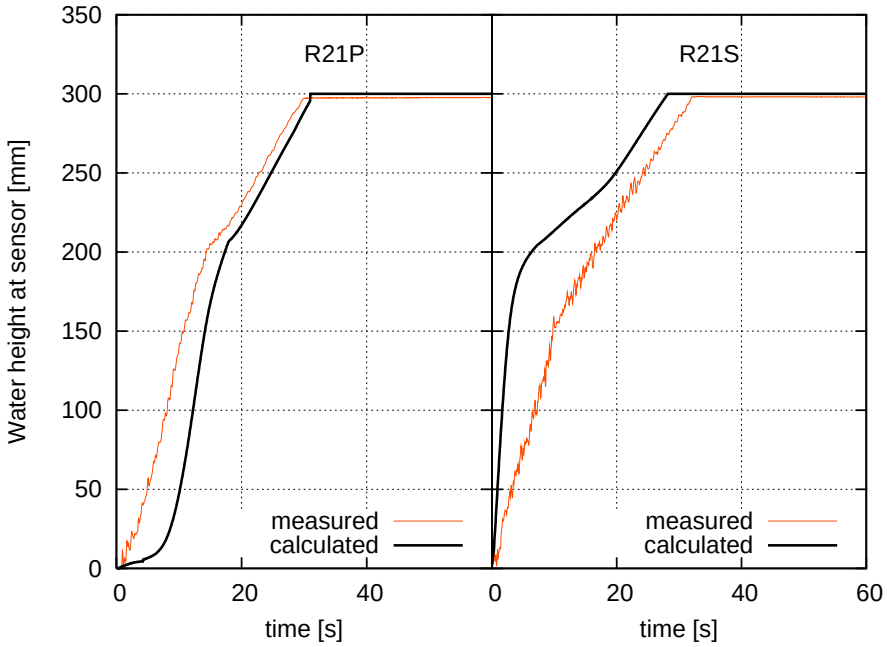

Figure 5.8 Case A – calculated and measured water heights in the rooms R21P and R21S

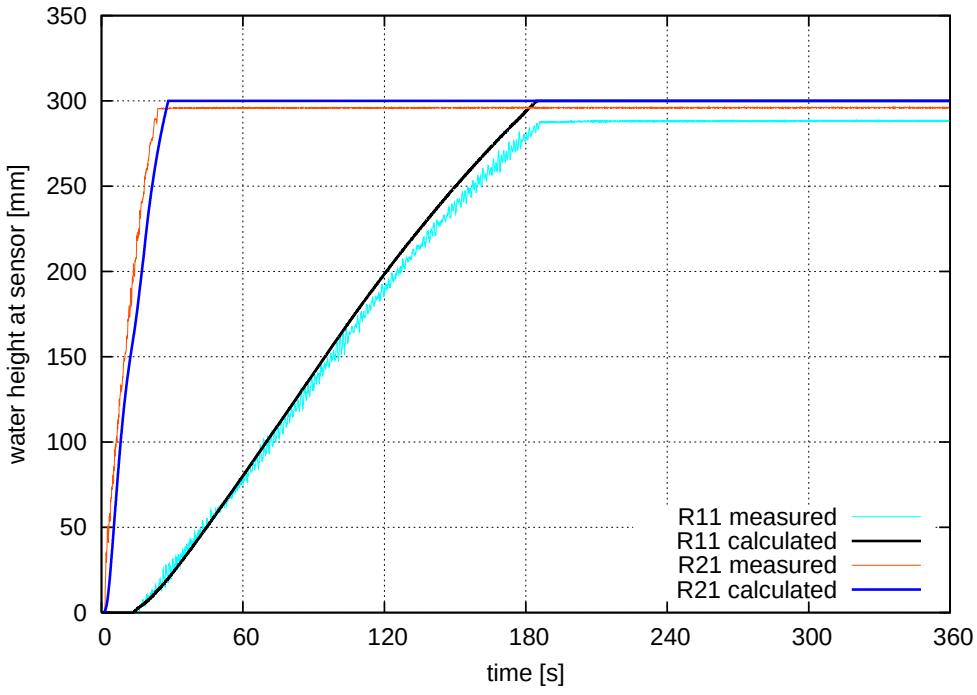

Figure 5.9 Case A – calculated and measured water heights on the lower deck in the rooms R11 and R21

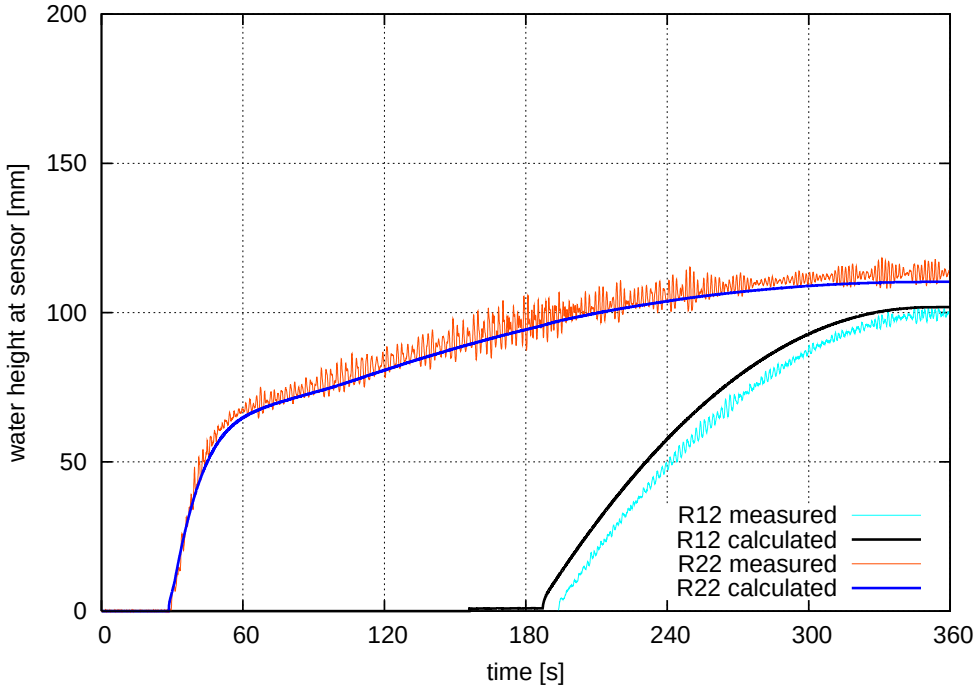

Figure 5.10 Case A – calculated and measured water heights on the upper deck in the rooms R12 and R22

Both the trim angle (Figure 5.6) and the heave motion (Figure 5.7) are predicted very accurately by the simulation tool.

The water height in the damaged room R21S is over-estimated in the start of the flooding (Figure 5.8) since the water jet through the damage hole allowed direct flooding of the rooms R21 and R21P directly from the sea. Consequently, the water height in R21P is under-estimated by the simulation. After about 20 s (phases 1 – 3 in Figure 5.4) the jet from the sea is submerged and it becomes less significant. As a result, the correlation between the measured and calculated water heights is much better. The water levels in the rooms that are subjected to pure progressive flooding (R11, R12 and R22) are predicted very accurately, Figure 5.9 and Figure 5.10.

Compression of air is takes place in the side compartments R21S and R21P when the water level reaches the opening to R21, and air can escape only through the small ventilation pipes. This can be seen as the sudden deceleration in the rise of the water levels, Figure 5.8. Qualitatively, the simulation predicts this phenomenon properly. Unfortunately, air pressures in these rooms were not measured. The maximum

calculated over pressure in the air pocket is about 200 Pa, which is small when compared to the air pressures in the double bottom during the other validation cases.

On average, 42 iteration rounds per time step were needed. Some examples of the convergence are presented in Figure 5.11. At $t = 0.45$ s flooding from R21S to R21 starts. The iteration converges steadily but a little slower than on average. At $t = 12.65$ s the flooding to R11 starts, causing a minor delay in the convergence of air pressures. At $t = 31.00$ s the side rooms R21P and R21S are filled up. This causes temporary convergence problems, and the iteration is practically started again for the hydrostatic pressures after the volumes of air have vanished.

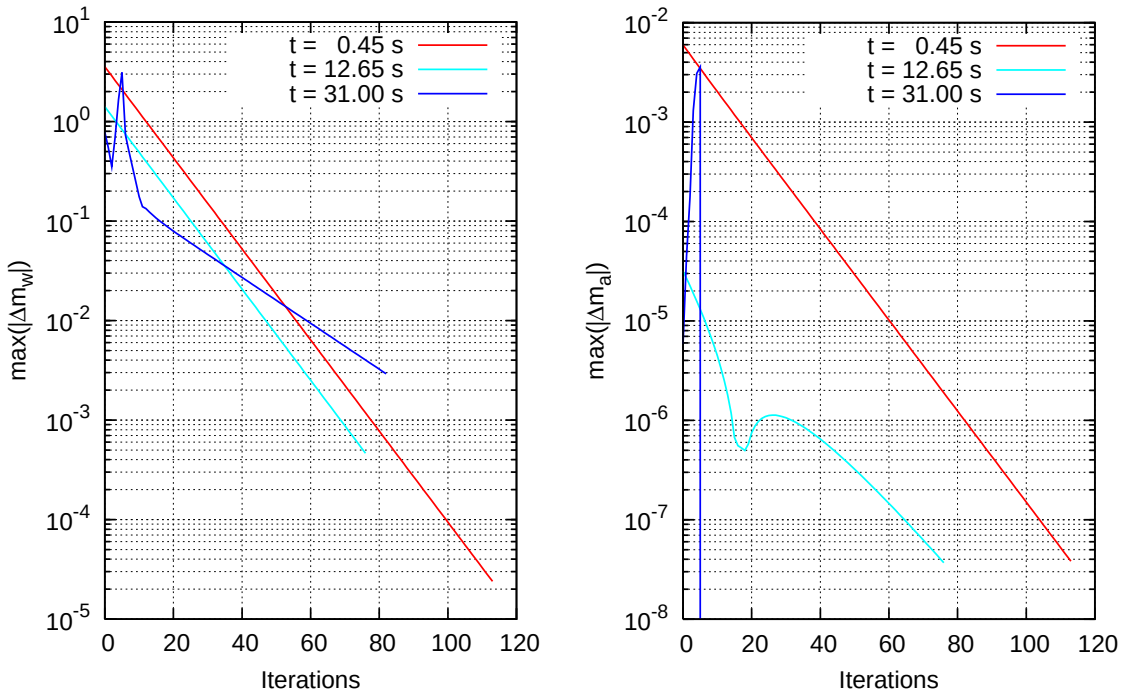

Figure 5.11 Examples of convergence in the validation case A

5.3.2 Validation Case B – Bottom Damage and Down-Flooding

The damage hole (60 mm × 40 mm) is located in the bottom of the room DB1 (Test03 in *Ruponen, 2006b*). Consequently, the forward compartment is flooded much faster than the aft compartment. On the upper deck there is an open door. As a result, there is a phase of down-flooding from the upper deck (R12) to the lower deck (R11) in the aft compartment. The opening in the deck is so large (100 mm × 100 mm) that basically all water that is flooded through the open door is drained down. When the room R11 is filled up, the flow direction in this opening is reversed to up-flooding. The phases of the flooding process are presented in Figure 5.12.

The results are presented in Figure 5.13 – Figure 5.19. Due to the symmetrical flooding in transverse direction and the large initial stability of the model, both the measured and the calculated heeling angles were zero throughout the flooding, and hence they are not shown.

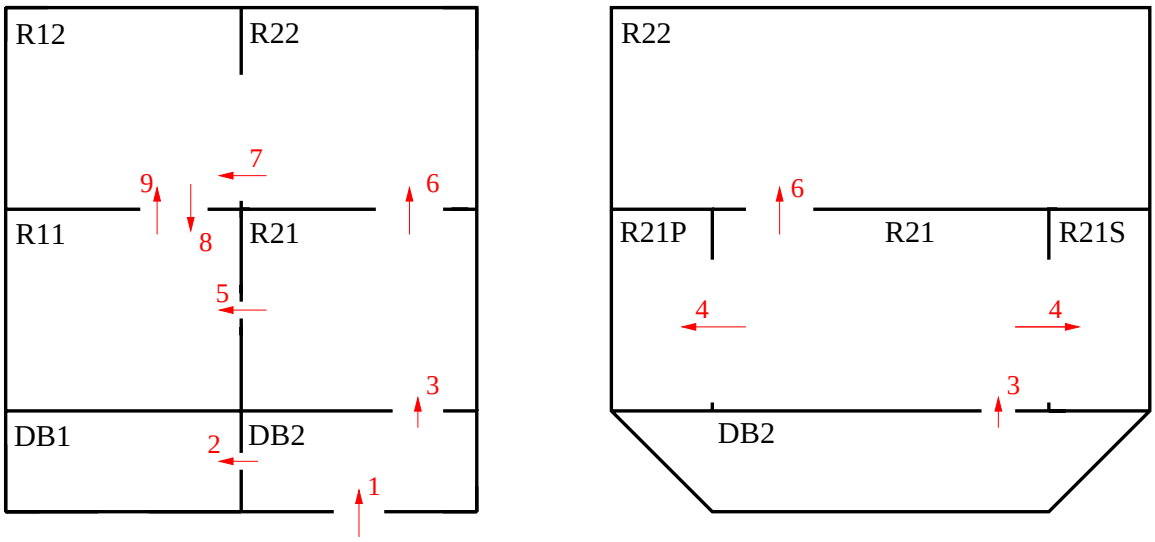

Figure 5.12 Progress phases of the flooding in the validation case B, the flow direction in the opening between R12 and R11 is changed during the flooding

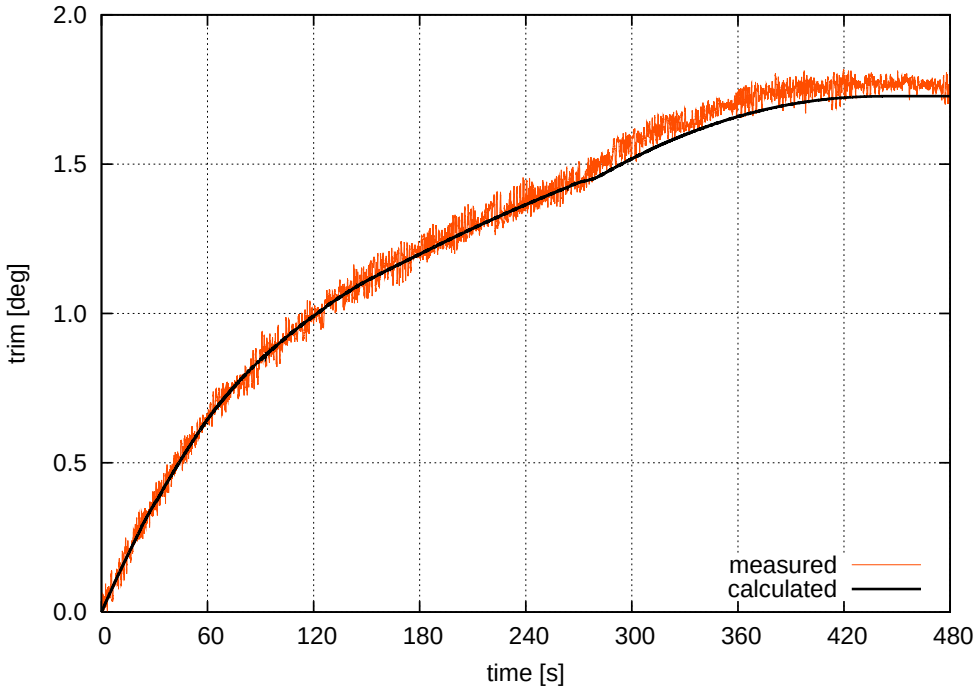

Figure 5.13 Case B – calculated and measured trim angle

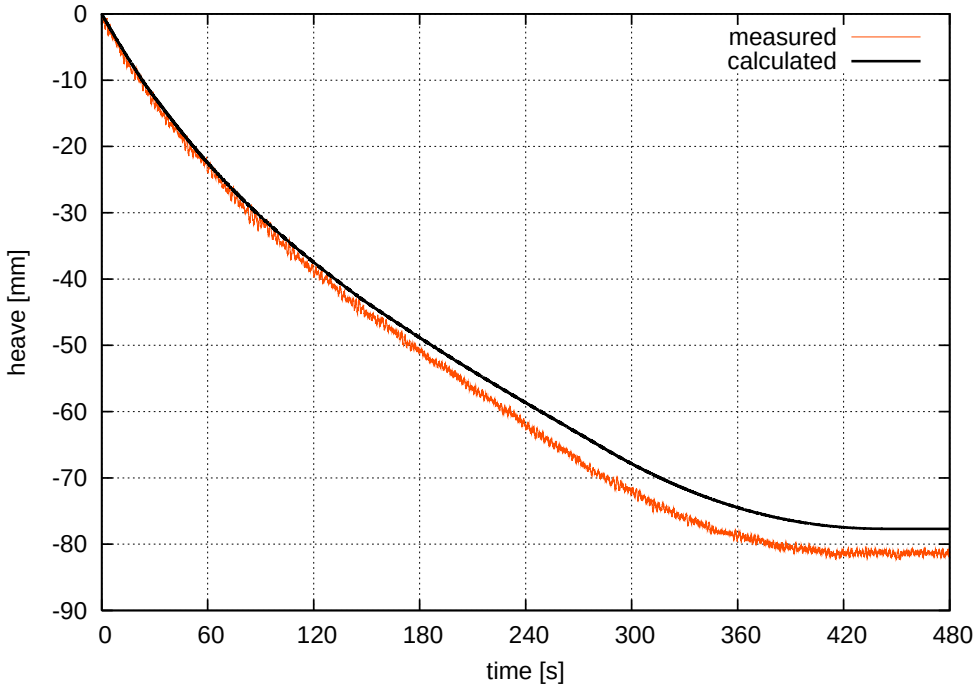

Figure 5.14 Case B – calculated and measured heave motion

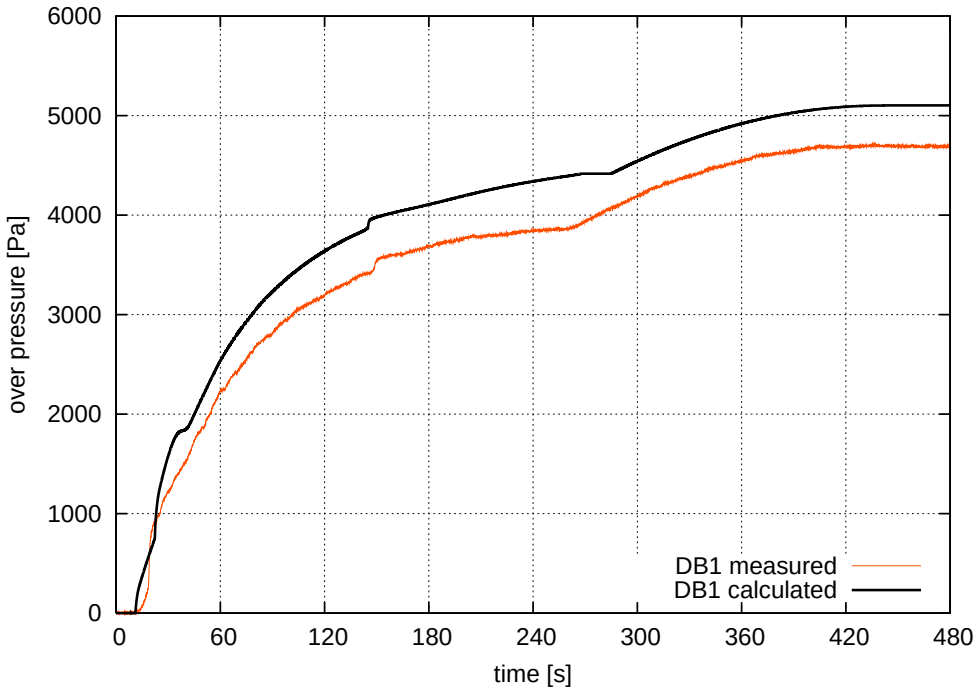

Figure 5.15 Case B – calculated and measured over pressure of the air pocket in the room DB1

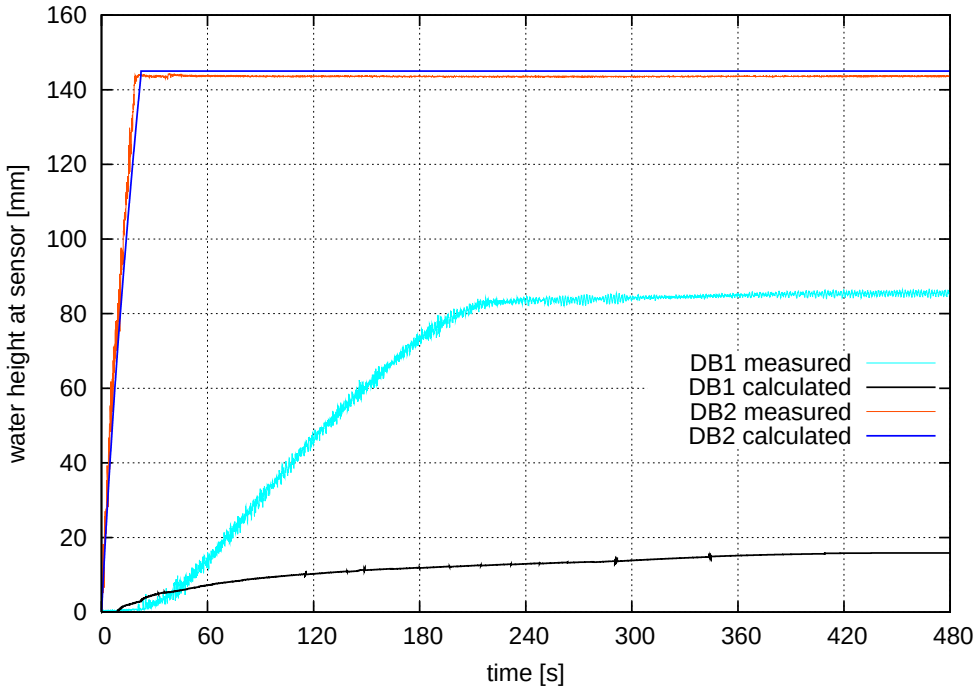

Figure 5.16 Case B – calculated and measured water heights in the double bottom rooms DB1 and DB2

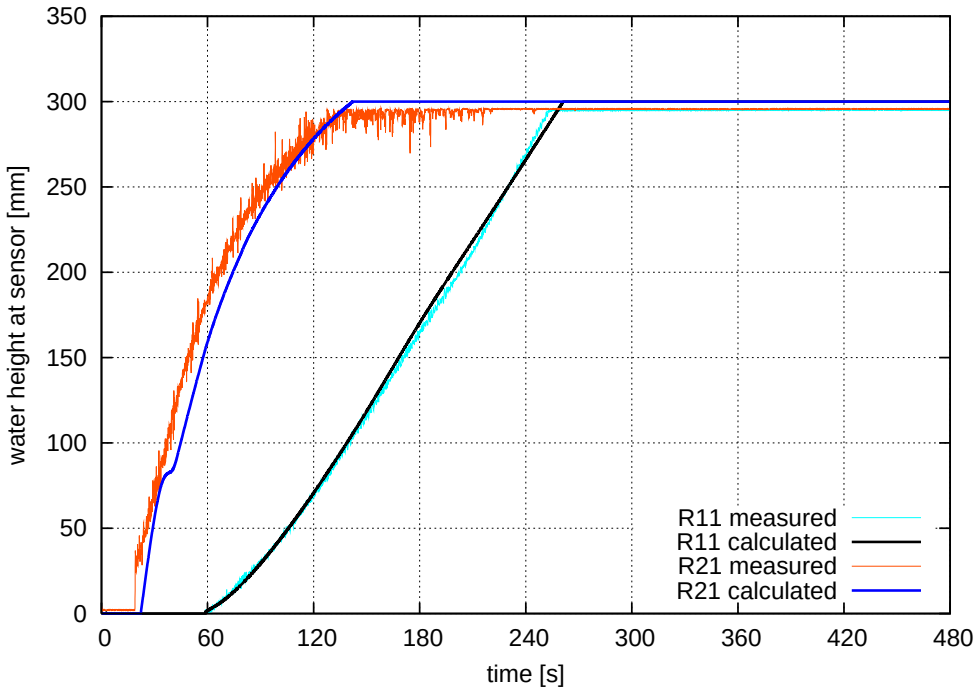

Figure 5.17 Case B – calculated and measured water heights on the lower deck in the rooms R11 and R21

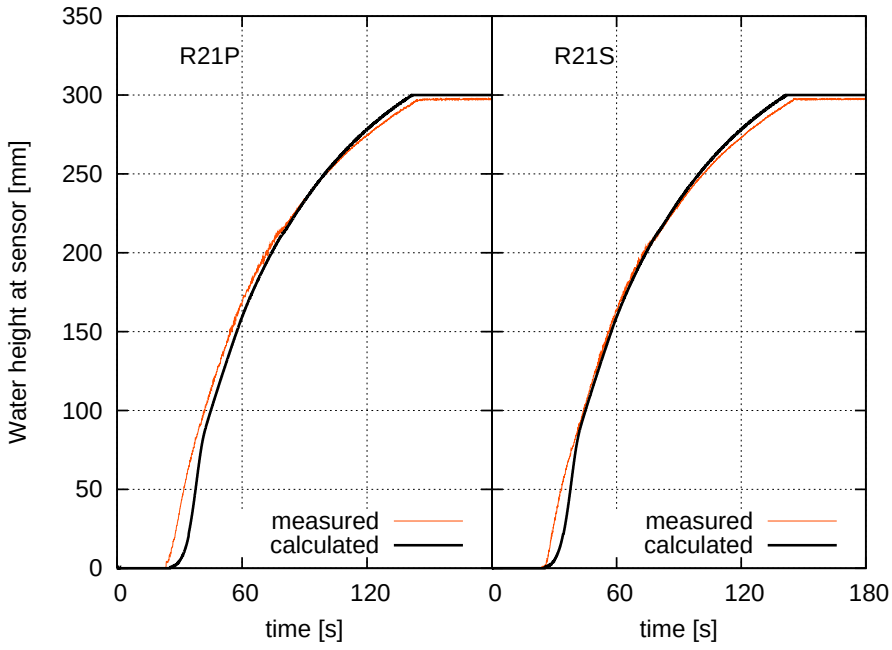

Figure 5.18 Case B – calculated and measured water heights in the rooms R21P and R21S

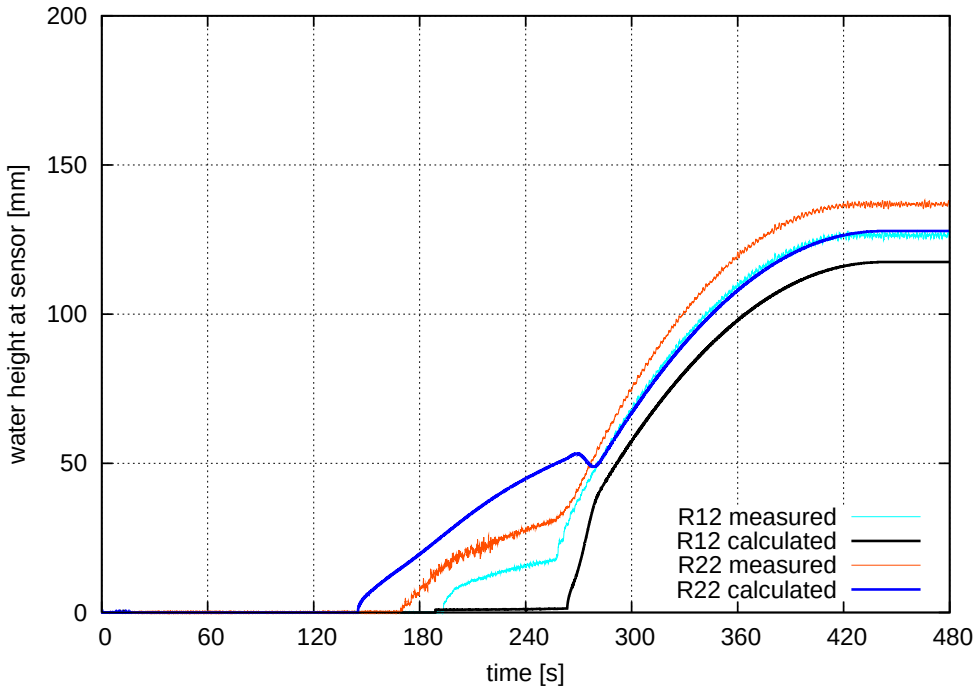

Figure 5.19 Case B – calculated and measured water heights on the upper deck in the rooms R12 and R22

In the double bottom room DB1, there is a significant difference between the measured and calculated water heights, Figure 5.16. This results from the fact that the numerical simulation tool cannot handle the situation, where air escapes in bubbles from an air pocket through the flooding opening. Some video captures of the bubble flow are shown in Figure 5.20. Instead, the calculated air pressure in the air pocket rises so much that it prevents further flooding of this room. The phenomenon is discussed in section 2.3.3. Consequently, the calculated volume of the air pocket is much larger than it actually was in the experiment. Correspondingly, the calculated air pressure is higher than that measured, Figure 5.15. Also, the calculated trim angle and heave motions of the barge are slightly under-estimated since the volume of flooded water is smaller than in reality, see Figure 5.13 and Figure 5.14.

Qualitatively, the calculated air pressure in DB1 corresponds well with the measurements (Figure 5.15) and even the sudden pressure increase at $t = 150$ s (when the room R21 is filled up) is predicted properly.

The calculated water heights on the lower deck correspond very well with the measurements (Figure 5.17 and Figure 5.18).

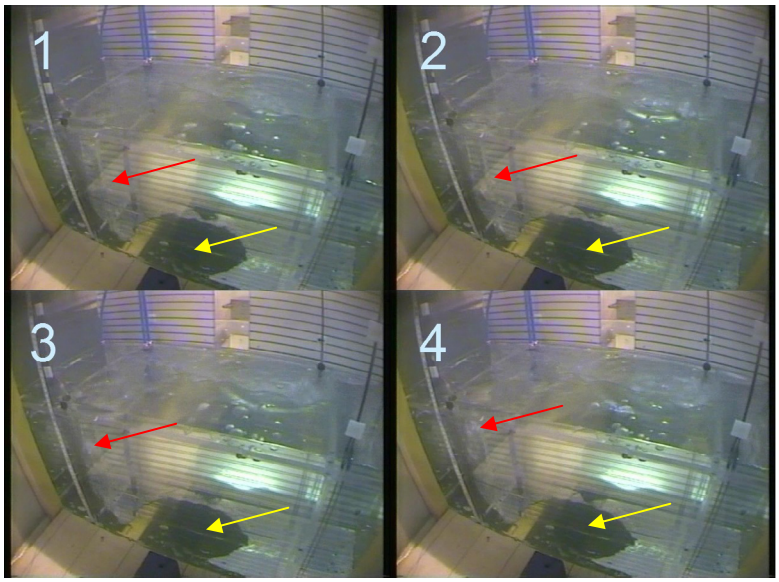

Figure 5.20 Video captures from an in-model camera showing the air bubble flow (pointed by the red arrows) from the double bottom; the period between the captures is 0.08 s; the dark area (pointed by the yellow arrows) is a thin air pocket on top of the double bottom

The calculation of down-flooding from R12 to R11 did not produce any problems. During this phase, the water height in R12 remains minimal (Figure 5.19), which is rather realistic. The measured water height is larger, but this difference is likely caused, at least partially, by the exclusion of surface tension.

About 200 iteration rounds were needed per time step. Due to the very slow rise of the water level in room DB1, more under-relaxation was applied after this room was flooded. Consequently, a factor $\alpha = 0.1$ was used for most of the steps. This ensured the convergence but also slowed it down. In fact, about five times more iteration rounds were needed than in the case A. When all rooms were modelled to be fully vented, only 77 iteration rounds per time step were needed on average.

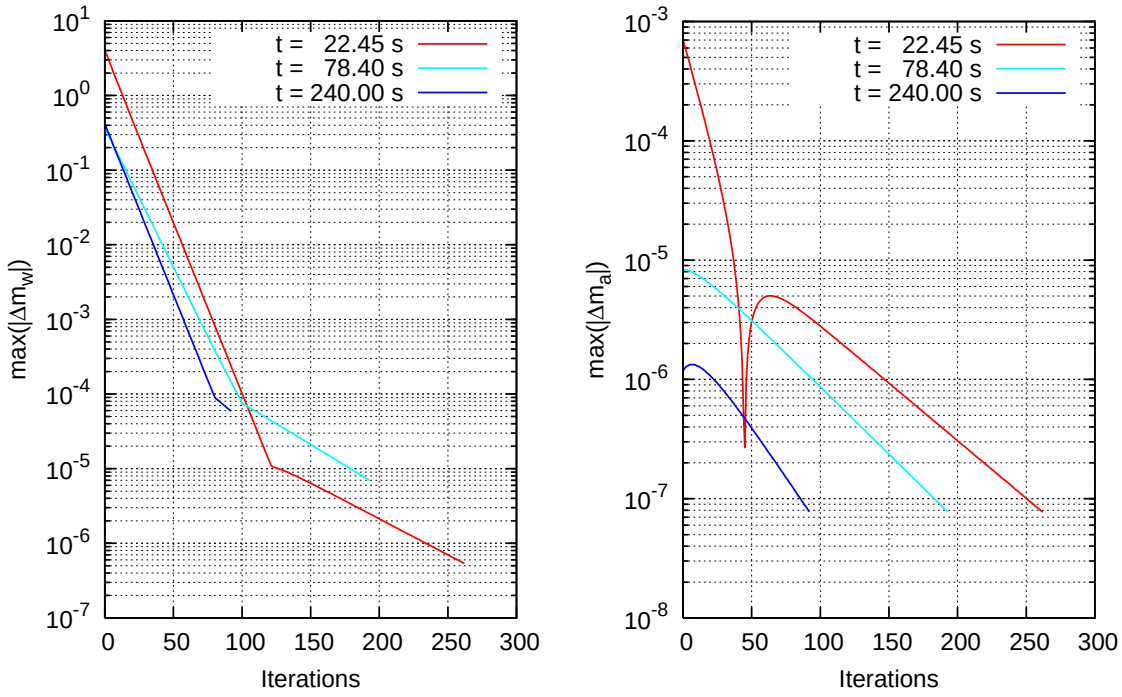

Figure 5.21 Examples of the convergence in the validation case B

Some examples of the convergence are presented in Figure 5.21. At $t = 22.45$ s up-flooding from the damaged room DB2 to R21 starts, at $t = 78.40$ s the openings to R21P and R21S become fully submerged and at $t = 240.00$ s there is down-flooding from R12 to R11. In all of these steps the applied under-relaxation factor was $\alpha = 0.1$ and hence the convergence is rather slow, yet the residuals decrease steadily, except for the air at $t = 22.45$ s. In the early phases of the flooding, the residuals for water drop several decades, while later the decrease is much slower.

5.3.3 Validation Case C – Slow Progressive Flooding

The damage opening (60 mm × 40 mm) is located in the bottom of the aft compartment (DB1) and the watertight (WT) door on the upper deck is closed (Test05 in *Ruponen, 2006b*). Water proceeds from the damaged room to the forward compartment (DB2) through a small opening (diameter 20 mm) and further up to the lower deck (R21). The chain of flooded compartments is relatively long (five rooms). The phases of the flooding process are presented in Figure 5.22. The time-to-flood is long since the floodwater must flow through several openings in order to reach all flooded rooms.

The results are presented in Figure 5.23 – Figure 5.29. Due to the symmetrical flooding in transverse direction and the large initial stability of the model, both measured and calculated heeling angles were zero throughout the flooding, and hence they are not included.

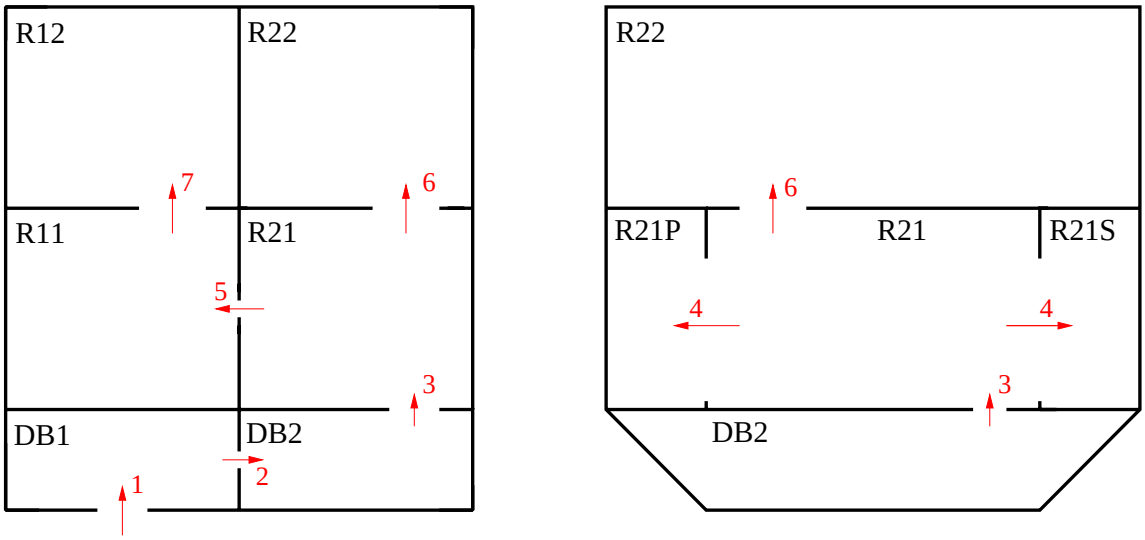

Figure 5.22 Progress phases of the flooding in the validation case C

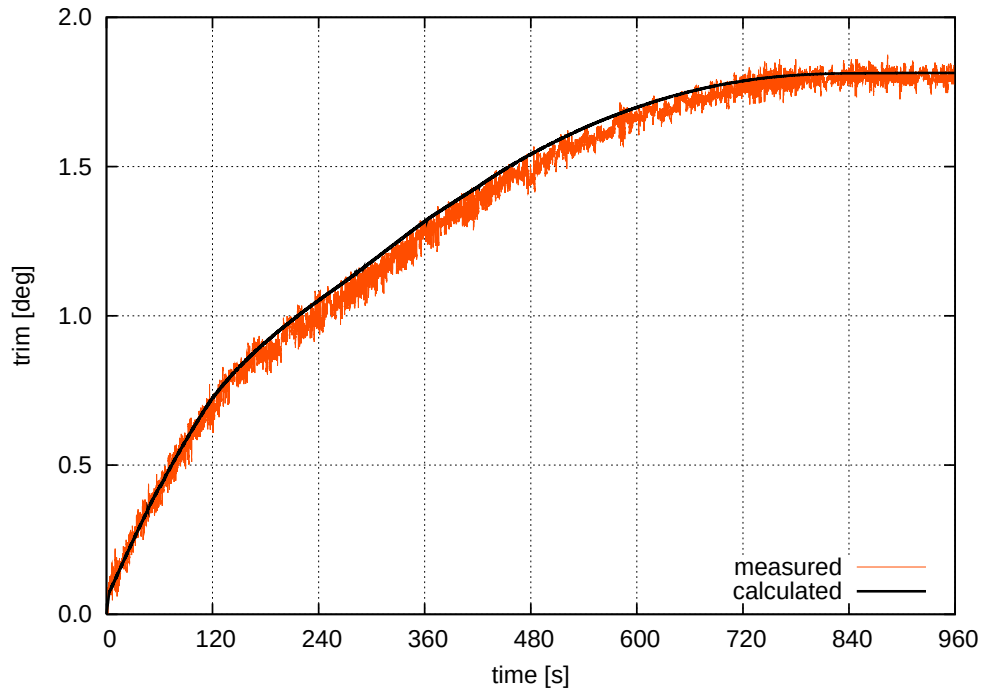

Figure 5.23 Case C – calculated and measured trim angle

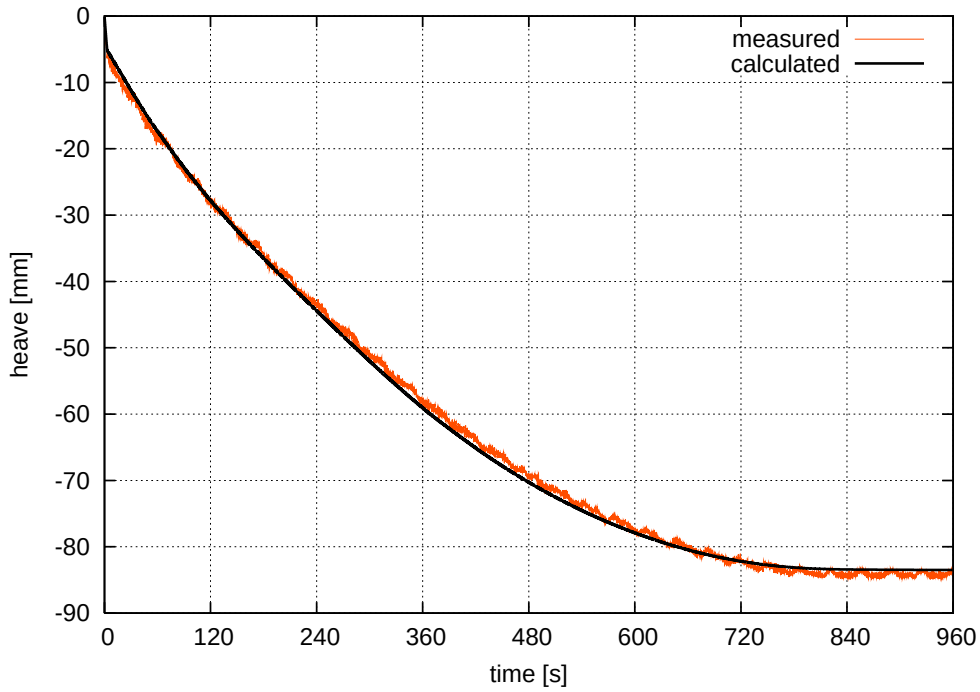

Figure 5.24 Case C – calculated and measured heave motion

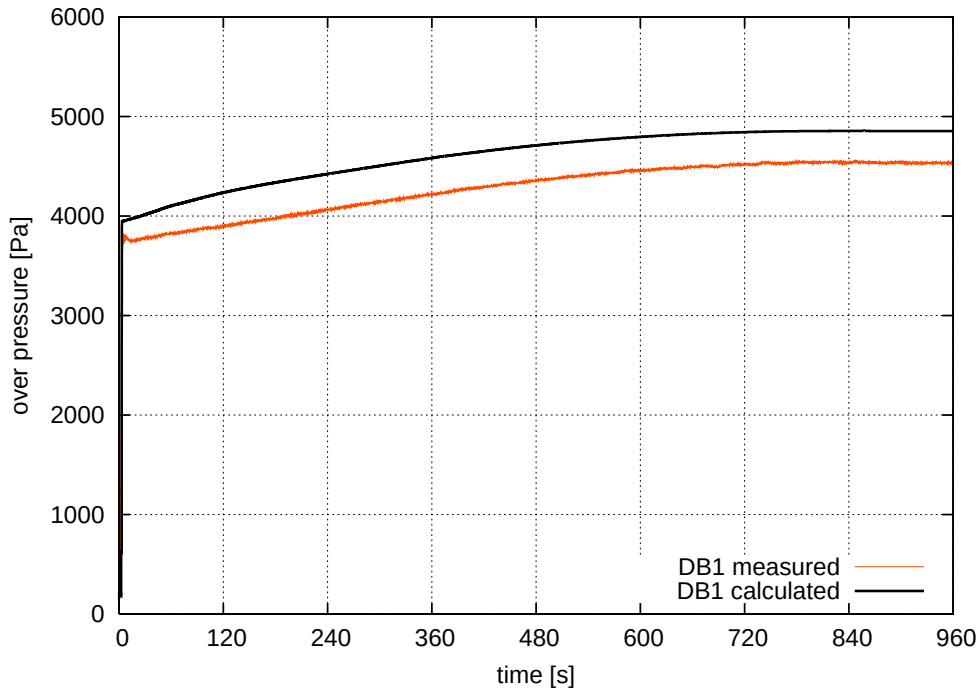

Figure 5.25 Case C – calculated and measured over pressure of the air pocket in the room DB1

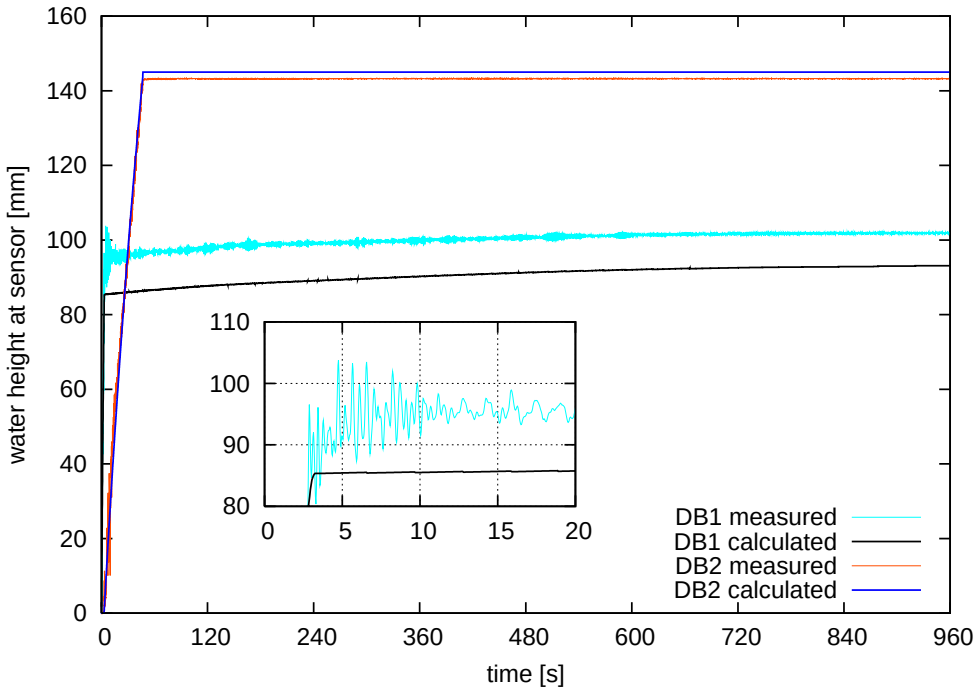

Figure 5.26 Case C – calculated and measured water heights in the double bottom rooms DB1 and DB2; the smaller figure shows a detail from the start of the flooding

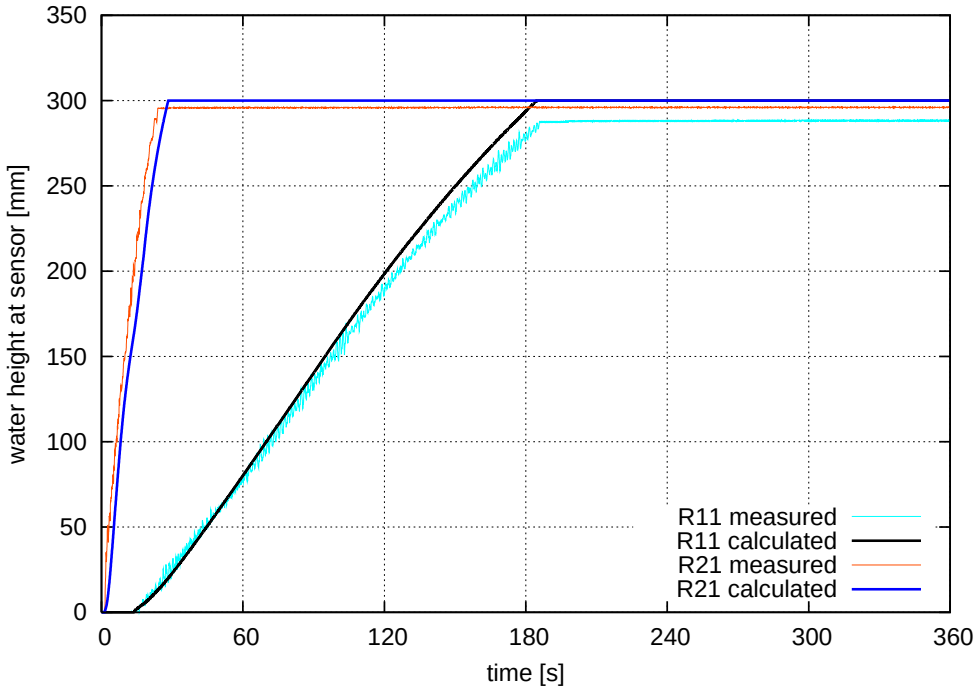

Figure 5.27 Case C – calculated and measured water heights on the lower deck in the rooms R11 and R21

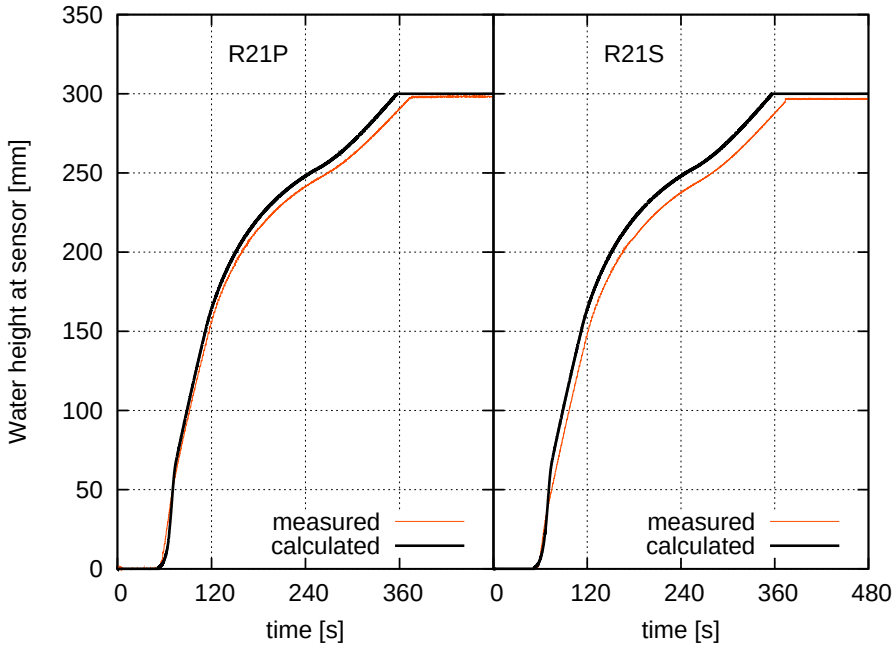

Figure 5.28 Case C – calculated and measured water heights in the rooms R21P and R21S

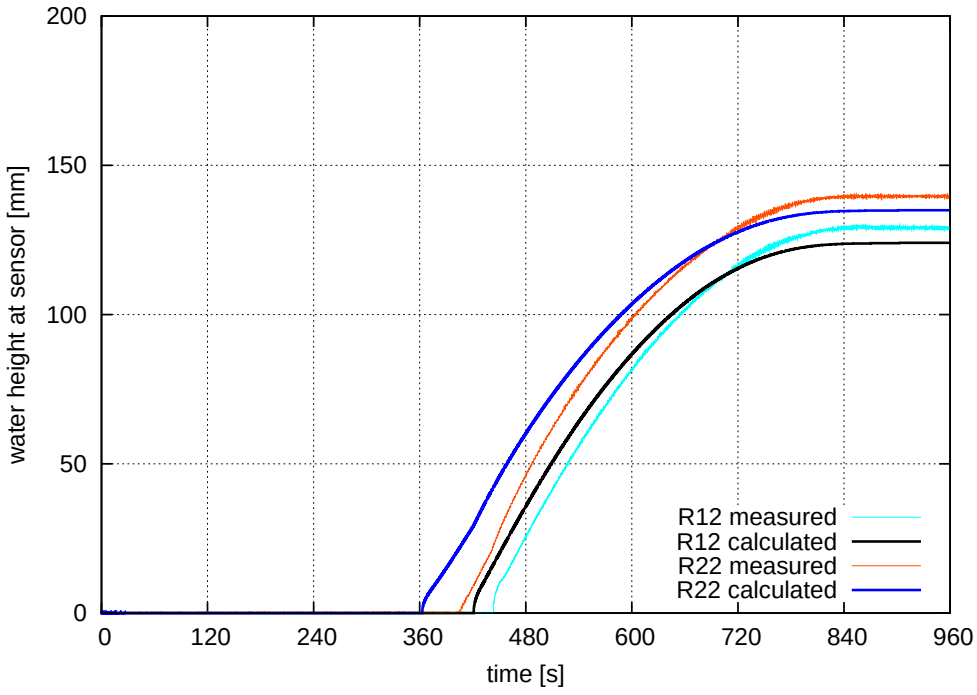

Figure 5.29 Case C – calculated and measured water heights on the upper deck in the rooms R12 and R22

The calculated floating position corresponds very well with the measurements throughout the flooding process (Figure 5.23 and Figure 5.24). In general, very good results were obtained for the water heights as well. However, the water height in the damaged room DB1 is under-estimated by 8 mm. The difference originates from the start of the flooding, where high waves due to the very fast flooding are formed, see Figure 5.26. These waves allow more air to escape to DB2 than predicted by the simulation method, which is based on the assumption of flat water surfaces. Correspondingly, the air pressure in the damaged room is slightly over-estimated by the simulation (Figure 5.25).

The calculated water heights on the lower deck correspond well with the measurements (Figure 5.27 and Figure 5.28). However, the difference between the measured and calculated results increases slightly towards the end of the flooding in these rooms. This may be caused, at least partially, by the under-estimation of the pressure losses in the openings when the jet discharges into water since the applied values were obtained from tests, where the jet discharged into air. The water heights on the upper deck are estimated well (Figure 5.29); only the flooding is predicted to start about 40 s too early due to the slightly over-estimated flooding of the lower deck.

On average, 40 iteration rounds were needed per time step. On a few occasions the iteration did not converge properly, in which case the iteration was restarted with more under-relaxation. This procedure ensured convergence in all time steps. An example of this is given in Figure 5.30. These kinds of convergence problems were observed mainly near the final equilibrium condition, where the time derivatives of the pressures were very small.

Significantly less iteration rounds were needed (27 on average) when all rooms were modelled as fully vented.

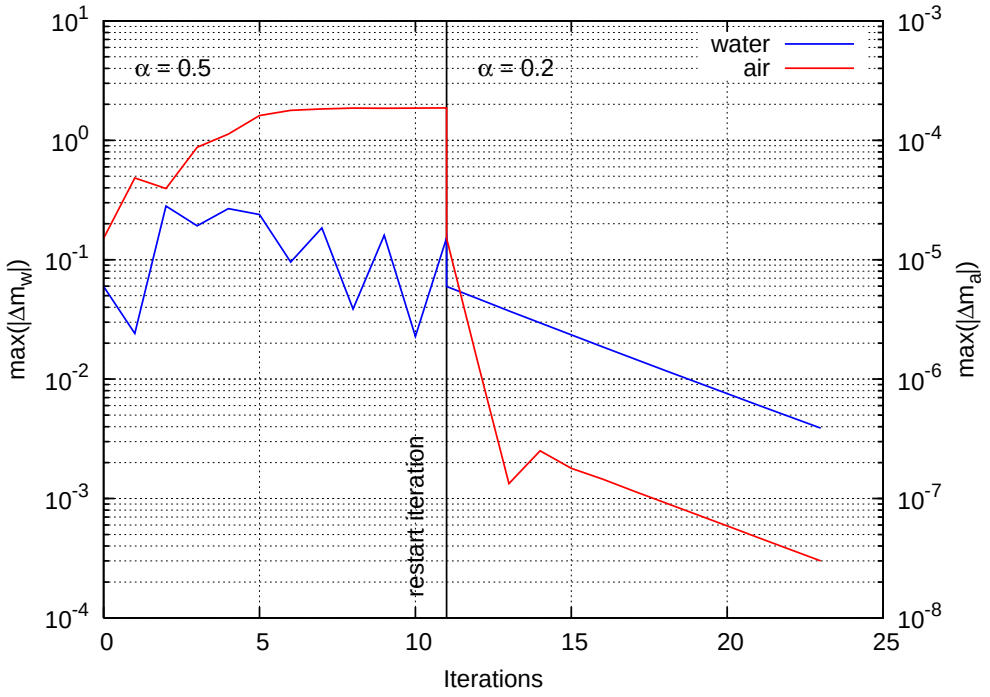

Figure 5.30 Example of a situation, where more under-relaxation is needed in order to achieve convergence (*t* = 784.65 s, i.e. near the equilibrium)

5.4 Conclusions from the Validation

The correspondence between measured and calculated floating position is generally very good. The small differences in the test case B are explained by the fact that the mathematical model could not take into account the escape of air from the double bottom compartment DB1 in a bubble flow through the rooms DB1 and R21. Excellent correlation between measured and calculated results is found in the cases A and C, where practically all the assumptions of the simulation method are valid and there was no notable bubbling of air during the experiment.

The calculated water heights correspond well to the measurements. Only in the beginning of test A, the results are only moderate due to the fact that the jet flew straight from the damage opening to undamaged rooms. Also the pressure in the air pocket in DB1 was estimated well with the simulation method and the qualitative correspondence is excellent.

In general, the pressure-correction iterations converged properly and relatively fast. However, in some cases more under-relaxation was needed in order to avoid diverence.

Furthermore, for some time steps, up to a thousand iteration rounds were needed, although there was no sign of actual convergence problems. In principle, more under-relaxation means slower convergence, and hence small values of α should not be used unless it is necessary in order to avoid divergence.

Case B required many more iterations per time step than the cases A and C. This was mainly caused by the large air pocket in the double bottom room DB1, preventing flooding from DB2. Also the down-flooding phase could have affected the convergence. However, when the convergence is compared to the simulation of the same case with fully vented rooms, the increase in the average number of iteration rounds is much larger in the case B than in the case C. This implies that the air pocket in DB1 causes the slow convergence.

In the presented simulations, the tall openings (R21-R21P, R21-R21S and R12-R22) were modelled as lines with a constant width. For these openings this technique should provide more accurate results than the first simulations (*Ruponen et al., 2006*), where these openings were modelled with 8 evenly distributed points. An example of the comparison for the water heights in the side rooms (R21P and R21S) in the validation case A is shown in Figure 5.31. The applied modelling technique for the openings has only a small effect on the result. However, neither technique results in good correlation with the measurements since the jet from the damage opening discharges partly to other rooms as well, as described in section 5.3.1. For other rooms, especially in the cases with slower flooding (i.e. cases B and C), the difference between the calculated results is much smaller. However, it is believed that the line opening should usually be more realistic than several opening points, besides it is easier to model in the grid generation.

In order to study the effects of the applied pressure correction equation for air pressures, some simulations were also performed by using the fully coupled pressure corrections. The applied pressure-correction equations do not affect the results of the simulation when the same time step and convergence criteria are applied.

The full coupling between the air pressure corrections and water height corrections allowed a slightly longer time step and the need for under-relaxation was reduced. However, the full coupling also slightly increased the number of iteration rounds and the solution of the pressure corrections was slower since the corrections could not be solved in two separate phases. For example, the calculation time was about 30 % shorter with the case C when the simplified version of the pressure-correction equation was used.

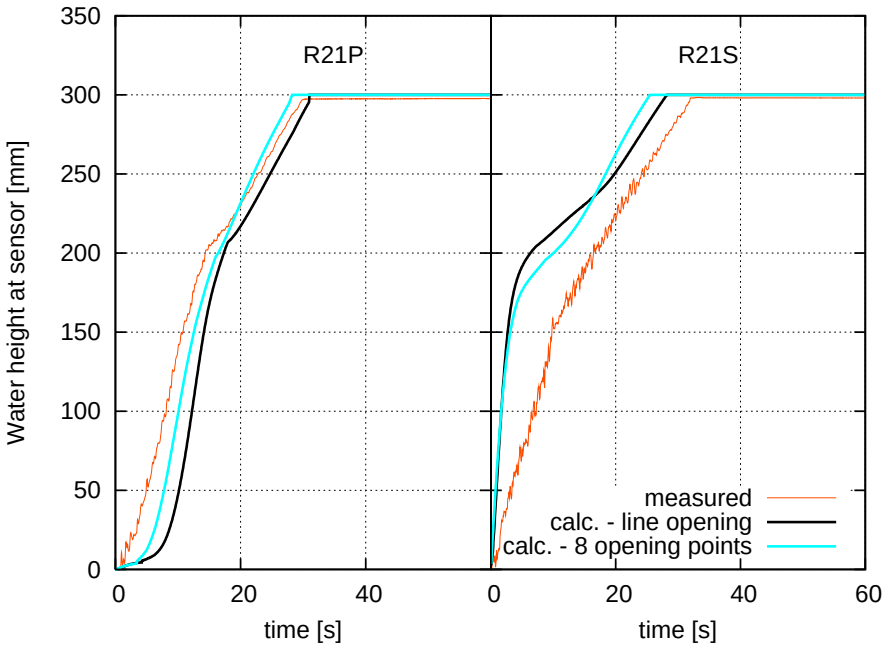

Figure 5.31 Effect of the modelling technique for the high openings (water heights in the side rooms in the validation case A)

6 Case Studies

6.1 General

6.1.1 Motivation

In addition to the validation of the developed method, also some case studies have been performed in order to check the capability to deal with realistic ship geometry and damage cases. The first case study, concerning the flooding of crew cabin and store compartments of a large passenger ship, was presented in *Ruponen et al. (2006)*. This study showed that the results depend on the applied modelling accuracy. Consequently, the applied detail level for modelling was selected on the basis of the results from this previous study.

This case study aimed at testing of the developed simulation method with realistic ship geometry and with an arrangement containing a large number of rooms and openings. The intention was not to investigate the survivability of the studied ship. Therefore, the damage scenarios for progressive flooding may not be very realistic as they were selected so that the flooding of the ship would be very complex and involve many different phenomena that might prove to be problematic to solve.

6.1.2 Details of the Passenger Ship

The studied ship is a modified version of a real passenger ship design. The side profile of the ship is presented in Figure 6.1. The length of the ship is 193 m and the gross tonnage (GT) is approximately 40 000.

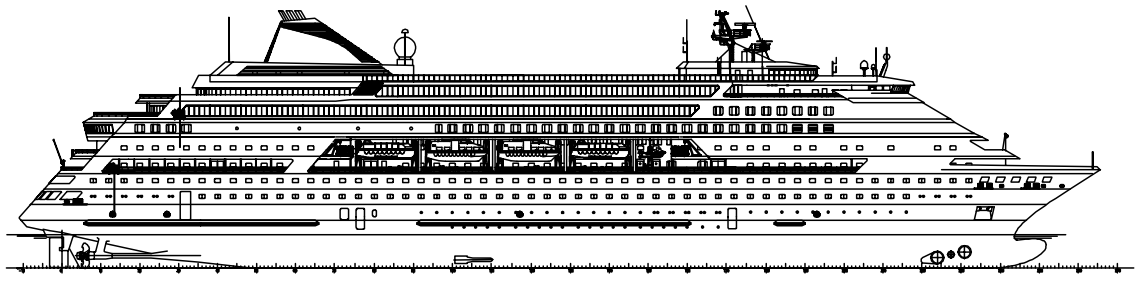

Figure 6.1 Profile of the studied passenger ship

All presented simulations were performed using an intact condition, where the draft is 6.0 m and the metacentric height is 2.38 m. All tanks are considered to be either full or empty so that there is no moving liquid load.

6.2 Cross-Flooding

Time-domain simulation tools have been used for cross-flooding calculation ever since the first codes were developed. *Vredeveldt and Journée (1991)* have validated their method with model tests for cross-flooding in a box-shaped ship. Later *Mustonen (1998)*, *Xia et al. (1999)*, *Palazzi and de Kat (2002)* and *Peters et al. (2003)* have presented similar studies for the effectiveness of various cross-flooding arrangements. All of these studies, except *Peters et al. (2003)*, considered also the effects of air compression.

In this study, the applicability of the developed simulation method for the estimation of the cross-flooding time is tested. This is a typical design case, where time-domain simulation of flooding can be used to provide new insights and to define the sufficient area for the tank air pipes.

The side tanks of a U-shaped void are connected through a single cross-flooding opening with an area of 2.0 m^2. Both the damaged and the equalizing side tank are equipped with an air pipe. The inlet of the pipes is in the top of the tank and the outlet is in the atmosphere, high above the bulkhead deck. The cross-sectional area of the air pipe is 0.2 m^2, i.e. 10 % of the area of the cross-flooding opening. The modelled connections are shown in the cross-section of the damage compartment in Figure 6.2. The net volume of each side of the U-void is 417.5 m^3. A constant discharge coefficient $C_d = 0.6$ was applied for both the openings and the air pipes.

Two different scenarios were investigated. First, also the damage opening, with an area of 5.0 m^2, was modelled 2.0 m below the intact water line; and the simulation was started with the creation of the damage. In the second approach, the damaged tank was flooded instantly before the equalizing flooding through the cross-flooding opening started. The same approach is used in the *IMO Resolution A.266 (VIII)*. In practice, this was done by considering the damaged part of the void as lost buoyancy.

Both cases were also tested with the area of the air pipes halved and with the assumption of full ventilation in the tanks.

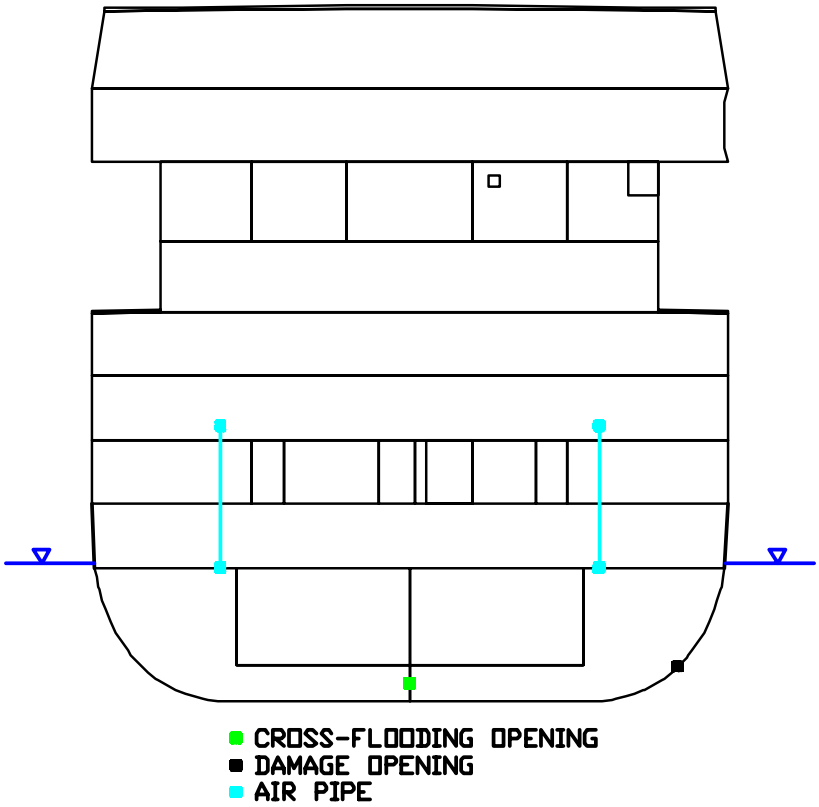

Figure 6.2 Cross-section of the rooms and openings in the cross-flooding case

Simulations were performed with a constant time step of 0.2 s and the applied convergence criterion corresponds to a water height difference of 0.1 mm. A stricter criterion or a shorter time step did not have any notable effect on the results. On average, 11 pressure-correction iterations were needed per time step. The ventilation level (i.e. the air pipe diameter) and the modelling of the damage did not affect the convergence. Examples of the convergence at three time steps in the case, where the damage opening was modelled and the air pipe size was reduced by 50 %, are shown in Figure 6.3. The iteration converges smoothly and rather fast even though the applied under-relaxation factor is 0.5. The residuals decrease about three decades. This decrease is smaller near the equilibrium condition since the time derivatives of the pressures are then smaller. Consequently, the initial guess values for the iteration from the previous time step are much closer to the solution.

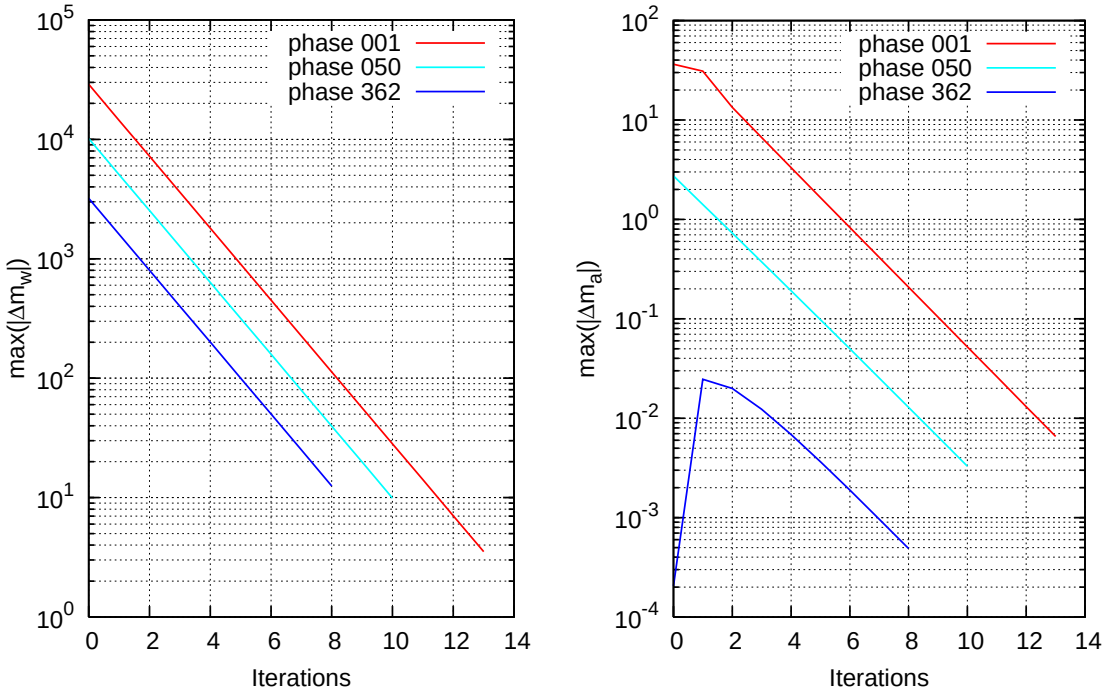

Figure 6.3 Examples of the convergence for water (left) and air (right) on three different time steps: t = 0.2 s (phase 001), t = 10.0 s (phase 050) and t = 72.4 s (phase 362)

The case was also calculated according to the *IMO Resolution A.266 (VIII)*, which is based on the equations derived in *Solda (1961)*, assuming that no air compression takes place. The applied pressure losses were selected so that the discharge coefficient, equation (2.6), is 0.6 as used in the simulations. Therefore, $\sum k_L \approx 1.78$ is used. This corresponds well to the proposed revision of the Resolution A.266, *IMO SLF 50/10 (2007)*, where $k = 2.8$ is suggested for a single orifice, and the unity in the formula for the flow reduction coefficient, equivalent to equation (2.6), is omitted. The procedure in the NAPA software was used for the calculation; resulting in an equalizing time of 52 s. this is in good correlation with the simulation results when the air pipes are large (10 % of the cross-flooding opening) or when full ventilation is assumed.

The results of the simulations are presented in Figure 6.4 and Figure 6.5. During the first 4 seconds, the flooding is independent of the air pipe size. After that period, air in the damaged side is compressed so much that it delays the flooding, and consequently, decreases the maximum heeling angle, when compared to the fully vented case. If the

damaged room is considered to be flooded immediately, as in the Resolution A.266, the decrease of the air pipe size only delays the equalization.

The roll motion is very slow in both damage scenarios. Therefore, it is believed that the quasi-stationary approach is a reasonably good approximation in this particular case.

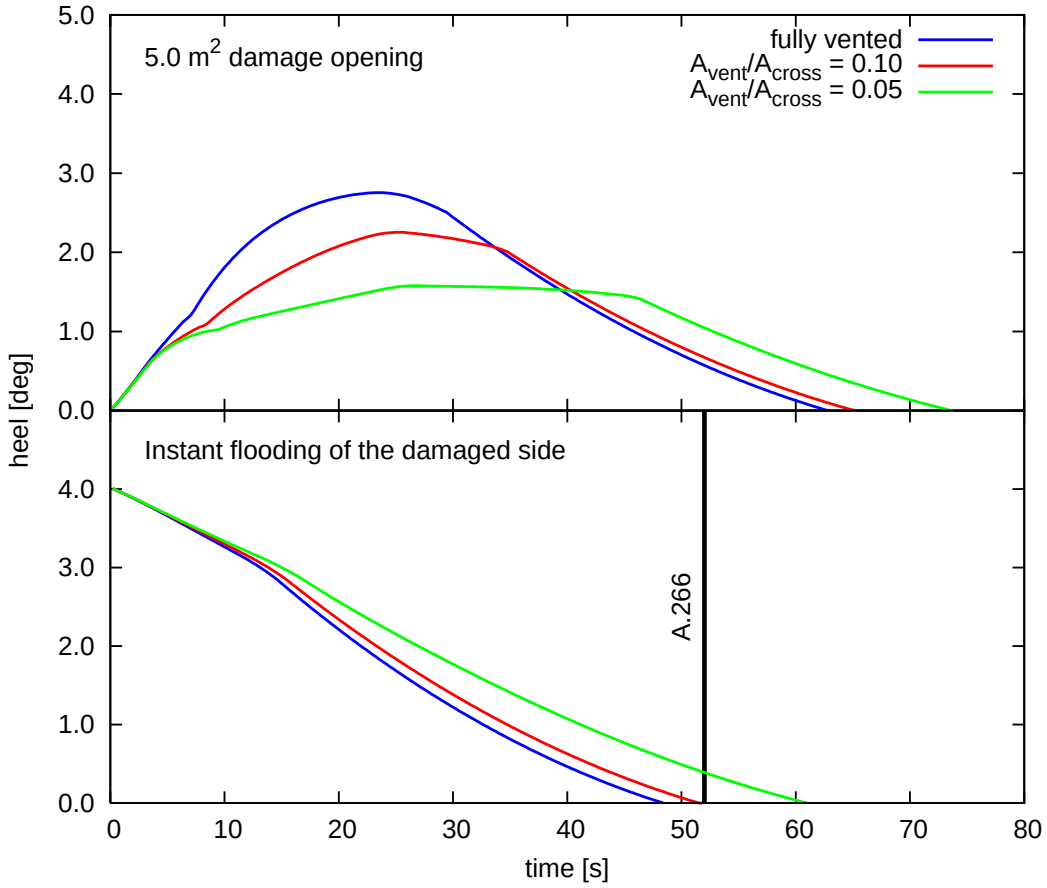

Figure 6.4 Calculated heel angle during the cross-flooding with two different approaches: simulation is started from the creation of the damage opening (above) and from the instantly flooded damaged room (below)

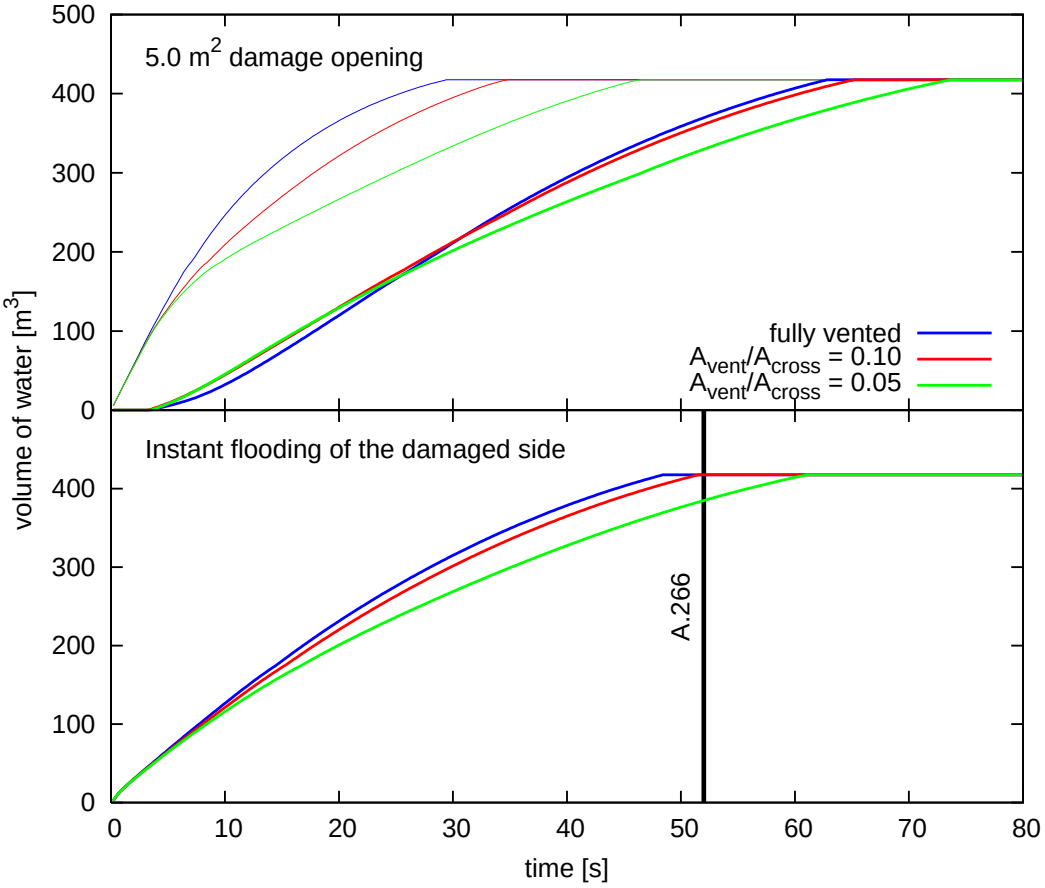

Figure 6.5 Calculated volumes of water during the cross-flooding with two different approaches: simulation is started from the creation of the damage opening (above) and from the instantly flooded damaged room (below); the thin lines represent the damaged room and the thick lines represent the equalizing room

6.3 Progressive Flooding

6.3.1 Damage Case

The studied case is an extensive damage in the starboard side of the ship, for example due to a grounding to a reef, see Figure 6.6. Four watertight compartments are flooded and the damage length is 30.8 m, which is far beyond the so-called SOLAS damage, where the damage length ($3\text{ m} + 0.03 \cdot L_{pp} = 8.129\text{ m}$) is calculated on the basis of the ship's length between perpendiculars L_{pp}.

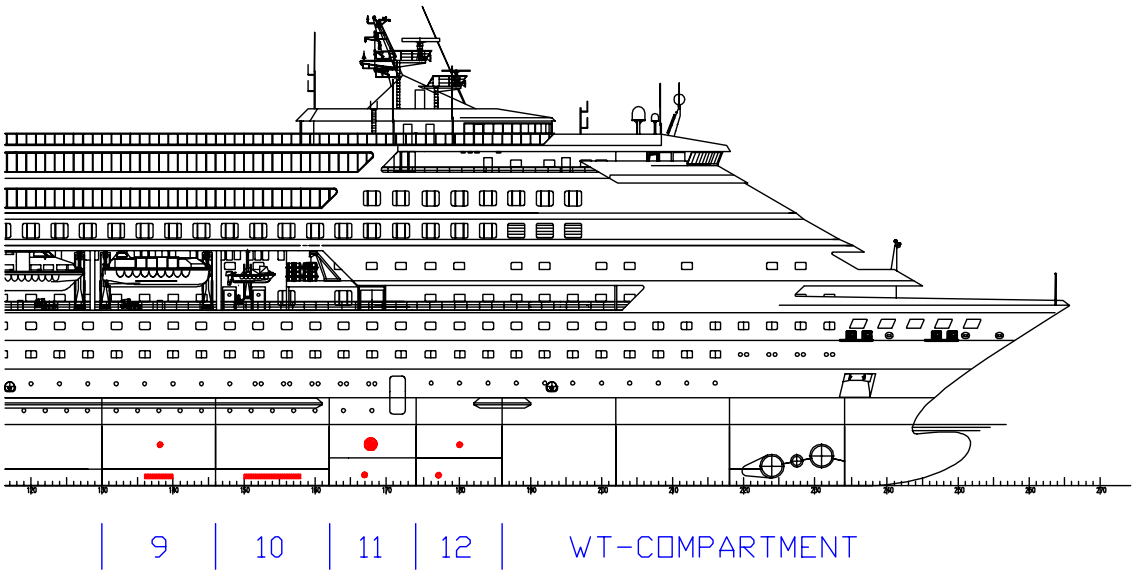

Figure 6.6 Modelled damage openings (red)

Table 6.1 Details of the damage openings

WT-comp.	Deck	Height from BL	Area	Modelling type
9	DB	1.0 m	0.5 m^2	Line
10	DB	1.0 m	0.5 m^2	Line
11	DB	1.0 m	0.5 m^2	Point
12	DB	1.0 m	0.5 m^2	Point
9	Deck 1	4.0 m	0.2 m^2	Point
11	Deck 1	4.0 m	5.0 m^2	Point
12	Deck 1	4.0 m	2.5 m^2	Point

The damage consists of several holes that are presented in detail in Figure 6.6 and Table 6.1. Two damage holes in the double bottom are modelled as narrow horizontal lines while the others are modelled as single points with given areas. A constant discharge coefficient $C_d = 0.6$ is applied for all damage openings.

6.3.2 Modelling of the Flooded Compartments

The detailed model for the flooding simulation includes the potentially flooded rooms and openings below the bulkhead deck (deck 3) in the four damaged WT-compartments (identified with numbers 9 – 12).

The feasible modelling of cabin areas has been discussed in *IMO SLF47/INF.6 (2004)* and *van't Veer et al. (2004)*. *Vartiainen (2006)* has also compared various modelling techniques. In general, it seems to be justified to group several small rooms, such as crew cabins, into larger objects. Furthermore, it is not necessary to model all doors separately so that the total area of the modelled openings corresponds to the sum of the door areas in the group of cabins. This simplification is valid only when both heel and trim angles are small. However, especially heel angle may be significant during the flooding. Therefore, two openings are modelled in transverse direction; one at each end of the grouped room. The modelling principle is presented in Figure 6.7; the version L3 is used for the simulation.

The number of cabins in one compartment of the studied ship is rather small, and hence only up to seven cabins have been grouped together. In general, this corresponds to the highest detail level that was tested in the first case study, presented in *Ruponen et al. (2006)*. Consequently, it can be considered that there is no need to study the effects of the modelling accuracy since the applied model of the ship is already considered to be as accurate as possible with feasible modelling work. The total number of flooded rooms in the model is 67 and the number of modelled connections, including the damage holes, is 81.

The corridors in the cabin areas are modelled as several separate rooms that are connected by openings. This approach is similar to the modelling technique for asymmetric flooding of symmetrical compartments, for example engine rooms, presented in *Santos et al. (2002)*. The connecting openings have the same area as the cross-section of the transverse corridor.

The original general arrangement and the computational grid with all modelled openings for the flooded compartments are presented in Figure 6.8, Figure 6.9 and Figure 6.10 for deck 2, deck 1 and double bottom, respectively. The opening types are presented with colour codes and the hatched areas mark the rooms that are not flooded.

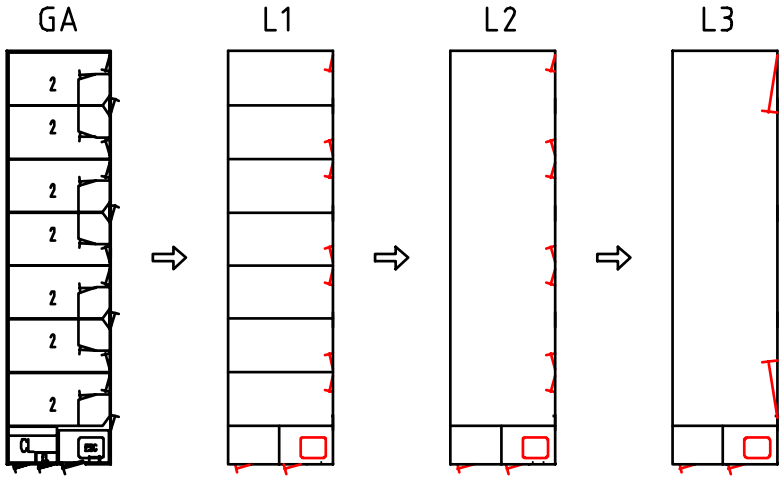

Figure 6.7 Simplified modelling of a group of cabins

The voids in the double bottom (Figure 6.10) are considered to be equipped with sufficient ventilation pipes. Therefore, on the basis of the cross-flooding study (section 6.2), it is assumed that the compression of air does not have a major effect on the flooding since the damage openings to the voids are small. Consequently, all modelled rooms are considered to be fully vented.

The floodwater can progress up to deck 2 through the staircases, escape trunks and in the most forward compartment (no. 12), also through the service lift shaft and the dirty linen canal. The openings in the decks are modelled as single points with the given area. The portholes of the crew cabins on the deck 2 are considered to be watertight, and thus they are excluded from the model.

The aim of this case study is to test the applicability of the developed simulation method, not to assess the survivability of the ship. Therefore, contrary to the regulations and good seamanship, two watertight (WT) doors on the deck 2 are considered to be open throughout the flooding process. These openings allow progress of the floodwater also to the undamaged spaces on deck 2 in the compartments 9 and 11. The damage opening on deck 1 in the WT-compartment 9 is small when compared to the damage in the compartment 11. Therefore deck 2 is flooded faster and there is a phase of slow down-flooding from deck 2 to deck 1 through an escape trunk in compartment 9. The assumption of two open WT-doors thus results in a very complex flooding scenario that is considered to be very suitable for testing the developed simulation method.

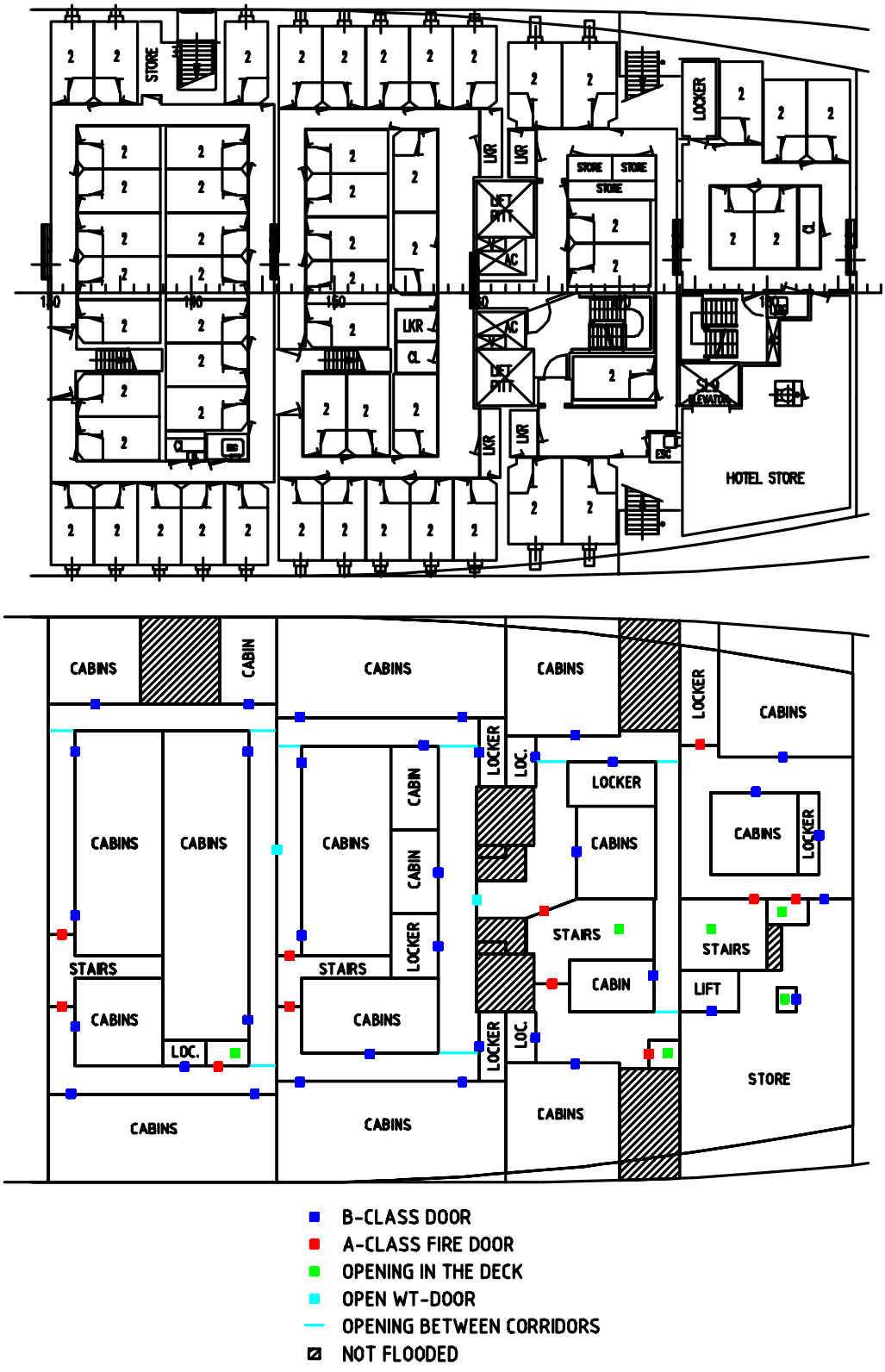

Figure 6.8 General arrangement of the damaged compartments on the deck 2 (above) and the corresponding part of the computational grid for flooding simulations (below)

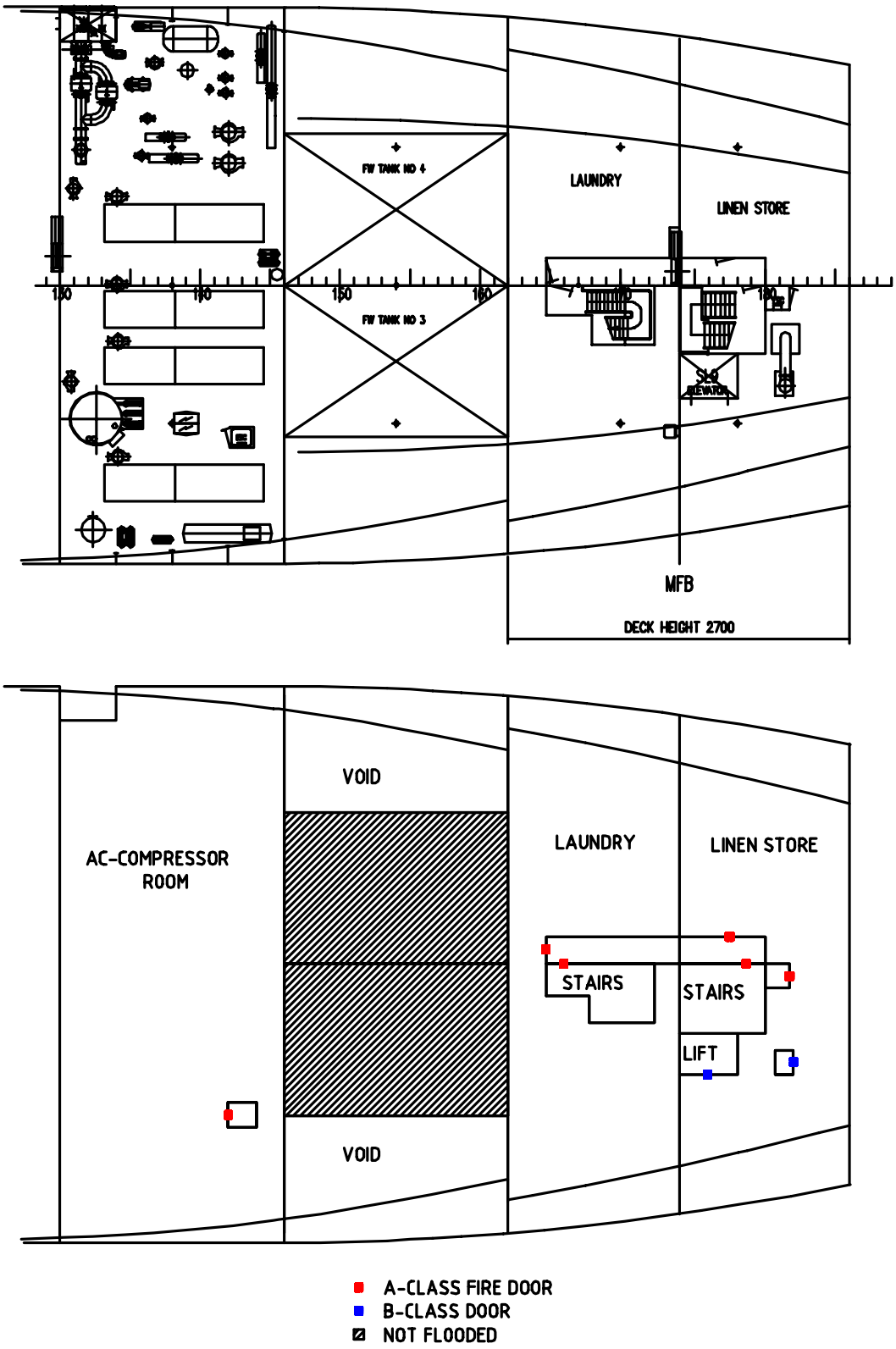

Figure 6.9 General arrangement of the damaged compartments on the deck 1 (above) and the corresponding part of the computational grid for flooding simulations (below)

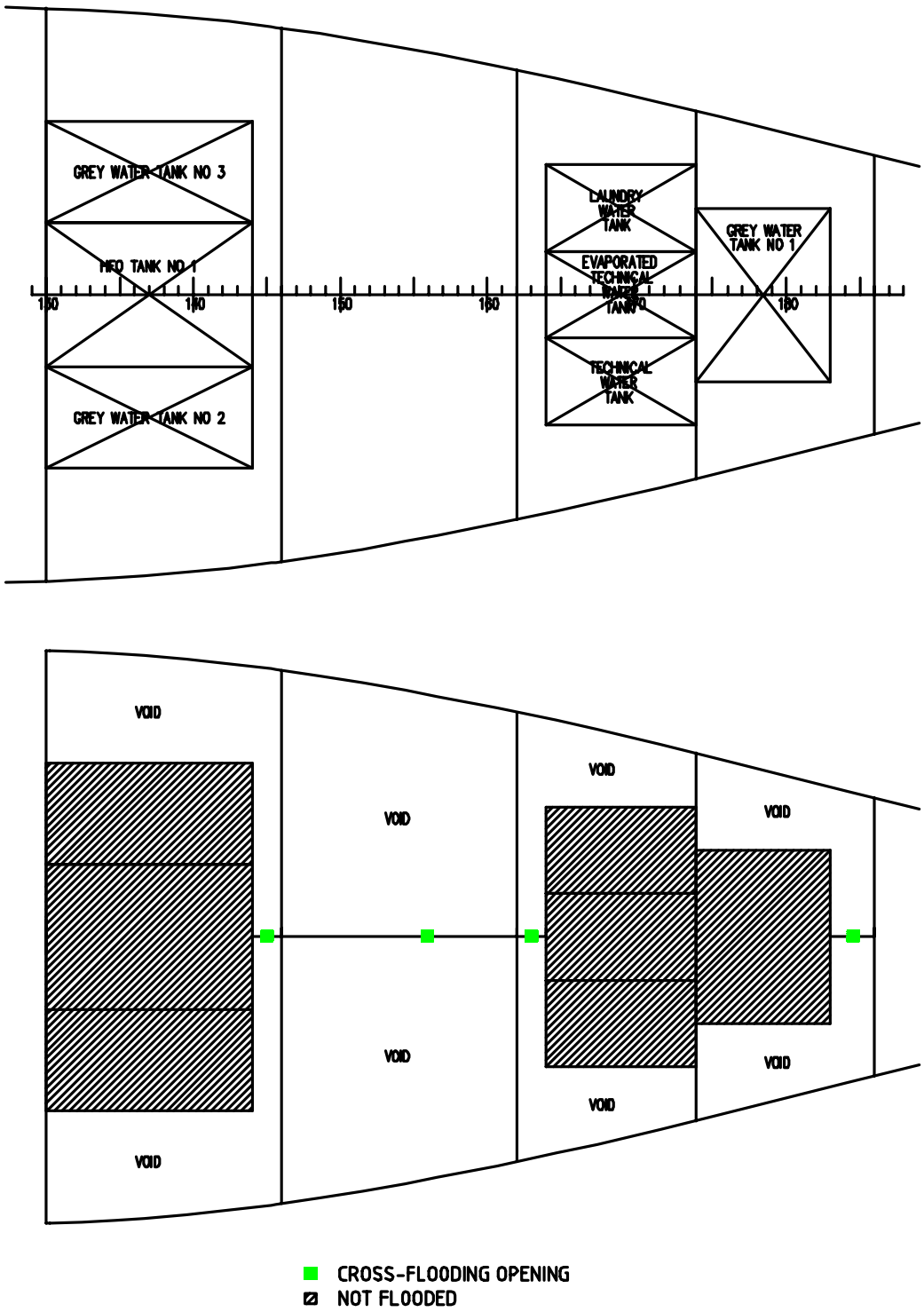

Figure 6.10 General arrangement of the damaged compartments in the double bottom (above) and the corresponding part of the computational grid for flooding simulations (below)

6.3.3 Applied Parameters

The applied permeabilities are listed in Table 6.2. The values were selected on the basis of SOLAS II-2, Regulation 7-3.

Table 6.2 Applied permeabilities

Room type:	Permeability:
AC compressor room	0.85
cabins	0.95
cabin corridors	0.95
laundry	0.95
linen store	0.60
locker	0.60
staircase / lift trunk	0.95
store	0.60
void	0.95

A constant discharge coefficient $C_d = 0.6$ is used for all openings in the case of water flow. This is the value that was suggested in *Vassalos et al. (1997)* on the basis of model test experiments, and it has been widely used in flooding simulations, e.g. *van't Veer (2004)*. However, also other values have been used. *Santos et al. (2002)* used 0.6 only for the damage opening and 0.4 for all internal openings in the flooding simulation of the "European Gateway" accident.

All doors are considered to be closed when the flooding starts, except for the two open WT-doors on deck 2. The critical pressure heads and leaking area ratios, suggested in *IMO SLF47/INF.6 (2004)* are used for A-class fire doors and B-class joiner doors. The values are listed in Table 6.3. The same values were also used in the MARIN study for the time-to-flood analysis of a large passenger ship, *van't Veer et al. (2004)* and *van't Veer (2004)*. It is important to recognize that these values are mainly estimations and they are not based on systematic full scale tests. However, at the moment there is no better knowledge available on this subject.

The closed watertight doors are considered to be tight, not leaking at all, under any circumstances.

Table 6.3 Critical pressure heads for doors and area ratios for leaking doors, *IMO SLF47/INF.6 (2004)*

Door type:	H_{leak} [m]	H_{coll} [m]	A_{leak} / A_{coll}
B-class joiner door	0.0	1.5	0.2
A-class fire door	0.0	2.0	0.1

6.3.4 Simulations

The simulation was performed with a constant time step of 1.0 s. The applied convergence criterion corresponds to a water height difference of 0.05 mm. A shorter time step or a tighter criterion did not cause notable difference in the results. The initial under-relaxation factor was 0.8 and more under-relaxation was applied when the time derivatives of the water heights were very small, i.e. especially near the final equilibrium condition.

6.3.5 Results

The calculated time histories for total volume of floodwater, heel, trim and mean draft are presented in Figure 6.11 – Figure 6.14, respectively. In the beginning, the phase of fast transient flooding takes about 90 s. During this phase the damaged rooms are flooded rapidly, causing a small transient heel. Thereafter, the flooding is significantly slowed down since most of the damaged rooms are filled up with water. The total time-to-flood is 42 minutes.

The maximum heel angle is about 2.5° and it is reached 24 s after the creation of the damage openings. This can be slightly under-estimated due to the assumption of quasi-stationary motions. Furthermore, the exclusion of ship's inertia results in too fast changes of heel angles, also during the phase of progressive flooding. However, these changes are very small. In general, the heel angle is quite small throughout the flooding. Hence the assumption of the quasi-stationary motions is not likely to have a significant effect on the results.

The final floating position is shown in Figure 6.15. The bulkhead deck is submerged at the bow. However, in the flooded compartments the bulkhead deck is just above the sea level and hence the rooms on the deck 3 are not flooded through the staircases from the

damaged compartments. Therefore, in this particular case, there was no need to model these rooms and openings. When the results of a flooding simulation are analyzed, it is necessary to check that no opening that has been excluded from the model was submerged at any stage during the flooding process. Thus for a ship model that is used for flooding simulation onboard the ship, also the rooms and openings on the bulkhead deck must be included.

A slightly more extensive damage or a severe sea state could cause more trim to the bow, thus leading to slow progressive flooding to the bulkhead deck. This might result in the loss of the ship but the long time-to-flood would likely allow enough time for safe and orderly evacuation and abandonment.

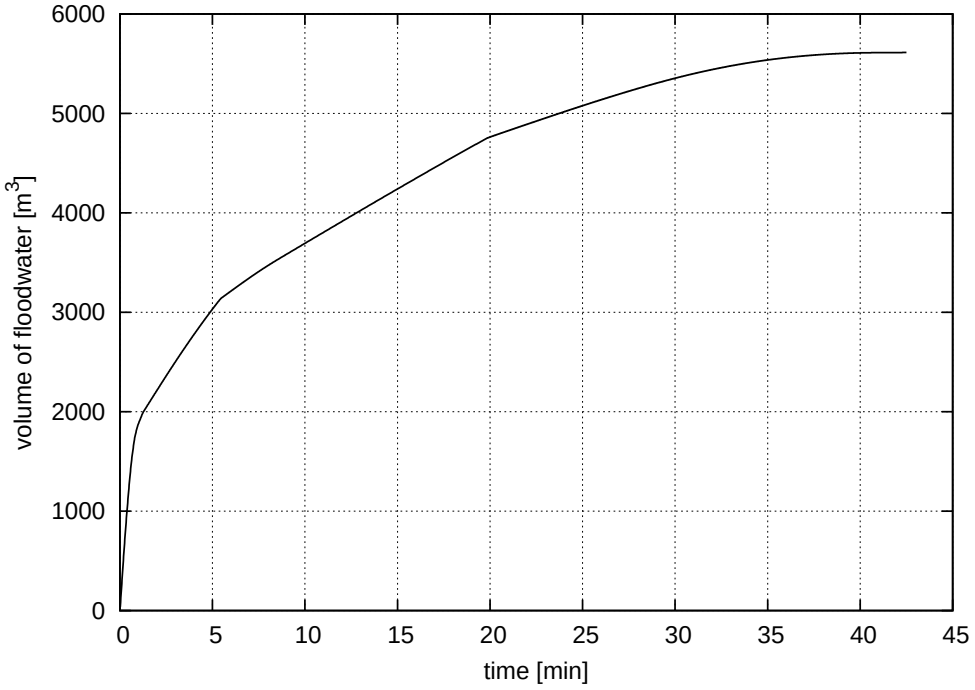

Figure 6.11 Calculated time history for the total volume of floodwater

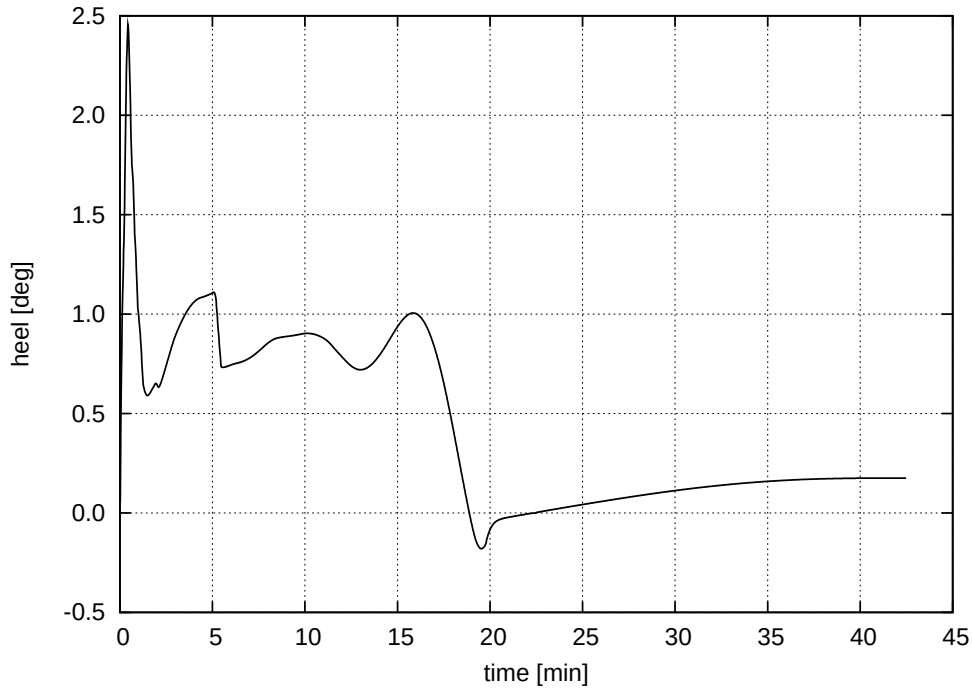

Figure 6.12 Calculated time history for the heel angle

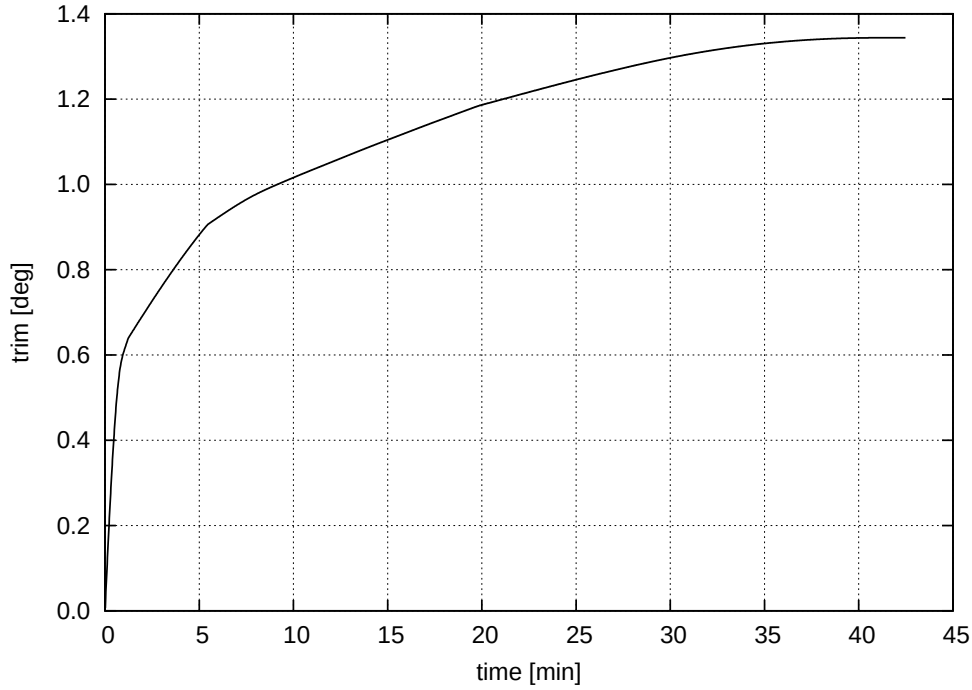

Figure 6.13 Calculated time history for the trim angle

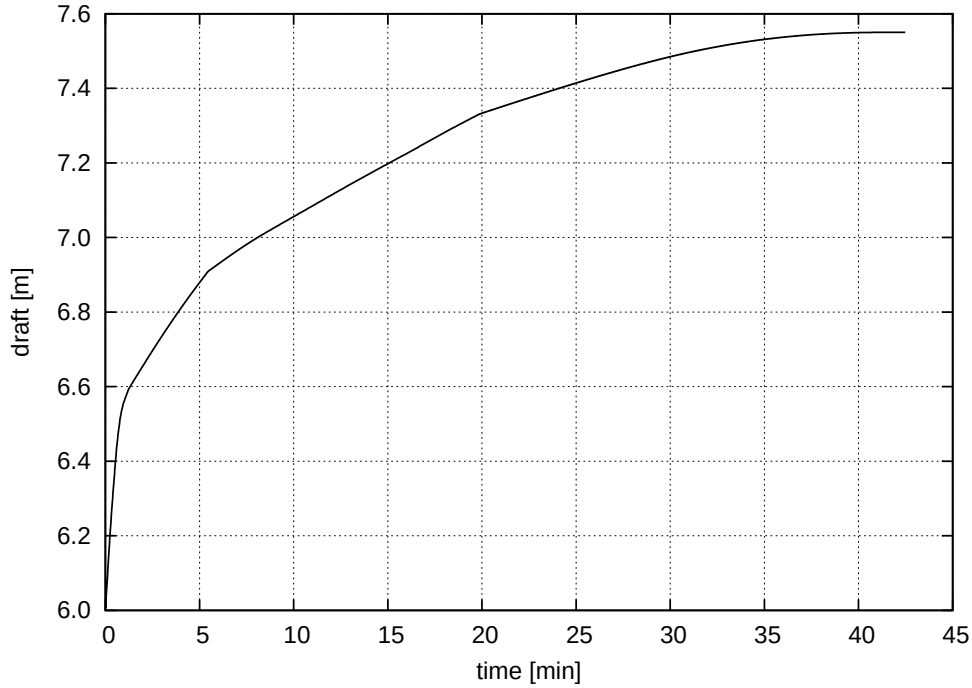

Figure 6.14 Calculated time history for the draft

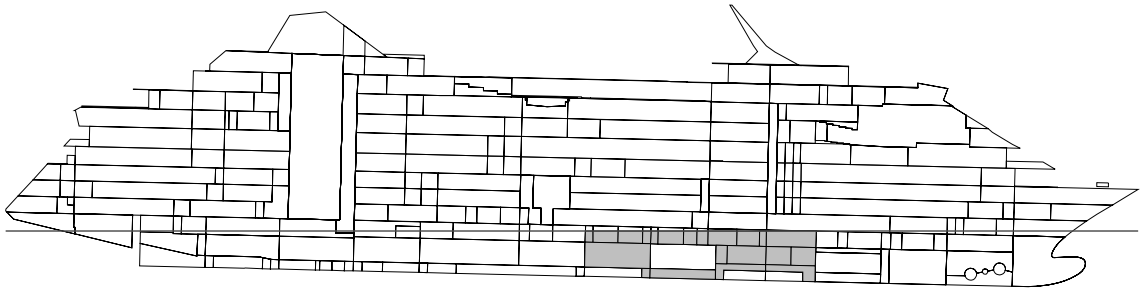

Figure 6.15 Floating position in the final equilibrium condition (the white parts in the four damaged compartments are the non-flooded tanks)

On average 91 iteration rounds were needed per time step. In general the convergence was rather fast. Some examples of the convergence histories are presented in Figure 6.16. The residuals decrease slowly on the time steps, where additional under-relaxation ($\alpha = 0.16$) is applied. However, in some cases, for example at $t = 1973$ s, this seems to avoid the divergence and the iteration is eventually converged. On the other hand, the discontinuities, such as the collapsing of a closed fire door, do not necessary mean slow convergence (e.g. at $t = 40$ s).

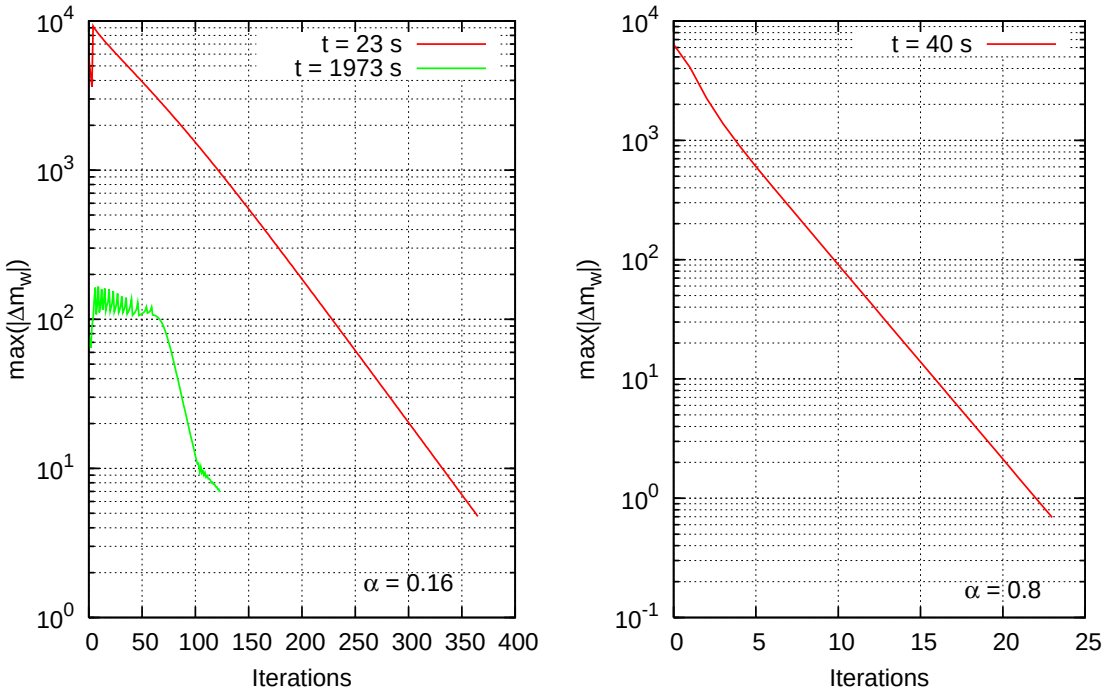

Figure 6.16 Some examples of the convergence in the case study

The down-flooding in the escape trunk in the compartment 9 is subjected to very slow flooding from the corridor on deck 2. Therefore, the calculation of the down-flooding in the trunk requires a lot of iteration rounds. The same phenomenon can be calculated much faster by modelling the whole trunk as a single room (Figure 6.17). This does not affect the results since the openings on the deck are so large when compared to the area of the room. Similar modelling of other vertical rooms, such as staircases, can significantly improve the convergence speed in the case of slow down-flooding.

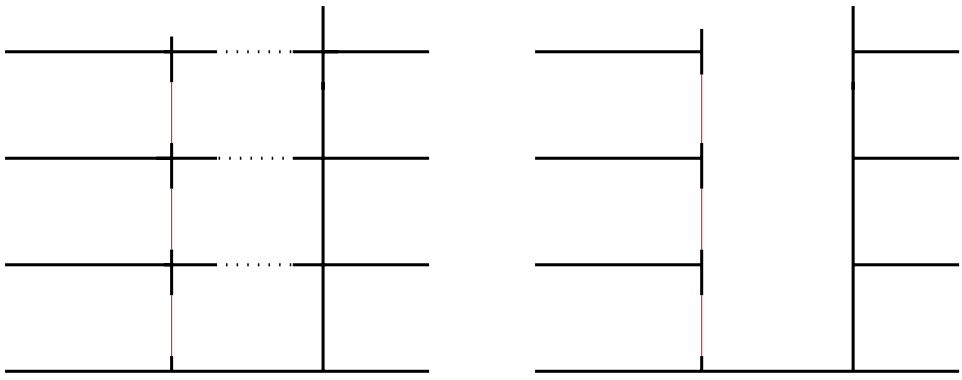

Figure 6.17 Vertical trunk, modelled as separate rooms (left) and as a single room (right)

7 Conclusions

A novel time domain simulation tool for progressive flooding in damaged passenger ships has been developed, using the pressure-correction technique that is well-established in the field of computational fluid dynamics. The implicit and iterative nature of the method ensures solution for complex flooding problems, including air compression and the subsequent airflows. The main emphasis of this study was the efficient and accurate modelling of progressive flooding, and hence the sea is assumed to be calm and a quasi-stationary approach is used for the motions of the damaged ship.

The simulation tool has been extensively validated by performing simulations for three flooding cases of a box-shaped barge and comparing the results with the experimental data. The simulations provide very accurate results for both water heights in the compartments and the floating position. Also the pressure in the air pocket was estimated reasonably well. The applied discharge coefficients for the pressure losses in the openings were known relatively accurately since they were evaluated experimentally by draining water through each opening. Furthermore, the motions of the model were slow, and consequently, the assumption of quasi-stationary motions was justified.

The presented case study simulations for a medium sized (40 000 GT) passenger ship show that the developed simulation method is a suitable and efficient tool for cross-flooding investigations, especially if the counter pressure of compressed air is significant. In the case of full ventilation, the simulation results agree with the simplified calculation method of the *IMO Resolution A.266 (VIII)*.

The study for the slow progressive flooding confirmed that the simulation method can deal with a large number of flooded rooms and openings, including rooms with complex geometry and collapsing non-watertight structures, such as closed doors.

For practical reasons, a rather coarse computational grid is needed for feasible simulation times, especially in the case of extensive progressive flooding. Furthermore, the air compressibility must be ignored in many compartments since it is not practical to model the whole ventilation system accurately enough. In addition, the inertia of the floodwater is not taken into account. These simplifications result in discontinuities in the governing equations and this makes the efficient numerical solution of the problem more complex. However, the developed simulation method can deal with these issues.

In the case of very slow progressive flooding, it is practical to use a longer time step than in the beginning of the flooding. Alternatively, a stricter convergence criterion should be used, but this will further slow down the simulation. The presented simulations were performed with a constant time step, but the method could easily be enhanced to deal with an adaptive time step. However, it must be recognized that for example the collapsing of a closed door may suddenly change the characteristics of the flooding process so that a shorter time step is needed again.

The pressure-correction iterations seem to converge properly but in some cases a little too slow for convenient use since up to a thousand iteration rounds can be needed. Usually, this seems to result from the increased under-relaxation due to small time derivatives of the pressures. Occasionally this procedure is necessary in order to avoid divergence, but in many cases it only slows down the convergence. However, it is believed that these steps can be identified and unnecessary under-relaxation can be avoided in order to speed up the iteration process.

The validation case was in general much more difficult to solve than the flooding of the cruise ship in the case study, since significantly more iteration rounds were needed. This is likely due to the very small air compression in model scale and the very short time step. Consequently, also the under-relaxation was increased. The average number of iteration rounds was substantially decreased when all rooms were modelled as fully vented. Moreover, the calculation of the pressure in the air pocket that prevented flooding from an adjacent room slowed down the convergence in the validation case B, when compared to the similar case C, where such prevention of flooding did not take place. In the experiment, this situation did not occur since air escaped in bubbles from the air pocket, thus allowing slow flooding to the room.

The applied quasi-stationary approach on the motions of the flooded ship evidently restricts the application of the simulation method. This simplification results in under-estimation of the transient heeling in the first phase of the flooding. Furthermore, the resulting time history of the heel angle is not always as smooth as in reality. This is clearly caused by the exclusion of the inertia of the ship. In order to widen the applicability of the developed simulation method, the inertia of the ship should be taken into account, at least in the evaluation of the roll motion.

The pressure-correction equation was simplified by assuming that the corrections of the air pressures are independent of the water height corrections. As a result, the solution of the pressure corrections becomes much easier and faster. All the cases in this study

could be solved by using this simplified version, where the air pressure corrections are solved first and the results are used in the solution of the water height (i.e. hydrostatic pressure) corrections. However, it is recognized that in some cases the coupled solution of the pressure corrections could be needed in order to ensure convergence, even though such a situation was not found in the studied cases. Furthermore, coupled solution of the pressure corrections may not require so much under-relaxation as the simplified version.

The results of the flooding simulations can be highly dependent on the applied data for the openings. In the presented case study, widely used estimations of the discharge coefficients and critical pressure heads for the closed doors were applied. However, different results would have been obtained with different input data. Therefore, it is of uttermost importance that full scale tests on various typical structures are performed in order to be able to obtain more reliable simulation results. Furthermore dedicated finite element and RANSE computations could provide more information on the structural deformation and on the pressure losses.

Finally, it can be concluded that the developed simulation method works well and it provides accurate results if all the parameters for the openings are known and if all the assumptions are valid. Therefore, the simulation method can be used as an efficient and feasible tool for assessing the time-to-flood in compartments, where the pressure losses in the openings and critical pressure heads can be estimated with a reasonable accuracy.

8 Bibliography

Blevins, R. D. 1984. Applied Fluid Dynamics Handbook, van Nostrand Reinhold Company, 558 p.

Chang, B.-C., Blume, P. 1998. Survivability of Damaged Ro-Ro Passenger Vessels, *Schiffstechnik – Ship Technology Research*, Vol. 45, pp. 105-112.

Chang, B.-C. 1999. On the Damage Survivability of Ro-Ro Ships Investigated by Motion Simulation in a Seaway, *Schiffstechnik – Ship Technology Research*, Vol. 46, pp. 192-207.

Cho, S. K., Hong, S. Y., Kim, Y. H., Lee, K. J. 2005. Investigation of dynamic characteristics of the flooding water of the damaged compartment of an ITTC RORO Passenger Ship, *Proceedings of the 8th International Ship Stability Workshop*, Istanbul, Turkey, 6-7. October 2005.

de Kat, J. O., van't Veer, R. 2001. Mechanisms and Physics Leading to the Capsize of Damaged Ships, *Proceedings of the 5th International Workshop on Ship Stability*, Trieste, Italy, 12-13. September 2001.

de Kat, J. O., Peters, A. J. 2002. Model Experiments and Simulations of a Damaged Frigate, *Proceedings of the 10th International Conference of the International Maritime Association of the Mediterranean, IMAM'02*, Crete, Greece, 14-18. May 2002.

Dillingham, J. 1981. Motion Studies of a Vessel with Water on Deck, *Marine Technology*, Vol. 18, No. 1, pp. 38-50.

Ferziger, J. H., Perić, M. 2002. Computational Methods for Fluid Dynamics, 3rd Edition, Springer-Verlag, 423 p.

Fox, R. W., McDonald, A. T. 1985. Introduction to Fluid Mechanics, John Wiley & Sons, 741 p.

González, V., Talens, M., Riola, J. M., Valle, J., Quesda, T., Espín, M. 2003. Numerical Prediction of the Dynamic Behaviour of a Ro-Ro Ship after a Hull Side Damage, *Proceedings of the 8th International Conference on Stability of Ships and Ocean Vehicles*, Madrid, Spain, 2003, pp. 215-227.

Ikeda, Y., Ishida, S., Katayama, T., Takeuchi, Y. 2004. Experimental and Numerical Studies on Roll Motion of a Damaged Large Passenger Ship in Intermediate Stages of Flooding, *Proceedings of the 7th International Ship Stability Workshop*, Shanghai, China, 1-3. November 2004, pp. 42-46.

IMO MSC.1/Circ.1226 2007. Interim Explanatory Notes to the SOLAS Chapter II-1 Subdivsion and Damage Stability Regulations, 15. January 2007.

IMO Resolution A.266 (VIII) 1973. Recommendation and a Standard Method for Establishing Compliance with the Requirements for Cross-Flooding Arrangements in Passenger Ships, adopted 20. November 1973.

IMO SLF46/INF.3 2003. Large Passenger Ship Safety: Time-to-Flood Simulations for a Large Passenger Ship – Initial Study, MARIN Report No. 17870-1-CPS, 40 p.

IMO SLF47/INF.6 2004. Large Passenger Ship Safety: Survivability Investigation of Large Passenger Ships, submitted by Finland, 11. June 2004.

IMO SLF50/10 2007. Revision of Resolution A.266 (VIII), Report of the SDS Correspondence Group, submitted by Sweden and United States, 26. January 2007.

ITTC 2002. The Specialist Committee on Prediction of Extreme Ship Motions and Capsizing – Final Report and Recommendations to the 23rd ITTC, *Proceedings of the 23th International Towing Tank Conference* – Volume II, Venice, Italy, 8-14. September 2002, pp. 619-657.

ITTC 2005. The Specialist Committee on Stability in Waves – Final Report and Recommendations to the 24th ITTC, *Proceedings of the 24th International Towing Tank Conference* – Volume II, Edinburgh, United Kingdom, 4-10. September 2005, pp. 369-408.

Jasionowski, A., Vassalos, D. 2001. Numerical Modelling of Damage Ship Stability in Waves, *Proceedings of the 5th International Workshop on Stability and Operational Safety of Ships*, September 2001, Trieste, Italy, 9 p.

Journée, J. M. J., Vermeer, H., Vredeveldt, A. W. 1997. Systematic Model Experiments of Flooding of Two Ro-Ro Vessels, *Proceedings of the 6th International Conference on Stability of Ships and Ocean Vehicles*, Varna, Bulgaria, 22-27. September, 1997.

Katayama, T., Ikeda, Y. 2005. An Experimental Study of Fundamental Characteristics of Inflow Velocity from Damaged Opening, *Proceedings of the 8th International Ship Stability Workshop*, Istanbul, Turkey, 6-7. October 2005.

Lee, D., Hong, S. Y., Lee, G.-J. 2007. Theoretical and Experimental Study on Dynamic Behaviour of a Damaged Ship in Waves, *Ocean Engineering*, Vol. 34, pp. 21-31.

Mustonen, P. 1998. Simulation Model of a Ship's Flooding Mechanism and Rolling Motion, Master's Thesis, Helsinki University of Technology, (in Finnish), 57 p.

Palazzi, L., de Kat, J. 2002. Model Experiments and Simulations of a Damaged Ship with Air-Flow Taken into Account, *Proceedings of the 6th International Ship Stability Workshop*, New York, U.S.A., 13-16. October, 2002.

Papanikolaou, A., Zaraphonitis, G., Spanos, D., Boulougouris, E., Eliopoulou, E. 2000a. Investigation into the Capsizing of Damaged Ro-Ro Passenger Ships in Waves, *Proceedings of the 7th International Conference on Stability of Ships and Ocean Vehicles*, Launceston, Tasmania, Australia, 7.-11. February 2000, pp. 351-362.

Papanikolaou, A., Spanos, D., Zaraphonitis, G. 2000b. Simulation of Large Amplitude Ship Motions and of Capsizing in High Seas, in *Contemporary Ideas on Ship Stability* (ed. Vassalos et al.), Elsevier, pp. 279-290.

Papanikolaou, A., Spanos, D. 2002. On the Modelling of Floodwater Dynamics and its Effects on Ship Motion, *Proceedings of the 6th International Ship Stability Workshop*, New York, U.S.A., 13-16. October, 2002.

Papanikolaou, A., Spanos, D., Boulougouris, E, Eliopoulou, E, Alissafaki, A. 2003. Investigation into the Sinking of the Ro-Ro Passenger Ferry Express Samina, *Proceedings of the 8th International Conference on Stability of Ships and Ocean Vehicles*, Madrid, Spain, 2003, pp. 31-48.

Patankar, S. V. 1980. Numerical Heat Transfer and Fluid Flow, Hemisphere Publishing Corporation, 197 p.

Paterson, A. R. 1997. A First Course in Fluid Dynamics, Cambridge University Press, 528 p.

Pawlowski, M. 2003. Accumulation of Water on the Vehicle Deck, *Proc. Instn Mech. Engrs Vol. 217 Part M: J. Engineering for the Maritime Environment*, pp. 201-211.

Peters, A. J., Galloway, M., Minnick, P. V. 2003. Cross-Flooding Design Using Simulations, *Proceedings of the 8th International Conference on Stability of Ships and Ocean Vehicles*, Madrid, Spain, 2003, pp. 743-755.

Pittaluga, C., Giannini, M. 2006. Pressure Losses Estimation for Structural Double Bottom by CFD Technique, CETENA Technical Report, published in internet (cited 28.8.2006), http://www.sname.org/committees/tech_ops/O44/sdsiscg/49/A266-1.pdf and http://www.sname.org/committees/tech_ops/O44/sdsiscg/49/A266-2.pdf

Ruponen, P. 2006a. Pressure-Correction Method for Simulation of Progressive Flooding and Internal Air Flows, *Schiffstechnik – Ship Technology Research*, Vol. 53, No. 2, pp. 63-73.

Ruponen, P. 2006b. Model Tests for the Progressive Flooding of a Box-Shaped Barge, Helsinki University of Technology, Ship Laboratory, Report M-292, 88 p.

Ruponen, P., Sundell, T., Larmela, M. 2006. Validation of a Simulation Method for Progressive Flooding, *Proceedings of the 9th International Conference on Stability of Ships and Ocean Vehicles*, Rio de Janeiro, Brazil, 25-29.9.2006, Vol. 2, pp. 607-616.

Santos, T. A., Guedes Soares, C. 2000. The Influence of Obstructions on the Transient Asymmetric Flooding of Roro Ships, *Proceedings of the 7th International Conference on Stability of Ships and Ocean Vehicles*, Launceston, Tasmania, Australia, 7-11. February 2000, pp. 385-395.

Santos, T. A., Winkle, I. E., Guedes Soares, C. 2002. Time Domain Modelling of the Transient Asymmetric Flooding of Ro-Ro Ships, *Ocean Engineering*, Vol. 29, pp. 667-688.

Sen, P. Konstantinidis, C. 1987. A Time Simulation Approach to the Assessment of Damage Survivability of Ro/Ro Cargo Ships, *Transactions of Society of Naval Architects and Marine Engineers*, SNAME, Vol. 95, pp. 337-355.

Siikonen, T. 2001. Lecture notes for the course Ene-39.030 "Advances in Computational Fluid Mechanics and Heat Transfer", Laboratory of Applied Thermodynamics, Helsinki University of Technology (in Finnish).

Skaar, D., Vassalos, D., Jasionowski, A. 2006. The Use of a Meshless CFD Method in Modelling Progressive Flooding and Damaged Stability of Ships, *Proceedings of the 9th International Conference on Stability of Ships and Ocean Vehicles*, Rio de Janeiro, Brazil, 25-29.9.2006, Vol. 2, pp. 625-632.

Solda, G. S. 1961. Equalisation of Unsymmetrical Flooding, *Transactions of Royal Institute of Naval Architects*, RINA, Vol. 103, pp. 219-225.

Souto-Iglesias, A. S., Pérez-Rojas, L. P., Zamora-Rodríguez, R. Z. 2004. Simulation of Anti-Roll Tanks and Sloshing Type Problems with Smoothed Particle Hydrodynamics, *Ocean Engineering*, Vol. 31, pp. 1169-1192.

Spanos, D., Papanikolaou, A. 2001. Numerical Study of the Damage Stability of Ships in Intermediate Stages of Flooding, *Proceedings of the 5th International Workshop on Stability and Operational Safety of Ships*, September 2001, Trieste, Italy, 8 p.

Spanos, D., Maron, A., Papanikolaou, A. 2002. On the Motions of a Flooded Ro-Ro Ferry in Beam Seas, *Proceedings of the 10th International Conference of the International Maritime Association of the Mediterranean, IMAM'02*, Crete, Greece, 14-18. May 2002.

Spouge, J. R. 1986. The Technical Investigation of the Sinking of the Ro-Ro Ferry European Gateway, *Transactions of Royal Institute of Naval Architects*, RINA, Vol. 128, pp. 49-72.

Svensen, T. E., Vassalos, D. 1998. Safety of Passenger/RoRo Vessels: Lessons Learned from the North-West European R&D Project, *Marine Technology*, Vol. 35, No. 4, pp. 191-199.

Tabri, K., Määttänen, J., Ranta, J. 2007. Model-Scale Experiments of Symmetric Ship Collisions, Journal of Marine Science and Technology (in press).

Tagg, R., Tuzcu, C. 2002. A Performance-based Assessment of the Survival of Damaged Ships – Final Outcome of the EU Research Project HARDER, *Proceedings of the 6th International Ship Stability Workshop*, New York, U.S.A., 13-16. October, 2002.

Turan, O., Vassalos, D. 1994. Dynamic Stability Assessment of Damaged Passenger Ships, *Transactions of Royal Institute of Naval Architects*, RINA, Vol. 136, pp. 79-104.

Valanto, P. 2002. Time-Dependent Survival Probability of a Damaged Passenger Ship, Volume 1 (Capsizing), HSVA Report No. CFD 05/2002, published as the IMO document SLF 45/INF.3, February 28, 2002.

Valanto, P. 2006. Time Dependent Survival Probability of a Damaged Passenger Ship II – Evacuation in Seaway and Capsizing, HSVA Report No. 1661, Hamburg May 31, 2006, 101 p, published in internet at http://www.hsva.de/10_downloads_content/ Valanto.pdf (cited 18.12.2006).

van der Vorst, H. A. 1992. BI-CGSTAB: a Fast and Smoothly Converging Variant of BI-CG for the Solution of Non-Symmetrical Linear Systems, *SIAM J. Sci. Stat. Comput.*, Vol. 13, No. 2, pp. 631-644.

van't Veer, R., de Kat, O. 2000. Experimental and Numerical Investigation on Progressive Flooding in Complex Compartment Geometries, *Proceedings of the 7th International Conference on Stability of Ships and Ocean Vehicles*, Launceston, Tasmania, Australia, 7-11. February 2000, pp. 305-321.

van't Veer, R., de Kat, O., Cojeen, P. 2002. Large Passenger Ship Safety: Time to Sink, *Proceedings of the 6th International Ship Stability Workshop*, New York, U.S.A, 13-16. October, 2002.

van't Veer, R., Serra, A. 2003. Large Passenger Ship Safety: Time to Sink Simulations, *Proceedings of the Passenger Ship Safety Conference*, Royal Institute of Naval Architects, London, UK, 25-26. March 2003.

van't Veer, R. 2004. Time to Flood (TTF) Simulations for a Large Passenger Ship – Final Study, Report No. 19289-1-CPS, MARIN, The Netherlands, August 2004, (published as the IMO document SLF 48/Inf.2), 30 p.

van't Veer, R., Peters, W., Rimpelä, A-L., de Kat, J. 2004. Exploring the Influence of Different Arrangements of Semi-Watertight Spaces on Survivability of a Damaged Large Passenger Ship, *Proceedings of the 7th International Ship Stability Workshop*, Shanghai, China, 1-3. November 2004.

Vartiainen, M. 2006. Evaluation of Flooding Simulation as a Ship Design Tool, Master's Thesis, Helsinki University of Technology, Ship Laboratory, 101 p.

Vassalos, D., Turan, O. 1994. A Realistic Approach to Assessing the Damage Survivability of Passenger Ships, *Transactions of Society of Naval Architects and Marine Engineers*, SNAME, Vol. 102, pp. 367-394.

Vassalos, D., Turan, O., Pawlowski, M. 1997. Dynamic Stability Assessment of Damaged Passenger/Ro-Ro Ships and Proposal of Rational Survival Criteria, *Marine Technology*, Vol. 34, No. 4, pp. 241-266.

Vassalos, D., Letizia, L., Shaw, M., MacPhearson, C. 1998a. An Investigation on the Flooding of Damaged Ro-Ro Ships, *Transactions of Royal Institute of Naval Architects*, RINA, Vol. 140, pp. 273-289.

Vassalos, D., Turan, O., Konovessis, D., Tuzcu, C. 1998b. Comparison between Prescriptive and Performance-Based Criteria for Assessing Ro-Ro Damage Survivability, *International Shipbuilding Progress*, Vol. 45, No. 444, pp. 351-382.

Vassalos, D. 2000. The Water on Deck Problem of Damaged Ro-Ro Ferries, in *Contemporary Ideas on Ship Stability* (ed. Vassalos et al.), Elsevier, pp. 163-185.

Vassalos, D., Letizia, L., Turan, O. 2000. Modelling the Accumulation of Water on the Vehicle Deck of a Damaged Ro-Ro Vessel and Proposal of Survival Criteria, in *Contemporary Ideas on Ship Stability* (ed. Vassalos et al.), Elsevier, pp. 315–337.

Vassalos, D., Jasionowski, A., Guerin, L. 2005. Passenger Ship Safety – Science Paving the Way, *Proceedings of the 8th International Ship Stability Workshop*, Istanbul, Turkey, 6-7. October 2005.

Vermeer, H., Vredeveldt, A. W., Journée, J. M. J. 1994. Mathematical Modelling of Motions and Damage Stability of Ro-Ro Ships in the Intermediate Stages of Flooding, *Proceedings of the 5th International Conference on Stability of Ships and Ocean Vehicles*, Melbourne, Florida, U.S.A.

Vredeveldt, A. W., Journée, J. M. J. 1991. Roll Motion of Ships due to Sudden Water Ingress, Calculations and Experiments, *RINA'91, International Conference on Ro-Ro Safety and Vulnerability the Way Ahead*, Vol. I, London, United Kingdom, 17-19. April 1991,.

Walshaw, A. C., Jobson, D. A. 1979. Mechanics of Fluids, Third Edition, Longman, 599 p.

Woodburn, P., Gallagher, P., Letizia, L. 2002. Fundamentals of Damage Ship Survivability, *Transactions of Royal Institute of Naval Architects*, RINA, Vol. 144, pp. 143-163.

Xia, J., Jensen, J. J., Pedersen, P. T. 1999. A Dynamic Model for Roll Motion of Ships Due to Flooding, *Schiffstechnik – Ship Technology Research*, Vol. 46, pp. 208-216.

Zaraphonitis, G., Papanikolaou, A., Spanos, D. 1997. On a 3-D Mathematical Model of the Damage Stability of Ships in Waves, Proceedings of the 6th *International Conference on Stability of Ships and Ocean Vehicles*, Varna, Bulgaria, 22-27. September, 1997, pp. 233-244.

Appendix A Derivation of Bernoulli's Equation

In the following Bernoulli's equation for a streamline is derived from the conservation of momentum for inviscid steady flow (Euler's equation). This follows mainly the reference *Fox and McDonald (1985)*.

The velocity field $\mathbf{U}$ is specified in rectangular co-ordinate system x, y, z. The corresponding velocity components are u, v, w. Euler's equation for steady flow in these rectangular co-ordinates is:

$$-\frac{1}{\rho}\nabla p - g\nabla z = \frac{D\mathbf{U}}{Dt} = u\frac{\partial \mathbf{U}}{\partial x} + v\frac{\partial \mathbf{U}}{\partial y} + w\frac{\partial \mathbf{U}}{\partial z}, \tag{A.1}$$

where ρ is the density of the fluid, p is the pressure and g is the acceleration due to gravity. With vector notation, this can be written as:

$$-\frac{1}{\rho}\nabla p - g\nabla z = (\mathbf{U}\cdot\nabla)\mathbf{U}. \tag{A.2}$$

The motion of a particle is governed by equation (A.2). In the time increment dt, the particle moves a distance $d\mathbf{s}$ along the streamline. Dot product:

$$-\frac{1}{\rho}\nabla p \cdot d\mathbf{s} - g\nabla z \cdot d\mathbf{s} = (\mathbf{U}\cdot\nabla)\mathbf{U}\cdot d\mathbf{s}, \tag{A.3}$$

where:

$$d\mathbf{s} = dx\mathbf{i} + dy\mathbf{j} + dz\mathbf{k}. \tag{A.4}$$

Let us consider the terms in equation (A.3) separately, along the streamline. The first one is:

$$-\frac{1}{\rho}\nabla p \cdot d\mathbf{s} = -\frac{1}{\rho}\left[\frac{\partial p}{\partial x}dx + \frac{\partial p}{\partial y}dy + \frac{\partial p}{\partial z}dz\right] = -\frac{1}{\rho}dp \tag{A.5}$$

and the second one is:

$$-g\nabla z \cdot d\mathbf{s} = -g\,dz. \tag{A.6}$$

Using the vector identity, the last term of (A.3) can be written as:

$$(\mathbf{U}\cdot\nabla)\mathbf{U}\cdot d\mathbf{s} = \left[\frac{1}{2}\nabla(\mathbf{U}\cdot\mathbf{U}) - \mathbf{U}\times(\nabla\times\mathbf{U})\right]\cdot d\mathbf{s}\,. \tag{A.7}$$

The second term in this equation is zero since $\mathbf{U}$ is parallel to $d\mathbf{s}$, consequently:

$$\begin{aligned}(\mathbf{U}\cdot\nabla)\mathbf{U}\cdot d\mathbf{s} &= \frac{1}{2}\nabla(\mathbf{U}\cdot\mathbf{U})\cdot d\mathbf{s} \\ &= \frac{1}{2}\left[\frac{\partial U^2}{\partial x}dx + \frac{\partial U^2}{\partial y}dy + \frac{\partial U^2}{\partial z}dz\right] \\ &= \frac{1}{2}d\left(U^2\right)\,.\end{aligned} \tag{A.8}$$

As a result, the equation (A.3) can be written as:

$$\frac{dp}{\rho} + g\,dz + \frac{1}{2}d\left(U^2\right) = 0\,. \tag{A.9}$$

Integration of this equation results in:

$$\int\frac{p}{\rho} + g\,z + \frac{1}{2}U^2 = C \text{ (along s)}, \tag{A.10}$$

which is Bernoulli's equation.

Appendix B Linearization of Bernoulli's Equation

Bernoulli's equation for incompressible flow can be presented in a form of a pressure loss (as described in section 3.3.2). Let us consider water flow through an opening k that connects the rooms i and j:

$$\frac{1}{2}K'_{w,k}\dot{m}_{w,k}\left|\dot{m}_{w,k}\right| = P_i - P_j . \tag{B.1}$$

The flow from i to j is defined to be positive.

Let us define an auxiliary function:

$$F^*_{w,k} = \frac{1}{2}K'_{w,k}\dot{m}^*_{w,k}\left|\dot{m}^*_{w,k}\right|. \tag{B.2}$$

This can be approximated with a linearization from the previous value $F^n_{w,k}$:

$$\begin{aligned} F^*_{w,k} &= F^n_{w,k} + \Delta F_{w,k} \\ &= F^n_{w,k} + \frac{\partial F^n_{w,k}}{\partial \dot{m}_{w,k}}\Delta\dot{m}_{w,k} \\ &= F^n_{w,k} + \left(\frac{1}{2}K'_{w,k}\left|\dot{m}_{w,k}\right| + \frac{1}{2}K'_{w,k}\dot{m}_{w,k}\,\mathrm{sign}\left(\dot{m}_{w,k}\right)\right)\cdot\Delta\dot{m}_{w,k} \\ &= F^n_{w,k} + K'_{w,k}\left|\dot{m}_{w,k}\right|\Delta\dot{m}_{w,k} . \end{aligned} \tag{B.3}$$

Therefore, the linear approximation of the change is:

$$\Delta F_{w,k} = K'_{w,k}\left|\dot{m}_{w,k}\right|\Delta\dot{m}_{w,k} . \tag{B.4}$$

Let us now use the equation (B.3) for corrected mass flow $\dot{m}^*_{w,k} + \dot{m}'_{w,k}$ by applying $\dot{m}^*_{w,k}$ as the initial guess for mass flow $\dot{m}_{w,k}$ and the mass flow correction $\dot{m}'_{w,k}$ as the change of mass flow $\Delta\dot{m}_{w,k}$:

$$\Delta F_{w,k} = K'_{w,k}\left|\dot{m}^*_{w,k}\right|\dot{m}'_{w,k} . \tag{B.5}$$

On the other hand, $\Delta F_{w,k}$ can also be expressed as the change in the pressure difference:

$$\Delta F_{w,k} = F^*_{w,k} - F^n_{w,k} = \left(P^*_i - P^*_j\right) - \left(P^n_i - P^n_j\right) = P'_i - P'_j . \tag{B.6}$$

Equations (B.4) and (B.6) can be combined, resulting in the following equation:

$$K'_{w,k}\left|\dot{m}^{*}_{w,k}\right|\dot{m}'_{w,k} = P'_i - P'_j . \tag{B.7}$$

This equation forms the basis of the pressure-correction equation for water flows.

Airflow needs to be handled separately due to its compressibility. The linearization of Bernoulli's equation is done similarly to the case of an incompressible flow, but now the mass flow must be expressed as a product of the density and the volumetric flow:

$$F^{*}_{a,k} = \frac{1}{2}K'_{a,k}\rho_{a,k}Q^{*}_{a,k}\left|\rho_{a,k}Q^{*}_{a,k}\right| = p_i - p_j . \tag{B.8}$$

So here it is assumed that Bernoulli's equation for incompressible flow is valid also for compressible flow. This assumption simplifies the pressure-correction equation significantly.

The density is assumed to depend linearly on the pressure. Furthermore, the air pressure is always positive so the absolute value is not needed. Consequently, equation (B.8) can be written as:

$$F^{*}_{a,k} = \frac{1}{2}K'_{a,k}\left(\frac{\rho_0}{p_0}\right)^2 p_k^2 Q^{*}_{a,k}\left|Q^{*}_{a,k}\right| = p_i - p_j . \tag{B.9}$$

Similarly to the previous case, equation (B.3), we obtain:

$$\begin{aligned}\Delta F_{a,k} &= \frac{\partial F^{n}_{a,k}}{\partial Q_{a,k}}\Delta Q_{a,k} + \frac{\partial F^{n}_{a,k}}{\partial p_k}\Delta p_k \\ &= \frac{1}{2}K'_{a,k}\left(\frac{\rho_0}{p_0}\right)^2\left[p_k^2\left(\left|Q_{a,k}\right| + Q_{a,k}\,\mathrm{sign}\left(Q_{a,k}\right)\right)\cdot\Delta Q_{a,k} + 2\cdot Q_{a,k}\left|Q_{a,k}\right|p_k\Delta p_k\right] \\ &= K'_{a,k}\left(\frac{\rho_0}{p_0}\right)^2\left[p_k^2\left|Q_{a,k}\right|\cdot\Delta Q_{a,k} + Q_{a,k}\left|Q_{a,k}\right|p_k\cdot\Delta p_k\right].\end{aligned} \tag{B.10}$$

Let us now use the equation (B.10) for corrected volumetric flow $Q^{*}_{a,k} + Q'_{a,k}$ by applying $Q^{*}_{a,k}$ as the initial guess for mass flow $Q_{a,k}$ and the mass flow correction $Q'_{a,k}$ as the change of volumetric flow $\Delta Q_{a,k}$. Moreover,

$$\Delta p_k = p'_k . \tag{B.11}$$

It should also be noted that the hydrostatic pressure has no effect on the airflows, and therefore, the effective pressure is always equal to the air pressure. Consequently, equation (B.6) is reduced to:

$$\Delta F_{a,k} = p'_i - p'_j \,. \tag{B.12}$$

Furthermore, equations (B.10) and (B.12) can be combined, resulting in:

$$K'_{a,k}\left(\frac{\rho_0}{p_0}\right)^2 \left[p_k^2 \left|Q^*_{a,k}\right| \cdot Q'_{a,k} + Q^*_{a,k}\left|Q^*_{a,k}\right| p_k\, p'_k\right] = p'_i - p'_j \,. \tag{B.13}$$

This equation forms the basis of the pressure-correction equation for airflows.

ISBN 978-951-22-9012-3
ISBN 978-951-22-9013-0 (PDF)
ISSN 1795-2239
ISSN 1795-4584 (PDF)